CHEMOSTRATIGRAPHY, PALEOCEANOGRAPHY, AND SEQUENCE STRATIGRAPHY OF THE PENNSYLVANIAN – PERMIAN SECTION IN THE MIDLAND BASIN OF WEST TEXAS, WITH FOCUS ON THE WOLFCAMP FORMATION

by

MILTON CORTEZ III

Presented to the Faculty of the Graduate School of

The University of Texas at Arlington in Partial Fulfillment

of the Requirements

for the Degree of

MASTER OF SCIENCE IN GEOLOGY

THE UNIVERSITY OF TEXAS AT ARLINGTON

MAY 2012

ACKNOWLEDGEMENTS

Foremost, I would like to thank God for providing my wife and me sufficient patience, strength, and love to achieve our goals over the last few years. Additionally, I would like to sincerely thank my wife for her support, encouragement, and unfailing love through these stressful times. Also, I truly thank my advisor, Dr. Harry Rowe, for his guidance, insight, and provision during the last two years.

Major thanks go to the Geology Department Chair at the University of Texas at Arlington, Dr. John Wickham, for all of his assistance and participation on my thesis committee. I would also like to thank several members of the Texas Bureau of Economic Geology, in Austin, Texas. First, I would like to thank Dr. Stephen Ruppel and the Mudrock Systems Research Lab (M.S.R.L.) consortium for providing access to several cores and funding for travel expenses. Also, I would like to especially thank Dr. Scott Hamlin and Robert Baumgardner for their collaborative work on the cores used for my research. Their meticulous core descriptions and interpretations have been a key factor in the final product of my research. Dr. Hamlin also provided many of the detailed maps and well log interpretations presented in the thesis, and served on my thesis committee. Similarly, Mr. Baumgardner was an essential sounding board and collaborator throughout several stages of my research. An often overlooked group that I would like to thank is the B.E.G. core repository staff. Nathan Ivicic, James Donnelly, Kenneth Edwards, and Josh Lambert were an integral part of my physical data collection process. Their incredible courtesy and hard work should not go unrecognized.

I would also like to thank Liz Clechenko, Terra George, and Jason Stein from ConocoPhillips for assisting in the attainment and interpretation of XRD data.

I am very grateful for many members of the geochemistry research group at University of Texas at Arlington. I would like to especially thank Niki Hughes for the development of the calibrations used to interpret raw XRF data. Also, I would like to thank Krystin Robinson, Robert Nikirk, Brian Turner, Karen McCreight, and Pukar Mainali for their help in the lab and as sounding boards for ideas and results.

Special thanks go to Cory and Jessica Daniels for their hospitality throughout my writing process. Thanks for putting up with my clutter and re-appropriation of the kitchen table.

Finally, I would like to thank my parents and extended family for their lifelong encouragement and support.

April 12, 2012

ABSTRACT

CHEMOSTRATIGRAPHY, PALEOCEANOGRAPHY, AND SEQUENCE STRATIGRAPHY OF THE PENNSYLVANIAN-PERMIAN SECTION IN THE MIDLAND BASIN OF WEST TEXAS, WITH FOCUS ON THE WOLFCAMP FORMATION

Milton Cortez III, M.S.

The University of Texas at Arlington, 2012

Supervising Professor: Harold Rowe

The late Pennsylvanian to early Permian rocks (Wolfcampian and Leonardian) of the Midland Basin represent a single lithologic unit composed primarily of calcareous mudrocks, siliceous mudrocks, muddy carbonate-clast conglomerates, and skeletal packstones/grainstones at the approximate depositional center located in Reagan County, Texas. Pure versions of these lithologic end-members are discretely distributed among a multitude of transitional lithofacies. The Midland Basin evolved in the foreland of the Ouachita Fold-belt from Mississippian to early Permian time along-side several sub-basins of the Permian Basin. These basins were formed by disseverance and uplift associated with the continental collision of Laurasia and Gondwana to form Pangea in the Late Paleozoic. Wolfcampian and Leonardian clastics were deposited into the basin as a result of a rapid increase in accommodation due to basin subsidence and proximal uplift of the Central Basin Platform, in concurrence with glacially-driven eustatic sea-level fluctuations influenced by the Late Paleozoic

Ice Age (LPIA). Various aspects of Penn-Perm strata that were studied include degree of basin restriction, redox conditions, sediment input, paleoceanography, bulk geochemistry, and sequence stratigraphy. Four drill cores located in Reagan and Martin Counties were scanned at a 1-foot interval with a hand-held energy-dispersive x-ray fluorescence (HH-ED-XRF) spectrometer to provide quantitative analysis of major (e.g. Fe, Si, Al) and trace (e.g. Mo, Cr, V) elements. In addition, total organic carbon (TOC), total inorganic carbon (TIC), X-Ray Diffraction (XRD) spectroscopy, and stable isotopes of organic carbon ($\delta^{13}C_{org}$) were analyzed in two of the cores. Focus of the project was to thoroughly define the chemostratigraphy of a continuous core through the Leonardian and Wolfcampian strata in Reagan County. Secondarily, study of intermittent core through the Spraberry, Dean, Strawn, and Atoka Formations in the Martin County core provided insight into the overall evolution of the Midland Basin from Atokan to the Guadalupian time. The area of study is located off of the shelf slope into marginal basin settings, and is oriented parallel to the Eastern Shelf between the Ozona Arch and the Eastern Shelf Nose.

The physical paleoceanography of the Penn-Perm section reveals an overall high degree of basin restriction at the time of deposition, while large scale study revealed an overarching trend of basin deepening along-side an increase in primary production seen in several scales of cyclic stair-stepping negative $\delta^{13}C_{org}$ excursions. Fluctuations in the degree of restriction and water mass mixing were studied through the chemical paleoceanographic interpretation of several distinct zones enriched in redox sensitive trace metals (Mo, V, Ni, and Zn) and/or detrital sediments (Ca, Fe, Si, Mg, and K) normalized to clay. Individual zones labeled Detrital (DZ), Detrital-Anoxic (DAZ), and Anoxic (AZ) were linked to changes in basin dynamics and ultimately associated with a complete LPIA-driven lowstand-to-highstand sequence stratigraphic cycle. Ultimately, a thorough chemostratigraphy was developed on Late Pennsylvanian through Permian age mudrocks. Correlations between chemostratigraphy, paleoceanography, and sequence stratigraphy have enhanced the ability to assess the

economic potential of Midland Basin Penn-Perm rocks as an unconventional source/reservoir. Furthermore, the study has laid the groundwork for future attempts to make similar correlations between mudrock geochemistry to marine basin dynamics.

TABLE OF CONTENTS

LIST OF ILLUSTRATIONS

Figure Page

LIST OF TABLES

CHAPTER 1

INTRODUCTION

1.1 Purpose of Study

1.1.1 Hydrocarbon Research

In recent years, technology related to the study of oil- and gas-bearing rocks has rapidly evolved. Highly sophisticated methods and instrumentation have been implemented worldwide to determine and exploit every possible economic hydrocarbon reservoir. Unprecedented global demand for energy has placed an enormous pressure on geologists and engineers to increase production rates while simultaneously decreasing the costs related to hydrocarbon procurement processes. An overwhelming demand for energy has been stimulated by concurrent exponential growths in population and technology. Assareh et al. (2011) estimate current global oil, natural gas, and coal consumption to slightly exceed 7 billion barrels of oil equivalent (BBOE) per year. The study also predicts an increase in global usage to 31 – 47 BBOE per year by 2040. Although renewable energy production is steadily on the rise, matching the 400 – 700 percent increase will be a daunting task. Although many industry officials quote a much higher number, the Organization of the Petroleum Exporting Countries (OPEC) and the Energy Information Administration (EIA) both estimate global reserves at approximately 1.2 trillion Barrels of Oil Equivalent (TBOE) (Energy Information Administration, 2012; OPEC, 2012). Discounting a number of complex production factors and the inevitable growth of technology, the area under the best fit exponential growth line shown in **Figure 1** predicts current global reserves (1.2 TBOE) to last a mere 43 years with the currently modeled usage prediction. This is an oversimplification of the numerous dynamics related to oil reserve forward modeling. Although, taken as a worst case scenario, it successfully creates a visual example of our desperate need for contemporaneous increases in

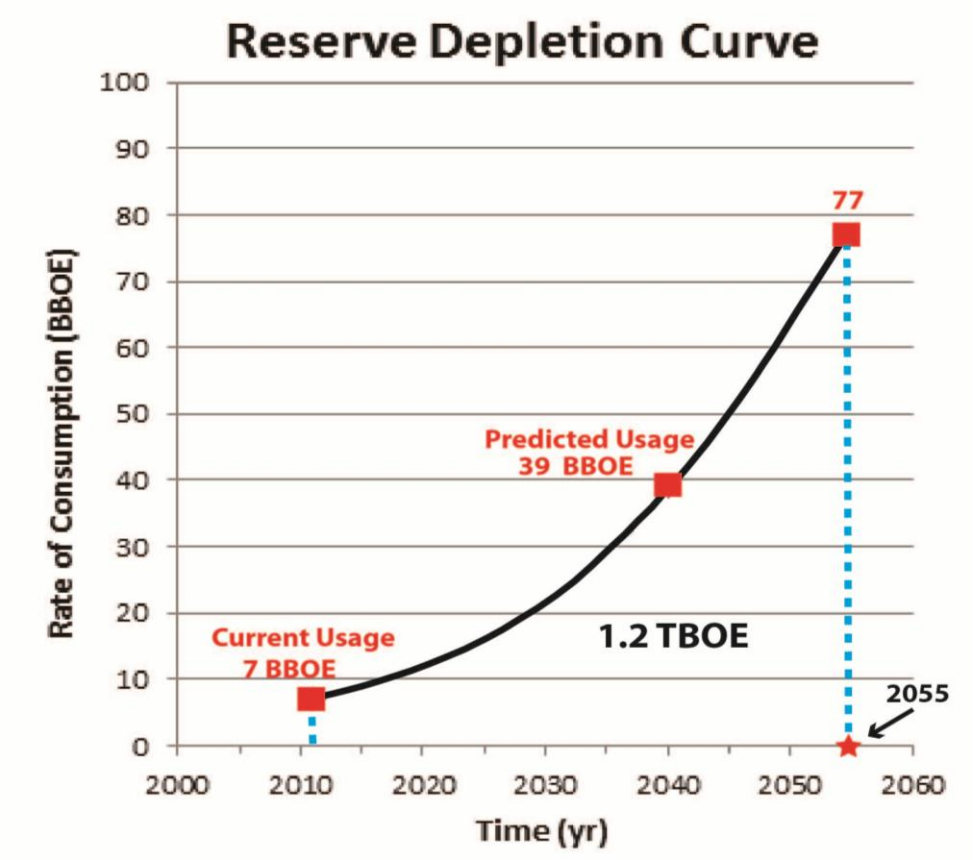

Figure 1. Modeled Reserve Deletion Curve with best fit exponential curve and estimated current reserve depletion date. (Energy Information Administration 2012; OPEC, 2012; Assareh et al., 2011)

production and decreases in consumption. These sobering estimates assure us that work to further our knowledge of unconventional systems will not be an act of futility.

A major shift in industry focus from conventional to unconventional reservoirs has led a similar shift in academic research. The factors driving the shift are discussed in detail below. A byproduct of a simple database search confined by topic and date reveals that a recent upswing in fine-grained sediment research has been vastly overwhelmed by porosity, permeability, and other reservoir based research. This study has been designed and developed alongside several similar projects in order to compile a comprehensive collection of source/reservoir mudrock geochemical and the relative paleoceanographic assimilations of various packages across the North American continent. It is our goal to successfully integrate our procedures and

findings into the standard protocol for evaluating a potential mudrock based hydrocarbon source/reservoir by demonstrating the importance of depositional and post-depositional geochemical processes to the accumulation and preservation of organic matter within mudrocks.

Idyllic timing of industry pressures, technological advances, and academic fervor have generated circumstances for a profound breakthrough in mudrock characterization. Recent developments in technology have converged upon a common point of interest between industry and academia. Engineers have developed complex hydraulic fracturing methods allowing industry to now view mudrocks as potential reservoirs. Similarly, improvements in geochemical analytical methodology and instrumentation allow geoscientists to refine their knowledge of pre- and post-depositional chemical signatures in source rocks. This unorthodox portrayal of Darwinian convergent evolution points to the next era of global hydrocarbon production.

In the course of the search for oil and gas plays based on Hunt's anticlinal theory of oil entrapment (1861), industry has successfully discovered and exploited structurally trapped conventional oil and gas reservoirs for over one-hundred years (Selley, 1998). J. F. Carll (1880) opened an additional bank of potential reservoirs with research depicting stratigraphic traps in the Vanango sands of Pennsylvania (Selley, 1998). Although these two major breakthroughs occurred within twenty years, the next significant step forward was not taken until 1949 when Stanolind Oil introduced modern hydraulic fracturing. Their discovery opened the door to the expansive vault we now know as tight-sand and shale-gas by expanding and improving small scale theories and practices first used in the 1860's. Solidified nitroglycerin was initially used as a fracturing agent and eventually replaced by various types of acids in the 1930's. These highly volatile and corrosive materials have since been replaced by simple mixes of water, sand, and a small set of proprietary chemicals. The development of hydraulic fracture technology coupled with lateral drilling capability allows industry to explore the vast storehouse of mudrocks that were previously overlooked as reservoirs due to their low porosity and permeability. It is

estimated that 60% of all wells drilled today are hydraulically fractured (Montgomery and Smith, 2010).

Conventional plays are defined as hydrocarbon reservoirs that have a well-defined areal extent and can produce resources at economically advantageous flow rates without extensive stimulation treatments or special recovery processes (Holdich, 2003; Vidas and Hugman, 2008). These reservoirs typically contain rocks of medium- to high-permeability and are profitable with a simple vertical drilling scheme. Conventional hydrocarbon reservoirs also consist of a source rock, reservoir rock, hydrocarbon trap, and a sufficient impermeable seal (Selley, 1998). Such plays have dominated global production for over one hundred years. The Barnett Shale of the Fort Worth basin in central Texas has changed this dynamic.

In conjunction with state and federal tax credits related to production, The United States government defined unconventional tight-gas reservoirs as systems expected to have a permeability to gas flow less than 0.1 millidarcy (Holdich, 2006). Industry, however, uses a much more complex definition. A widely used integration of Darcy's law relates flow rate as a function of permeability, net thickness, average reservoir pressure, flowing pressure, average fluid properties, drainage area, well-bore radius, and skin factor. Therefore, the most accurate definition for an unconventional reservoir refers to a number of diverse systems that can only be economically beneficial after large-scale stimulation or special recovery schemes are performed (Holdich, 2003; Vidas and Hugman, 2008). Common unconventional systems include gas shale, tight-gas sand, coal-bed methane, and heavy oil (Holdich, 2003). Processes that are typically used to promote production in these reservoirs include hydraulic fracturing, flooding, and steam injection. These processes allow mudrocks with permeability flow rates on the order of microdarcies (~0.001 millidarcy) that were previously viewed only as sources and seals to now be exploited for economical hydrocarbon production. It is clear that we must understand a number of physical and chemical characteristics of tight-gas plays in order to exploit their resources in the most economically advantageous manner.

The present study will focus on the geochemical aspect of a prolific petroleum system in west Texas. Chemistry of source/reservoir rocks provides information related to sedimentology, provenance, paleoceanography, petrography, organic content, and even geo-mechanics (Selley, 1998). The focus is on developing an increased comprehension of source rock sedimentology and basin paleoceanography. Defining the depositional environment and paleo-oxygenation of bottom waters delivers insight at multiple scales into the likelihood of the location of preserved hydrocarbons throughout the Pennsylvanian – Permian boundary of the Midland Basin. Results will aid geologists and engineers in their efforts to concentrate on zones of greater potential. Furthermore, this will imply general conclusions as to the distribution and quality of analogous unconventional plays around the world.

1.1.2 Mudrocks

> *"Possibly many may think that the deposition and consolidation of fine-grained mud must be a very simple matter, and results of little interest. However, when carefully studied experimentally it is soon found to be so complex a question, and the results dependent on so many variable conditions, that one might feel inclined to abandon the inquiry, were it not that so much of the history of our rocks appears to be written in this language."*
>
> Henry Clifton Sorby, 1908

Sorby's quote describes the formerly bleak plight of geologists looking for significant revelations in fine-grained clastics everywhere. Shales and mudstones compose nearly two thirds of the sedimentary rock record, making them the most prevalent lithological storehouse of earth's history. Held in their seemingly homogeneous matrix are indications of climate change, tectonic movement, and paleoceanography to name a few (Sheiber and Zimmerle, 1998). Ambiguity of the widely used terms, "shale" and "mudstone," are a source of confusion throughout literature. The two terms depicting fine-grained terrigenous clastics (Sheiber and Zimmerle, 1998) are commonly used interchangeably, although their formal definitions differ

slightly. Industry related literature primarily uses the terms “shale” or “black shale” in reference to fine-grained mudstone source rock (e.g. Harris et al., 1970; Curtis, 2002; Bowker, 2007). Often, this term falsely implies some degree of fissility regardless of the true physical characteristics of the rock. The accepted definition for “mudrock” or “mudstone” refers to a fine- to very fine-grained siliciclastic sedimentary rock of which at least fifty percent is silt and clay. It is further supposed that cumulative composition of the silt and clay fraction have no connotation to the breaking characteristics or fissility of the rock (Grainger, 1984). The latter nomenclature will be used in this study, while it must be noted that virtually all of the geochemical characteristics associated with one applies to the other.

The detailed sedimentological and geochemical aspects of mudrocks and their contribution to oil and gas systems have been relatively overlooked in the past. Shieber and Zimmerle (1998) note that only 22 papers in the GEOREF data base focused on shales/mudstones from 1980 to 1995, while an average of 1332 papers on sandstone and carbonates were published each year. This staggering disproportion is a direct result of a century subjugated by conventional reservoir economics and drilling schemes that have subsequently compiled an enormous bank of knowledge related to sandstone and carbonate reservoirs. Now that technology has approached the desperate need for a further understanding of fine-grained clastic systems, we must work diligently to glean as much information from the sedimentary record as possible (Schieber and Zimmerle, 1998; Slatt, 2002).

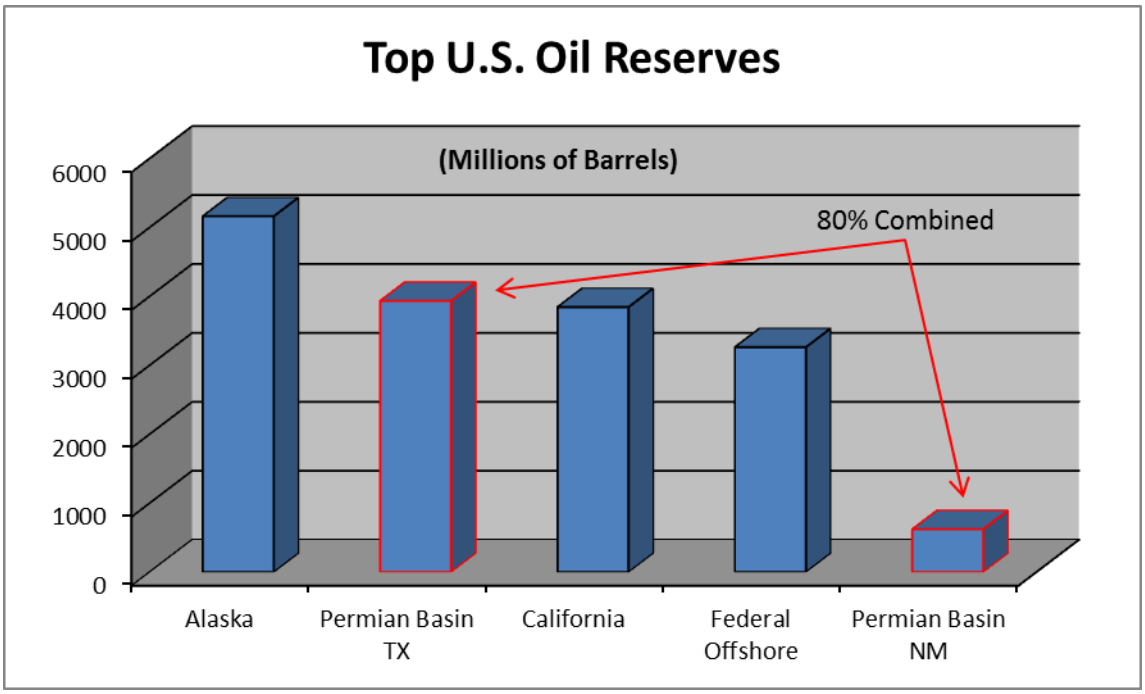

Figure 2. Top 5 U.S. oil producers and their relative contributions. *Compiled by the Center for Energy & Economic Diversification*. (University of Texas Permian Basin, 1998)

1.1.3 Permian Basin

Many legendary fields thought to have been exploited to their fullest extent in the past are now subject for a reassessment of their economic viability due to trapped hydrocarbons in mudrocks. One of the most famous examples is the Permian Basin of West Texas. This basin spans 52 counties throughout Texas and New Mexico over an estimated 86,000 square miles (Ball, 1995). Remaining oil-in-place estimates have been steadily climbing since 1995. Although roughly 29 billion barrels of oil (Bbbl) have been produced to date, it has been estimated that 23-30 Bbbl remain in place while an additional 2.5 Bbbl remain undiscovered (Ball, 1995; Dutton et al., 2004; Flamm, 2008). The Permian Basin has contributed a considerable amount of the cumulative oil production in the United States (**Figure 2**). Generally considered the most prolific oil-producing basin in U.S. history (Kim and Ruppel, 2005; Flamm, 2008), the Permian Basin is now attempting to continue its reign by proliferation into the realm of unconventional oil and natural gas. Focus has now shifted to the recovery of shale-oil/gas

found in the source rocks responsible for such fruitful production over the last eighty years. Pennsylvanian-Permian age strata have contributed greater than one-third of cumulative produced hydrocarbons from this system (Dutton et al., 2004). These impressive totals are owed to the discovery of Wolfcampian carbonate reservoirs in the early 1950's (Dutton et al., 2004; Flamm, 2008). Since then, conventional carbonate production has made up 75% of the total hydrocarbon contribution of the Permian Basin (Dutton et al., 2004). The present study will concentrate on the Wolfcampian and Leonardian clastic source rocks from a location in the Midland Basin that is accountable for such prolific hydrocarbon production.

1.2 Previous Mudrock Research

1.2.1 Geochemical Analysis

Although geochemical studies of mudrocks have been conducted for several decades, (e.g. Vine and Tourtelot, 1970; Demaison and Moore, 1980; Arthur and Sageman, 1994; Algeo and Lyons, 2006; Rowe et al., 2008) detailed core-based analysis in relation to depositional environment and paleo-oxygenation is only recently emerging as an accepted tool used in reservoir characterization. Several environmental factors, including bottom-water oxygenation and sediment characterization provide insight into the measurable appearance, enrichment, and depletion of chemical assemblages throughout vertical sections of rock. A better understanding of geochemical signatures, their causal relationships, and their linkages with the paleo-environment and -oceanography will help to refine well-to-well correlations. Additionally, an accurate and understood chemostratigraphy can help to better understand well-log results and spatial variability in depositional environments across the basin. Chemostratigraphic data may also prove valuable for assessing post-depositional signatures that may also change across the basin. Furthermore, a higher magnitude resolution of reservoir quality can be obtained through the integration of these relationships into the traditional reservoir characterization protocol.

Research using redox-sensitive trace metals, iron-sulfur-organic carbon relationships, iron speciation, and stable isotope or organic carbon and nitrogen has been sparsely distributed throughout literature (e.g. Morford et al., 2001; Algeo and Maynard, 2004; Rimmer et al., 2004; Brumsack, 2006; Lyons and Severmann, 2006; Cruse, Lyons and Hannigan, 2007). These studies have been predominantly focused on relating chemistry of modern anoxic basins, like the Black Sea or the Cariaco Basin, to similar environments in the geologic past (e.g. (Brumsack, 1989; Magyar et al., 1993; Schroder and Grotzinger, 2007; Aller et al, 2004; Arthur and Sageman, 2005; Dutkiewicz et al, 2004; Brumsack, 2006; Schroder and Grotzinger, 2007)

Research on mudrocks of varying characteristics and locations has been the focus of several theses from a group of geoscientists in association with University of Texas at Arlington, the Bureau of Economic Geology, and the Mudrock Systems Research Laboratory (MSRL) (e.g. Hoelke, 2011; Hughes, 2011; Manali, 2011). The complex chemostratigraphy and paleoceanography of several systems have been analyzed together and separately to form conclusions at several scales. Each mudrock package has been chosen for its unique characteristics in an effort to better represent the full range of possibilities achievable in basinal fine-grained depositional systems. Particular attention has been paid to packages referred to as “black shales” by the oil and gas industry. Mentioned before, black shale is a widely used term pertaining to dark-colored mudrocks containing organic matter and silt- and clay-sized mineral grains which are typically, but not exclusively, a product of an extremely sediment starved basin floor (Swanson, 1961; Tourtelot, 1979). This setting results in a chemically complex but relatively thin sequence of rock that can potentially represent vast amounts of time. Also referred to as a condensed section, the subsequent mudrock package often provides researchers the opportunity to observe various regional and global changes through the analysis of only a few hundred feet of core. Commonly laminated and fissile, black shales typically contain 2 – 10 percent organic carbon, minor amounts of authigenic carbonate, and considerable enrichments of trace metals (Tourtelot, 1979). Accumulations of biogenic and

terrigenous silica (SiO_2) as well as calcium carbonate ($CaCO_3$) can become significant bulk mineralogical fractions (Arthur and Sageman, 1994; Piper and Calvert, 2009). Major elemental (e.g. Si, Al, K, Fe, Mg) ratios and common substitutions (e.g. Rb, Sr, Na) into the clay fraction mineralogy are well known and predictable characteristics as a function of aluminosilicate diagenesis. Similarly, environmental conditions necessary for the enrichment of redox sensitive trace metals (e.g. Mo, V, Cr, Zn) in the sediment are a well-documented phenomenon (Morford and Emerson, 1999; Morford, et al., 2001; Algeo and Lyons, 2006; Tribovillard et al., 2006; Algeo and Maynard, 2008; Piper and Calvert, 2009; Algeo and Rowe, 2011; Tribovillard et al., 2011).

The present study will concentrate on determining the depositional environments and paleoceanography of carbonate-rich Pennsylvanian-Permian black shales and mudrocks in the Midland Basin through the analysis of chemostratigraphic properties. Geochemical analysis, as such, has four main categories of significance: 1) chemostratigraphic plots of elemental enrichments and depletions versus depth, to observe stratigraphic trends, cyclic sequencing, and unique elemental signatures found in the rock; 2) bulk geochemical compilations plotting all relative data points along significant lines of regression representing mineral stoichiometry, mineral phase shifts, or mineralogical assemblage ratios; 3) isotopic ratios and trends reflective of paleoceanography, circulation, and productivity and 4) sequence stratigraphic implications by the integration of basin hydrography and chemostratigraphic proxies. Results obtained from each of these categories are based on basic proxies and pragmatic tendencies which will be addressed below. Ultimately, paleo-environmental geochemical studies are based on observations of modern marine and theorized paleo-marine chemistry and the related oceanographic properties associated with each.

A number of studies have interpreted the chemical composition of sediments in modern upwelling zones and sapropels to exhibit theorized thermodynamic and diagenetic occurrences

preserved in the rock record (e.g. Berner, 1982; Brumsack, 1989; Schroder and Grotzinger, 2007). Influx of nutrient-rich waters promotes primary production, while subsequent anoxia encourages preservation of organic matter (Brumsack, 1989). This basic principle can be combined with several complex chemical signatures depicting the extent and timing of these events in order to expound on the generalized model for basinal mudstone deposition.

Chemostratigraphic analysis and interpretation of redox-sensitive and/or sulfide-forming trace metals has been historically one of the most used methods in the determination of paleo-redox conditions of oil and gas producing basins (Jones and Manning, 1994; Rowe et al., 2008; Tribovillard et al., 2011). An enormous amount of economic importance has been placed on pre- or post-depositional oxic levels of basinal bottom-waters as a result of the perceived control this parameter is thought to have over the locale and extent of organic preservation. In addition, intrinsic relationships with bottom water oxygenation levels have been linked to the genesis, deposition, and accumulation of economically significant ores (Jones and Manning, 1994). It is hypothesized that global expansion of the oxygen minimum zone during the late Paleozoic heightened the accumulation and preservation of organic material in open ocean settings (Jenkyns, 2010). More specifically, the presence of organic material in sediment relies on a complex interaction of three main factors: 1) Production: the amount of organic-matter input (primary or secondary), 2) Destruction: the mechanism responsible for the preservation or decomposition of organic-matter, and 3) Dilution: the degree of non-organic mineralogical constituents introduced along-side organic material in the sediment (Bohacs et al., 2005; Tyson, 2005). Organic matter preservation is ultimately a thermodynamically driven process acting along-side biogenic catalysts in a system. Fluctuations in the amount or type of biologic activity have considerable effect on the amount and location of several elemental controls in a system. The tendency of organic matter to react with oxygen is great; therefore, the strongest control on preservation is time of exposure to an oxic environment (Tyson, 2005). Obviously, this variable can be controlled by several different depositional regimes. It is noted that the majority of

preserved organic matter was deposited in marine sediments under oxygenated waters near continental margins (Hedges and Keil, 1995). This fact is attributed to high sedimentation and burial rates analogous to modern Papua New Guinea (Hedges and Keil, 1995; Milliman, 1995; Aller et al, 2004). Such modern analogs are products of tropical climates and extremely high accommodation resulting from active orogenic activity. These systems are characterized by rapid deposition, burial, and compaction of organics which, in turn, limits the time of exposure to oxygen in the water column. Conversely, silled and restricted basins limit the time of exposure of organics to oxygen by developing highly stratified and virtually stagnant water columns within basins. Efficient organic preservation in the Draupne and Dimmeridge formations was a direct result of a poorly oxygenated and highly stratified water column, rather than high primary production or sedimentation rates (Tyson et al., 1979; Jones and Manning, 1994). Such highly stratified water columns result from stable thermoclines or drastic salinity differences and eventually create anoxic bottom waters. Stability of the water column can also be influenced by regional weather patterns. An area with particularly fair weather and cold winters develops a thermal stratification that is increasingly difficult to overcome by seasonal mixing cycles (Jones and Manning, 1994). These conditions are not always permanent, especially within epicontinental seas. Longstanding anoxia only remains in the deepest of these basins. Summer dysoxia and anoxia is often broken up by winter re-oxygenation in many depth permitting cases (Jones and Manning, 1994). Examples of poorly mixed water columns leading to the development of anoxia and subsequent eutrophism have also been extensively studied in the modern Black Sea as well as the Mid-Cretaceous Western Interior Basin of North America, and the late Devonian Appalachian Basin (Arthur and Sageman, 2005). These notable accumulations are primarily related to increased primary production through the cyclic influx of nutrient rich waters associated with eustatic sea level rise and localized transgressions followed by a severely stratified water columns (Brumsack, 1989; Arthur and Sageman, 2005; Tyson, 2005). The positive influence of dysoxic to anoxic conditions alone on organic matter

preservation can only be possible at extremely low sedimentation rates (Tyson, 2005). The realistic empirical study of these systems show that suboxic to dysoxic environments tend to improve the preservation of organic matter by a multiple of three to six while dysoxic to anoxic waters in similar settings commonly result in total organic contents >10% (Tyson, 2005).

1.2.1.1 Geochemical Proxies

Ultimately, proxies used in the assessment of mudrock systems should be supported by recognized or inferred relationships between primary geologic processes and the corresponding variation of a geochemical component to the sediment. Proxies with a single or principal controlling factor are both ideal and rare (Mackenzie, 2005). Molybdenum has recently become one of the most empirically tested and useful trace metals found in black shales (Mackenzie, 2005; Algeo and Lyons, 2006; Rowe et al., 2008; Algeo and Tribovillard, 2009; Algeo and Rowe, 2011; Tribovillard et al., 2011). Enrichments of Mn, V, Cr, Ni, Co, U, and Th are also valuable and specific redox proxies (Brumsack, 1989; Magyar, Moor and Sigg, 1993; Morford and Emerson, 1999; Schulz, 2000; Morford et al., 2001; Archer, Morford and Emerson, 2002; Lyons et al, 2003; Mackenzie, 2005; Brumsack, 2006; Algeo and Tribovillard, 2010; Jenkyns, 2010; Algeo and Rowe, 2011; Tribovillard et al., 2011). A broad range of geochemical proxies will be presented along with a brief description of the properties involved. Each of these methods has advantages and limitations related to instrumentation accuracy, chemical interference, or shear practicality. The most reliable, consistent, and research specific proxies were used in the study.

Practically every identified element in the periodic table of elements has been discovered in modern seawater (Eby, 2004; Mackenzie, 2005). Elements found in concentrations <0.05 µmol kg^{-1} are primarily metals known as trace metals (Eby, 2004). These metals are primarily removed from the water column by incorporation into particles or being adsorbed onto a surface. Although, most trace metal concentrations are far below the amount

needed to precipitate out in a solid phase, many precipitate out as stable oxyhydroxides (Eby, 2004; Mackenzie, 2005). More commonly, trace metals are incorporated into clay minerals, particulate organic matter, and shell material (Eby, 2004). This study will focus on those trace elements that are incorporated into clay minerals. Trace metal concentrations in basin derived mudrocks are essentially enriched or depleted through several pre-, post-, and syn-depositional processes. These processes could act exclusively or in concert with others resulting in a complex combination of geochemical signatures. Translations of these signatures tell a significant amount of information about the depositional history of the basin. Particular mechanisms of interest to this study include, but are not limited to, diffusion, fixation, crystallization/incorporation, precipitation, and sedimentation. As one might expect, changes of varying degrees and scales to any or all facets of a basin (i.e. hydrography, stratification, tectonic setting, or sedimentation rate) result in an equally dynamic shift in the chemistry of related lithologic packages. These changes can bring about unique trends that are discernible through modern geochemical analysis.

Familiarity with all factors of a basin in relation to each element or basin property is crucial to our ability to decipher retrieved geochemical data. A major contributing factor to geochemical changes in a basin is a stratified water column immediately overlying the sediment (Jones and Manning, 1994). Enrichment of redox-sensitive trace metals is driven by oxidation-reduction (redox) conditions in the body of water within 1 meter of the sediment-water interface, also known as the bottom-waters (Tyson and Pearson, 1991; Jones and Manning, 1994) The character of these bottom-waters influences the sediment pore water, resulting in preserved mudrocks reflective of oxic, suboxic, dysoxic, anoxic or euxinic (sulfidic) conditions (Eby, 2004; Mackenzie, 2005; Schulz, 2000; Morford and Emerson 1999; McManus et al., 2006; Calvert and Pedersen, 1993; Piper, 1994; Cusius et al., 1996; Tribovillard et al., 2006; Hoelke, 2011). This study will depict several redox-sensitive trace metal enrichment peaks that are generally

indicative of the suboxic (2.0-0 ml O^2L^{-1}) to anoxic (euxinic) transition zone (Tyson and Pearson, 1991; Algeo and Rowe, 2011).

To observe these trends in a normalized manner, baseline concentrations of trace metals in shale must be defined to assess relative enrichments (Tribovillard et al, 2006). In order to remain consistent with earlier work, elemental point of reference is the "average grey shale," defined by Wedepohl (1971, 1991). Proxies used in the present study have been defined in previous work as redox sensitive trace metals, paleoproductivity indicators, and depositional environment proxies. (e.g. David Z., 1994; Crusius et al., 1996; Morford and Emerson, 1999; Rimmer, 2004; Rimmer et al., 2004; McManus et al., 2006; Tribovillard et al., 2006; Algeo and Tribovillard, 2009; Tribovillard et al., 2006; Piper and Calvert, 2009). Jones and Manning (1994) characterize paleo-oxygenation indices into three categories: 1) pyrite involved (C/S, DOP), 2) Uranium Thorium involved (U/Th, authigenic uranium), and 3) Trace Metal involved (V/Cr, Ni/Co, Ni/V, (Cu+Mo)/Zn).

Modern marine sediments beneath oxygenated water columns show covariant percentages of organic carbon (TOC, $\delta^{13}C$) and sulfur (S). As a result, sulfur-to-carbon ratios (S/C) tend to lie on a line of regression through the origin with an average slope of 0.36 in modern marine sediments (Jones and Manning, 1994). Ancient mudstone S/C ratios also show covariance but tended to be considerably higher (2x in study by Raiswell and Berner) than their modern analogs (Raiswell and Berner 1986; Jones and Manning, 1994). Conversely, sediments deposited under euxinic conditions generally reveal high sulfur values at low organic carbon concentrations, thus plotting above the oxygenated sediment line of regression (Berner and Raiswell, 1983; Raiswell and Berner, 1986; Rimmer, 2004). This process, however, is not always an adequate proxy for paleo-oxygenation on its own (Calvert et al, 1991; Jones and Manning, 1994; Rimmer, 2004). Sulfur-to-Carbon ratios are increased due to carbon loss in two distinct post-depositional processes: 1) methanogenesis and decarboxylation driven by

increased burial depth, and 2) hydrocarbon generation and migration (Jones and Manning, 1994). It is much more practical to rely on the generalized assumption that mudstones deposited under oxic conditions will have a line of regression through the origin while anoxic mudstones, especially at low carbon concentrations, will have a positive intercept on the sulfur axis (Jones and Manning, 1994; Rimmer, 2004).

Sulfur can be used in another ratio to help determine the paleo-oxygenation of the depositional environment related to a specific mudrock. The degree of pyritization (DOP) is defined as the percentage of iron bound in pyrite divided by the total amount of iron (Fe_{pyrite}/Fe_{total} or $Fe_{pyrite}/Fe_{pyrite} + Fe_{HCLsoluble}$) (Raiswell and Berner, 1985; Raiswell et al, 1988; Jones and Manning, 1994; Rimmer, 2004). This plot is often used in conjunction with the S/C plot to minimize the confusion caused by the tendency of iron to combine into several assemblages. When reliable sulfur and pyrite percentages are attained, a very precise set of lines can be drawn defining oxic, suboxic, dysoxic, and anoxic depositional conditions. DOP values <0.42 indicate oxic environments while values between 0.46-0.80 denote dysoxic depositional environments. Suboxic and anoxic conditions overlap dysoxic ranges slightly but usually remain between 0.55-0.93 (Jones and Manning, 1994).

The previous methods can be combined with iron measurements to study the paleoceanography of a basin. Organic carbon (TOC) and pyrite sulfur ratios distinguish between normal marine, freshwater, and euxinic environments (Leventhal and Goldhaber, 1977; Berner, 1982; Berner and Raiswell, 1983; Berner, 1984; Strauss and Beukes, 1996; Rimmer, 2004). The limitation of the formation of pyrite in marine sediments can be determined by a ternary diagram of iron, sulfur, and TOC (Dean and Arthur 1989; Calvert and Karlin, 1991; Lyons and Berner, 1992; Rimmer, 2004).

The relationship between uranium and thorium is commonly used to determine detrital influx and paleo-oxygenation (Swanson, 1961; Jones and Manning, 1994; Adams and Weaver,

1958; Rogers and Adams, 1969; Leventhal and Goldhaber, 1977; Leventhal and Finkelman, 1987). Uranium is typically found in one of two forms: 1) U^{6+} is soluble and easily weathered at the surface and 2) U^{4+} is insoluble at the surface and in oxic waters yet easily reducible under anoxic conditions. Detrital fractions of sediment have an enrichment of stable state U^{4+} after sufficient weathering, while oxic water columns tend to be enriched in dissolved U^{6+}. Thus, U_{total} value spikes seen in sediment can represent either a detrital influx into the basin or an episodic anoxic event. This ambiguous result is partially caused by frequent uranium replacement in the clay fraction of mudrocks. Under reducing conditions, U^{4+} is fixed into the sediment while additional U^{6+} is supplied to the rock by diffusion (Jones and Manning, 1994; Klinkhammer and Palmer, 1991). Furthermore, simple observance of the U_{total} curve will not be sufficient evidence for either detrital influx or the paleo-oxidation of the basin. Wignall and Myers (1988) used the properties of U^{4+} and U^{6+} in combination with the covariant nature of potassium and thorium found in aluminosilicate minerals as a detrital indicator (Wignall and Myers, 1988; Jones and Manning, 1994). Thorium, much like U^{4+}, is relatively immobile subaerially and when present in fine-grained sediments. This characteristic usually results in thorium concentration in the detrital fraction associated with heavy minerals and clays (Jones and Manning, 1994). Further discrimination of $U_{authigenic}$ from U_{total} associated with Th would depict both rocks with high amounts of detrital influence as well as episodes of anoxia. The authigenic portion of uranium is calculated as follows:

$$U_{authigenic} = U_{total} - Th/3$$

(Jones and Manning, 1994)

Wignall and Myers (1988) observed that $Th/U_{authigenic}$ ratios averaging $\geq 3.8 \pm 1.1$ were typical in the detrital fraction after weathering (Jones and Manning, 1994). Although this particular value is variable across the wide variety of preserved mudrocks, it is a usable base for initial observance. Hence, attention to the presence of a spike above the 3.8 threshold contains more

significance than the actual value of the spike. A comparison of Th/3 to K, Ti, and Al was explored in order to increase confidence in the obtained results. An acceptable linear regression was seen in all comparisons as well as an agreement of results using each as clay proxies. The chemical properties associated with thorium make it the most reliable proxy for this method. Variability seen in results is believed to be a result of carbonate or phosphate rich lithologies acting as secondary hosts to uranium (Wignall and Myers, 1988; Jones and Manning, 1994).

The most reliable paleo-oxygenation indicators are trace-metal ratios involving V, Cr, Cu, Mo, Ni, and Zn (Vine and Tourtelot, 1970; Jones and Manning, 1994; Morford and Emerson, 1999; Algeo and Maynard, 2004; Rimmer, 2004; Tribovillard et al, 2006; Cruse et al., 2007; Jenkyns, 2010; Tribovillard et al., 2011; Algeo and Rowe, 2012). Molybdenum is widely used to depict basin hydrography, partly because it is the most abundant and measurable transition element in the modern ocean (Algeo and Lyons, 2006; Rowe et al., 2008). This trace metal is extremely stable under oxic conditions in suspension as the molybdate oxyanion (MoO^{2-}_4) but adsorbs into humic substances, Mn-oxyhydroxides, or Fe-sulfides in anoxic environments (Berrang and Grill, 1974; Magyar et al., 1993; Morse and Luther III, 1999; Algeo and Lyons, 2006). Anoxic facies count for ~30 – 50% of the total Mo globally despite only composing ~0.3% of the total seafloor area (Algeo and Lyons, 2006). Molybdenum is a highly reliable proxy for benthic redox potential in sedimentary rocks (Algeo and Lyons, 2006). Algeo and Lyons (2006) performed a study of the Mo-TOC covariance in modern anoxic silled basins of differing aqueous chemistry. These modern analogs ranged from the Black Sea to the Saanich Inlet and included an upwelling zone off the Namibian Shelf. The correlation was based on the depletion of Mo in stagnant basins without the basin reservoir effect (Algeo and Lyons, 2006). The development of a fully stratified water column and basin floor anoxia creates a peak in Mo concentration in weakly sulfidic environments (Algeo and Lyons, 2006). The slope of a best-fit regressional line through data-points of a Mo and Total Organic Carbon (TOC)

cross-plot (Algeo and Lyons, 2006) can be used to determine the occurrence and amount of water-mass restriction and deep-water renewal time (Rowe et al., 2008; Rowe et al., 2009; Hoelke, 2011). This connection can be made because of the spatial and temporal effects of water restriction on the mass chemistry of the water column. Large scale changes in Mo/TOC trends can often be connected to known historical or geological events (Algeo and Lyons, 2006)

V/Cr ratio has been widely used due to the tendency of Cr to substitute for Al within clays while V bonds with organic matter and is concentrated under reducing conditions (Jones and Manning, 1994; Schulz, 2000; Rimmer, 2004; Mackenzie, 2005). This ratio provides a redox proxy normalized to the clay fraction. V/Cr values greater than 2 represent anoxia in the overlying water column when H_2S is present (Ernst, 1970; Jones and Manning, 1994) A ratio less than 2 is indicative of oxidizing conditions, while values near 1 suggest the rocks were deposited near the O_2-H_2S chemocline (Jones and Manning, 1994; Rimmer, 2004). It is noted by Ernst (1970) that grain-size and carbonate content may adversely affect the results (Jones and Manning, 1994).

A less complex, but more reliable, implementation of vanadium and chromium is the enrichment value of their sum. Usage of V+Cr takes advantage of their many valence states and additionally complex chemistries as they are precipitated out of seawater as hydroxides in conditions favorable to denitrification. The resulting enrichment, whether sudden or gradual, marks a reduction in the availability of oxygen in the system. This proxy, along-side Mo enrichment, is commonly used to mark the oxic-anoxic transition in bottom-waters (Mackenzie, 2005).

Ni/V ratios have also been used to assess depositional environments. Both metals are fixed into the sediment in stable tetrapyrrole complexes when the system remains open. These ratios decrease due to thermodynamic properties as the environment becomes more reducing (Jones and Manning, 1994). A solid number delineating the oxic boundaries has not yet been

defined, but the enrichment and depletion trends observed, along with other proxies, can be very telling. As performed with the V/Cr ratio, enrichments observed when plotting the relative presence of Ni to a clay proxy (Cr, Ti, or Al) delineate a reducing environment.

R. O. Hallberg has proposed the use of the ratio:

$$R = (Cu + Mo) / Zn$$

(Hallberg, 1981)

This ratio has proven to be a valuable and reliable oxygenation indicator of bottom waters in modern analogs like the Baltic Sea (Jones and Manning, 1994). This ratio increases under reducing conditions because the precipitation of Cu is favored over Zn in an oxic environment. The amount of Cu may even exceed Zn in sulphide rich zones, due to their respective solubility properties when combined with Sulfur. Mo is added to the ratio to decrease the effects of burial and compaction in mudstones. If the initial oxic environment was made anoxic by mudstone burial and compaction, Cu and Zn totals may be very similar due to reduction by chelation. Mo is only deposited under H_2S bearing waters (Jones and Manning, 1994). Adding this variable eliminates the contribution of post depositional effects on the ratio.

Lastly, several ratios involving stable isotopes of organic carbon ($\delta^{13}C_{org}$) and nitrogen ($\delta^{15}N$) and organic carbon-to-nitrogen (C/N) ratios are widely used in the study of paleoceanography. These isotopes have historically been used to determine the provenance of organic matter in mudrocks as well as the paleo-productivity and -climatology of the related depositional environments (Meyers, 1994; Meyers, 1997; Twichell et al., 2002; Meyers et al., 2006; Meyers et al., 2009A). Adhering to similar theory as trace metal paleo-oxygenation proxies, carbon-to-nitrogen relationships have been used as an oxygenation indicator (Meyers, 1994; Twichell et al., 2002; Meyers et al., 2006). Elevated C/N ratios found in black shales or

basinal mudrocks indicate enhanced organic preservation as a result of bottom-water anoxia (Meyers et al., 2006).

Organic carbon isotope ratios are useful in many ways; some of the most valuable applications include the determination of sedimentary organic matter sources, changes in deep-water production, water-mass age, and atmospheric conditions. The typical marine algae carbon source is dissolved bicarbonate with a $\delta^{13}C_{org}$ value near 0‰ resulting in a $\delta^{13}C_{org}$ value of sediments rich in marine algae between -22 and -20‰ (Meyers, 1994; Meyers et al., 1997; Twichell et al., 2002; Eby, 2004). Methane is highly negative, ranging from -40 to -70‰, while coal and petroleum $\delta^{13}C_{org}$ values typically range from -20 to -30‰ (Eby, 2004). C_3 land plants often discriminate against the heavier $\delta^{13}C_{org}$, creating a negative excursion ranging from -20 to -27‰ (Meyers, 1994; Meyers et al., 1997). Thus, measured excursions in sediment between -22 and -27‰ are indicative of terrestrial C_3 influence. Similarly, negative excursions in the deep basin sediments can often be linked to an increase in biologic activity and its tendency to consume light carbon ($\delta^{13}C_{org}$) (Hohbein et al., 2012). Positive excursions are typically caused by an increased in deep-water age and reductions of biologic activity (Hohbein et al., 2012). Ultimately, secession of any active process causing negative excursions will eventually produce a positive excursion.

This study will use isotopic relationships to link changes in bulk geochemistry to boundaries and known formation horizons representing large scale geologic events (Algeo and Lyons, 2006; Algeo et al., 2007; Algeo and Rowe, 2011). Additionally, this relationship can be paired with trace-metal analyses to indicate zones of anoxia and associated basin hydrography (Algeo and Lyons, 2006; Algeo and Maynard, 2008).

As the true heterogeneous nature of mudrocks becomes increasingly obvious, sequence stratigraphy is emerging as a useful and practical method for the characterization of the related depositional environments and their typical oxygenation levels based on known

relationships to event horizons (Vail et al., 1997; Posamentier and Allen, 1999; Catuneanu et al, 2009; Holbrook and Dunbar, 1992; Slatt, 2002). In some ways, this technique is the most reliable and accurate way to integrate physical, chemical, and biological observations at numerous scales to arrive at one hierarchical description (Bohacs, 1998). Such determination is done by creating chronostratigraphic boundaries through the correlation of stratal horizons representing periods of time and their subsequent genetically related rocks (Campbell, 1967; Bohacs, 1998). It must be noted, that any specific chemical trend or signature is not necessarily indicative of a particular depositional environment. Rather, a detailed correlation of the didactic stories told through sequence stratigraphy and chemostratigraphy will improve the small and large scale determination of these environments. The properties typically associated with mudrocks vary tremendously and are commonly observed at dissimilar scales. Many of these differences are generally produced by differential depositional environments and stratal stacking (Bohacs, 1998). Using multiple disciplines to further constrain these factors is especially important when considering the heterogeneous nature of basin mudrocks. Although cores through a number of black shale formations appear relatively featureless and homogeneous, observations of vast geochemical variations correlate to detailed sequence stratigraphic models. The combination of these two disciplines prove valuable when correlating cores and well logs on a local and regional scale by determining the chronological relationships of depositional and erosional events (Catuneanu et al, 2009; Hoelke, 2011). Additionally, there are innate implications relating to grain size and sediment sources of the sedimentary basin in question.

1.2.2 Previous Geochemical Studies

Because of a prolific history of oil and gas production, the Midland Basin has been studied to a great degree. Unfortunately, the vast majority of geochemical research has only been utilized to depict water and hydrocarbon migration through the use of isotopic analysis (e.g. Kvenvolden and Squires, 1967; Given and Lohmann, 1986; Wigginset al., 1993;

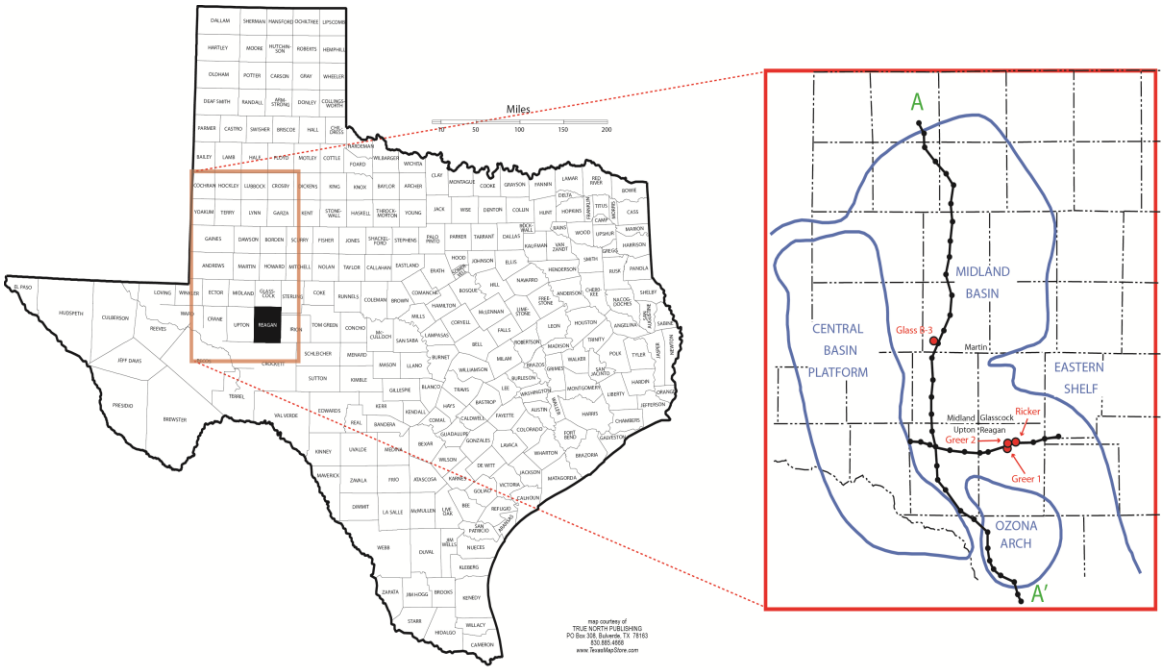

Figure 3. Area of study in relation to Texas counties and Permian Basin major features. Red circles mark wells used for geochemical analysis. Interpreted cross-section A-A' from Figure 6 shown. *Map modified from figure provided by Scott Hamlin, BEG Austin*

Dutkiewicz et al, 2004). Until now, instances of lithology-based geochemical research have been predominantly based on carbonate factories and reservoirs with favorable hydrocarbon production histories (e.g. Krumbein, 1951; Holser and Kaplan, 1966; Comer, 1991; Ulmer-Scholle et al., 1993). It is anticipated that chemostratigraphic research will slowly begin to gain precedent throughout academia and industry in the near future.

1.3 Geological Information

1.3.1 Geographic Setting

The area of study is the approximate depo-center of the Midland Basin through the Late Pennsylvanian and Early Permian periods. **Figure 3** shows relative positioning of the Midland Basin to the Eastern Shelf, Central Basin Platform, and Ozona Arch, as well as the modern location of Texas county lines. The Greer 1, Greer 2, Ricker, and Glass B3 core locations are marked by red dots in Reagan and Martin counties along a cross sectional line including several points along the estimated basin depocenter.

1.3.2 *Structural Geology and Tectonics*

The Permian Basin was a complex asymmetric basin undergoing active subsidence and increased levels of shale, limestone, and arkose deposition in the foreland of the Ouachita Fold-belt from Mississippian to early Permian time (Heckel, 1986; Cys and Gibson, 1988; Mazzullo and Reid, 1989; Hovorka, 1998). Intricate faulting and differential rates of subsidence produced several sub-basins by disseverance and uplift associated with the continental collision of Laurasia and Gondwana to form Pangea in the Late Paleozoic (Hills, 1972; Hills, 1984; Cys and Gibson, 1988). Major features of significance to this study are the Delaware Basin, Central Basin Platform, Midland Basin, Ozona Arch, and Eastern Shelf. **Figure 4** shows an interpretation of the active rifting between the modern North and South American continents with simultaneous eustatic seaway regression from the late Pennsylvanian (300 Ma) to the early Permian (270 Ma) periods. Sedimentary patterns suggest that the north and east parts of the Permian Basin were completely infilled with sediments by early to middle Permian (Leonardian Age) period (Cys and Gibson, 1988). The northern platform strata depict a stable tectonic

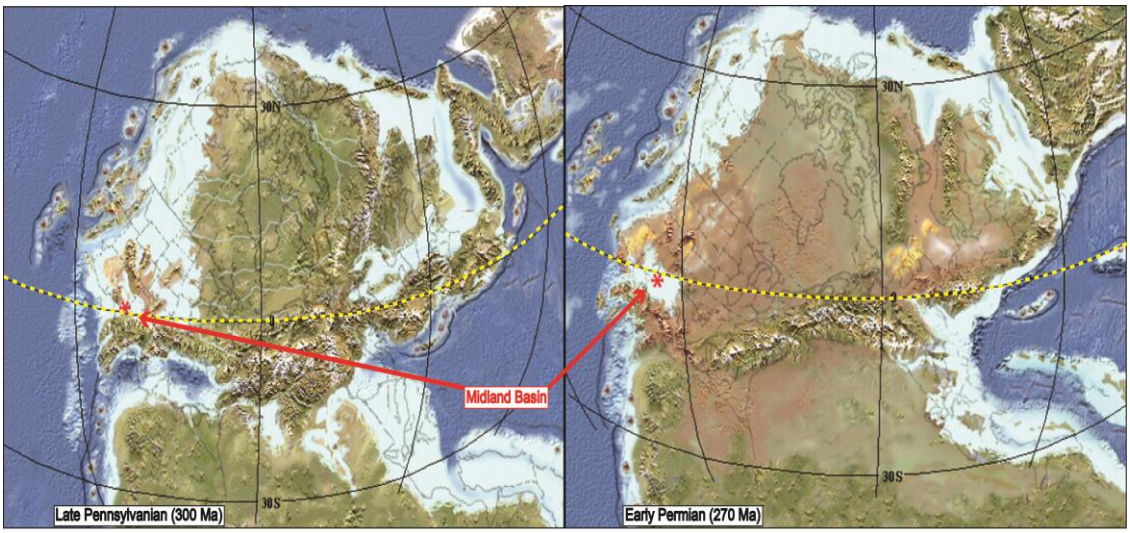

Figure 4. Tectonic setting of the Midland Basin relative to modern U.S. States. Equator marked in yellow. *Figure Modified from Blakey, 2008.*

history through the preservation of relatively complete and undeformed platform deposits, including carbonates, evaporites, and shales (Mazzullo and Reid, 1989). Evidence suggests that major lithologic changes are primarily influenced by glacially induced eustatic sea-level change (Blakey, 2008; Fielding et al., 2008). Such stability in the north is in stark contrast to southern shelf preserved strata due to Lower Permian syn- and post-depositional tectonism (Mazzullo and Reid, 1989). Stratigraphic discontinuity in this field has plagued the oil and gas industry for decades. In many ways, the depositional sequencing and stratigraphy can be related to strata of similar age (e.g. Witchita and Bone Spring formations) in the surrounding sub-basins (**Figure 5**) (Mazzullo and Reid, 1989; Broadhead et al., 2004). For example, coeval strata in the northern Delaware provide a quality analog for the understanding of Wolfcampian facies evolution (Mazzullo and Reid, 1989).

Wolfcampian clastics were deposited as a result of a rapid increase in accommodation from the local subsidence and proximal uplift of the Central Basin Platform along with glacially driven eustatic sea-level changes (Heckel, 1986; Blakey, 2008, Fielding et al., 2008). The development of the Permian and subsequent sub-basins can be broken into three distinct stages. First, a large expanse of time passed as enormous amounts of clastics were deposited into the broad marine Tobosa Basin from the Cambrian until Mississippian time (Alnaji, 2012). Paleo-reconstructions by Blakey (2008) and Scotese (1979) place the area now known as west Texas near the equator at the time of deposition (**Figure 4**). Literature defines the depositional climate related to the Wolfcampian strata of the Midland Basin as humid to sub-humid by to the occurrence and characteristics of a mixed carbonate and siliciclastic system at a paleolatitude near the equator (Walker, 1991; Flamm, 2008). Second, this long period of time was followed by a relatively short period of collision and related orogeny from the Early Pennsylvanian to the Early Permian. During this time, the North American land mass (Laurasia) collided with Gondwana, resulting in the formation of the Hercynian Orogeny and the Ouachita (Alleghanian) – Marathon Fold Belts (Hills, 1972; Flamm, 2008; Alnaji, 2012). This collision was the primary

factor in the differentiation of the Tobosa Basin into a series of horsts and grabens along high-angle reverse faults, ultimately creating several deep basins and shallow shelves (Hills, 1984, Horak, 1985; Hills, 1972; Flamm, 2008; Alnaji, 2012) By the late-Paleozoic, the Tobosa Basin had been divided into two northwest aligned asymmetric basins (Delaware and Midland) by the Central Basin Platform and Diablo Platform (Alnaji, 2012). Carbonate shelves began to develop along the photic zones around the basins, while increased accommodation lead to intense clastic deposition throughout the basins (Hills, 1972; Flamm, 2008). The Paradox Basin of Northern Colorado serves as a quality analog representing slow deposition of black shale and carbonates from the shelf of the Midland Basin (Peterson and Ohlen, 1963; Hills, 1972). Lastly, Mid-to-Late Permian time was relatively stable with regards to tectonics. At this time the basins were filled by terrigenous clastics, while carbonate factories built up on the shelves (Alnaji, 2012).

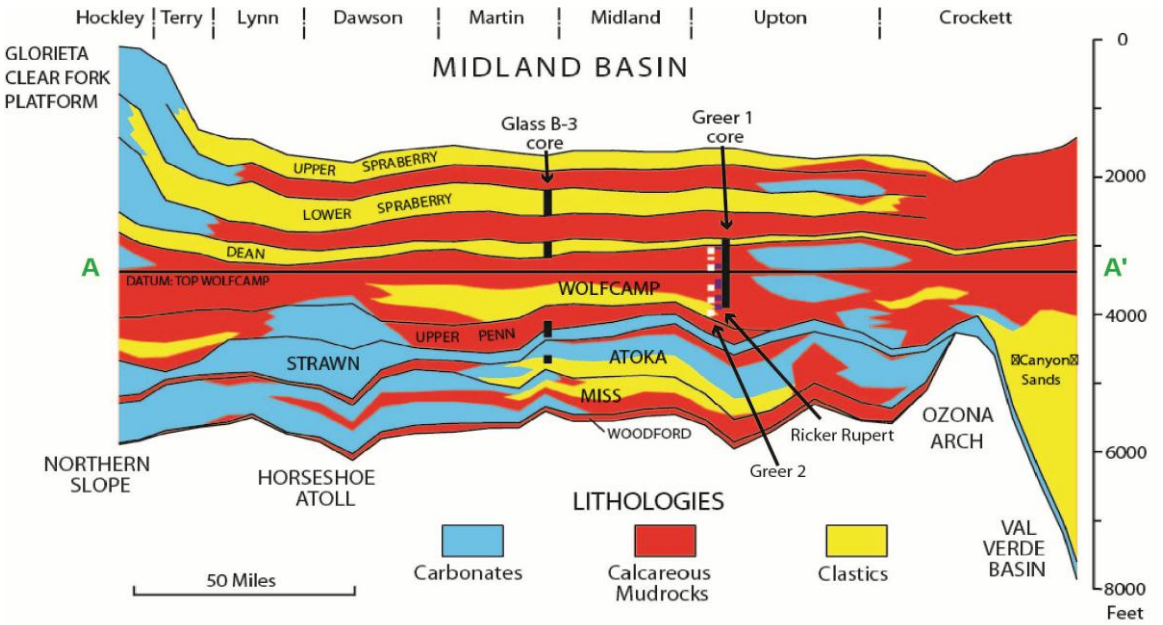

Figure 5. Regional Cross Section A-A' showing stratigraphy, lithology, and relative cored intervals. Greer 1, 2, and Ricker Rupert Cores are into the plane of the graph along cross-section in Figure 4.. This f*igure modified from: Scott Hamlin, B.E.G. Austin*

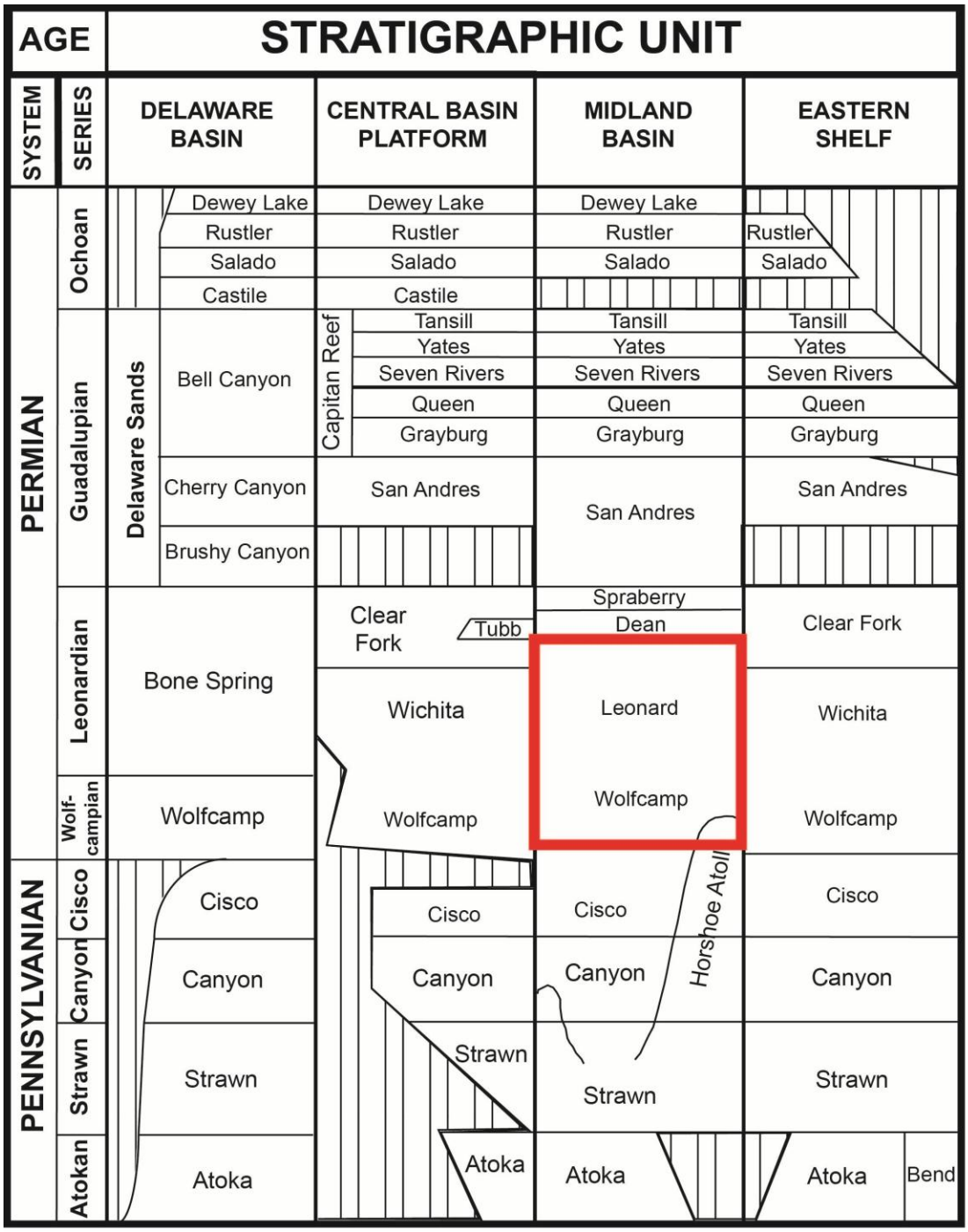

Figure 6. Stratigraphic column depicting coeval strata throughout the Permian Basin. (Mazzullo and Reid, 1989)

1.3.3 *Stratigraphy*

The Wolfcamp has been used throughout academia and industry as the first marker of the Permian System in this region since 1939 (Adams et al, 1939). However, recent conodont dating suggests that the true origin of the lower boundary is in the Upper Pennsylvanian (Gzelian) (Davydov et al., 1995; Ritter, 1995; Chernykh and Ritter, 1997; Flamm, 2008). A cross section and stratigraphic column have been combined in **Figure 5** to show the current accepted classifications of lithologies and nomenclature of rock packages. Similarly, **Figure 6** shows coeval strata of the Permian Basin system.

Likely named after the Wolfcamp Hills of West Texas, and first used by Udden et al. (1916) and Böse (1917), the Wolfcamp formation has been accepted as the lowermost Permian formation of the Glass Mountains and much of the surrounding area since the early 20th century. However, a paper published by Böse in 1917 suggested that previous paleontological studies by Udden and himself were clearly incomplete (Böse, 1917; Flamm, 2008). The upper portion of the Wolfcampian mudstone is commonly referred to as the Lower Leonard (Leonardian Age) by academia and Upper Wolfcamp by industry. The separation of rock packages was first used to describe a slight shift in lithology to a system containing more influence from sand and siltstone (Udden et. al., 1916; Böse, 1917). The Leonardian age rocks were observed to be immediately underlain by the Hess formation and an erosional unconformity that is the upper limit of the Pennsylvanian period in the Glass Mountain region. This unconformity migrates into the Lower Permian are rocks elsewhere. A cross-cutting relationship is observed through the lateral disappearance of the Hess formation, not seen in the Midland Basin (Böse, 1917). The Wolfcamp formation was suggested to be the first series marker of the Permian system in 1939 (Adams et al, 1939). A short lived division of the Wolfcamp occurred in the late 1950's into the Neal Ranch Formation and the overlying Lennox Hills Formation (Ross, 1959). This nomenclature was helpful in outcrop but proved to be inapplicable to subsurface correlations

(Flamm, 2008). Industry and the North American Stratigraphic Code (NASC) have adopted the terms “Wolfcamp” or “Wolfcampian” for the formation and stage names. The International Stratigraphic Code (ISC) nomenclature is Asselian (~285 Ma) and Sakmarian (~275 Ma) for early Permian age rocks and Gzelian (~290 Ma) and Kasimovian (~295 Ma) for Late Pennsylvanian rocks (Flamm, 2008; Alnaji, 2012). NASC terminology will be used in this study for consistency and correlation to previous studies.

Although initial dating and nomenclature was based on the vast array of ammonoid faunas, the Permian rocks of western Texas are well known for having one of the largest and most diversified brachiopod fauna worldwide. In the late 1960’s, nearly 1000 species and more than 200 genera provided an accurate and complete biostratigraphic definition of strata in the Midland Basin (Cooper and Grant, 1969). Permian strata outcrops in the “trans-Pecos” area of west Texas have been generally accepted as the standard for Permian stratal correlation across North America (Cooper and Grant, 1969). However, additional micro-fossil correlation has resulted in a slight migration in the top and base of the Wolfcampian stage over the last 25 years in areas where defining strata are lacking (Flamm, 2008). Fusulinids research in the early 1980’s determined that the Wolfcampian-Leonardian boundary actually lies beneath the Dean Formation (Tubb equivalent) in the Midland Basin (Mazzullo and Reid, 1988; Flamm, 2008). Reminiscent of earlier work by Udden (1916) and Böse (1917), research depicting conodont correlation of time equivalent fossils from the Ural Mountains of Russian to Penn-Perm Kansas conodonts suggest a change in the definition of the Wolfcamp base and subsequent lower one-third section to be upper Pennsylvanian (Ritter, 1995; Chernykh and Ritter, 1997; Flamm, 2008).

1.3.4 *Paleoclimate*

The late Paleozoic climate is referred to as the Late Paleozoic Ice Age (LPIA) (Gastaldo et al., 1996; Fielding et al., 2008). This particular event was characterized as the largest and most extensive of several glacial events during the Paleozoic (Blakey, 2008). Multiple stages of the LPIA gave rise to the most celebrated preservation of cyclic, glacially influenced sedimentary deposits in Phanerozoic history (Blakey, 2008).

Two distinct and profound long-term glacial cycles (**Figure 7**) have been identified from the Carboniferous to Permian periods (Gastaldo et al., 1996). Significance lies in the intense similarities shared between these cycles and late Cenozoic climate change (Gastaldo et al., 1996). Not only does this epoch represent the most recent icehouse event, but it is the only episode in Earth history since the occurrence of such a diversified terrestrial flora in which the climate has completed a full cycle of a long-lived icehouse state (Fielding et al., 2008).

Physical characteristics of the unconformity previously mentioned offer additional insight into the tectonics and paleoclimate of the Permian Basin during deposition. As uplift of the Central Basin Platform ceased, the regional erosional unconformity developed below what is now known as the "Wolfcamp Shale Marker" (Hoak et al., 1998; Flamm, 2008). This marker is used to represent the separation of the Middle and Upper Wolfcamp (Silver and Todd, 1969; Flamm, 2008). Studies have shown that an unconformity of this magnitude would generally be associated with a drop in sea level of 800-1500 ft. (250-450 m) (Mazzullo and Reid, 1988; Flamm, 2008). These events transpired in concurrence with the continental glacial growth in the southern hemisphere associated with the Pennsylvanian and Permian icehouse climate cycles (Flamm, 2008). In comparison to paleoclimate specifications for typical glacial eustatic change, this implied drastic sea level drop far exceeds the accepted 300 ft. (100 m) average fluctuations during icehouse conditions (Flamm, 2008). Mazzullo and Reid (1988) claim that the Wolfcamp shale marker resulted from rapid subsidence while recognizing the possibility of

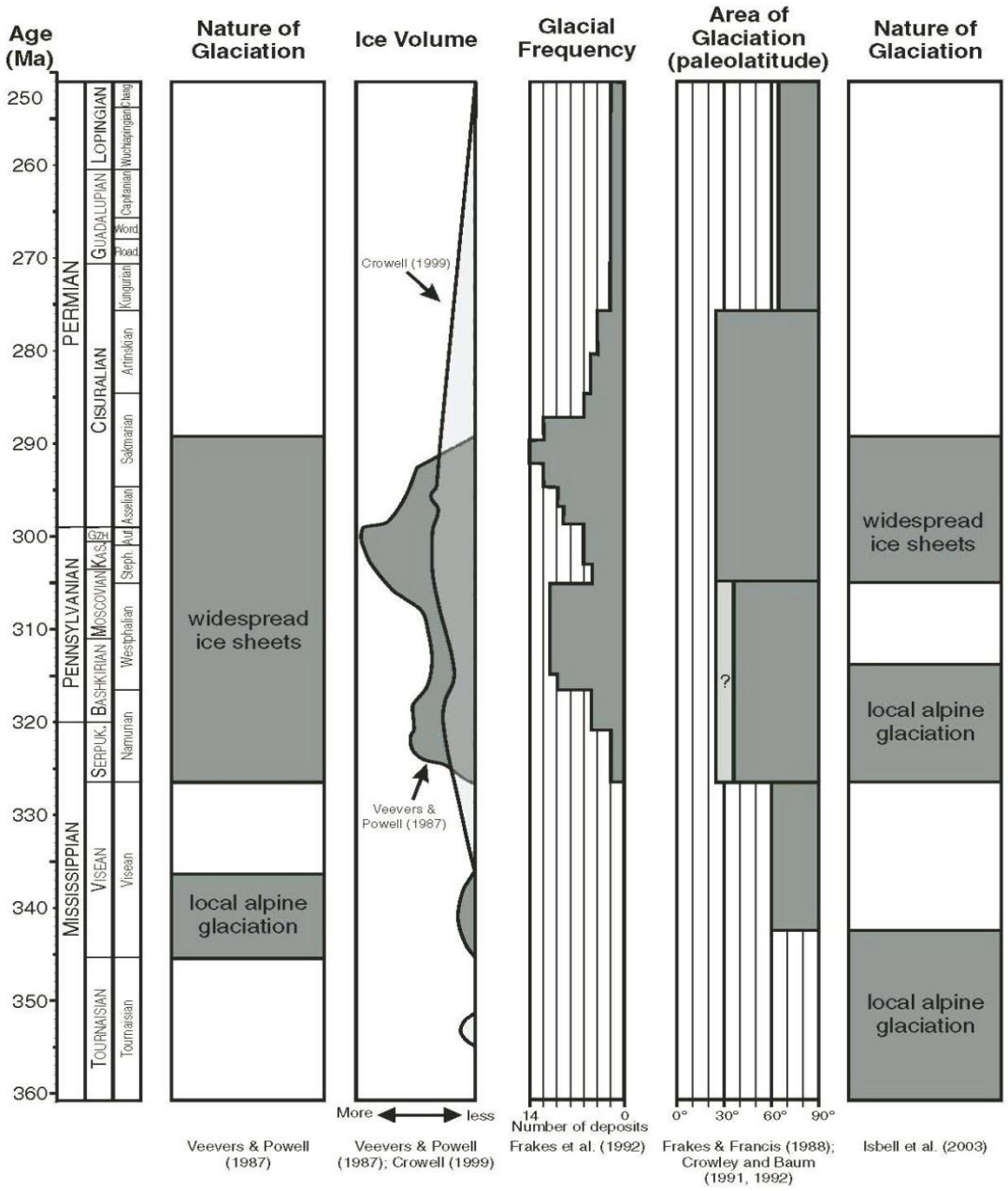

Figure 7. Stratigraphic column depicting Late Paleozoic Ice Age (LPIA) glaciation throughout the Carboniferous and Permian system. (Fielding et al., 2008)

subaerial erosion creating an unconformity on the shelf. It is most likely that a combination of these factors is the true cause of this marker.

1.3.5 *Lithologic Description*

Literature defines the Wolfcamp Formation as being a two-lithology system, dominated by limestone and shale (e.g. Walker et al., 1991; Flamm, 2008). Detailed core descriptions (Baumgardner and Hamlin, 2012) further expound on this rather simplistic look at the complex lithology of the Pennsylvanian – Permian section of the Midland Basin. Four facies have been observed: 1) siliceous mudrock, 2) calcareous mudrock, 3) muddy carbonate-clast conglomerate, and 4) skeletal packstone/grainstone. The following description is based on a core analysis done by Scott Hamlin and Robert Baumgardner, visual and geochemical analysis by myself, and XRD analysis performed by ConocoPhillips on the Greer 1, Greer 2, and Ricker Rupert cores of Reagan County.

Wolfcampian rocks appear to be dominated by dark grey to black non-fissile siliceous mudrock with an average clay content of 40%. Clay type is 95 – 99 percent illite with the remaining clay fraction made up of illite/smectite mix and discrete pulses of chlorite and kaolinite in trace amounts. The remaining 60% bulk mineralogy contains primarily carbonate, quartz, feldspar, pyrite, and apatite. Rocks designated into this lithologic classification contain carbonate composition <20% with an average of 6% bulk weight. These rocks typically have massive structure with discontinuous thin (mm-scale) laminae composed of vertically compacted sand-sized platy bioclasts. Thickness ranges from 3 cm to 4 m with an average thickness of 55 cm. Pyrite is dispersed most commonly as silt-sized framboids making up 4% mean weight and ranging from 0 – 13% bulk weight. Phosphatic nodules up to 35 mm in diameter are exclusively seen throughout the siliceous mudrock facies in local pulses with as many as 11 nodules observed in 3.3 m. Orientation and degrees of soft sediment compaction suggest early formation and 72% overall compaction of the surrounding sediments. These hemipelagic rocks contain higher TOC values than all other facies of the system with percentages ranging from trace amounts to 6.3% and an average of 3.01% (Baumgardner and Hamlin, 2012).

Leonardian rocks are comprised primarily of calcareous mudrocks that bear a remarkable resemblance to the siliceous mudrocks previously described. The overall color reveals a slightly lighter shade of grey to dark brown from the increase in the carbonate fraction. Bulk lithology percentages >20% carbonate were chosen to depict these rocks. The increase of carbonate is typically absorbed by the decrease in total percentages of quartz, feldspar, pyrite, apatite, and clay. These rocks contain less organic carbon, averaging only 2.14% TOC. Also considered hemipelagic sediments, these beds contain higher amounts of bioclasts and clay-sized carbonate with an average bed thickness of 50 cm ranging from 6 cm to 2.7 m. Silt-sized framboidal pyrite is also found throughout this section ranging from 1 – 6% and averaging 3% of the bulk mineralogy (Baumgardner and Hamlin, 2012).

Muddy conglomerates present as debris-flow deposits and represent an increase of carbonate influence into the Wolfcamp Formation. These rocks are predominantly bio- and litho-clasts in a calcareous mudrock matrix with an average of 62% carbonate in the bulk mineralogy. Conglomerates containing mudrock intraclasts (up to 9 cm) and fossiliferous limestone lithoclasts (up to 6 cm) generally contain higher average carbonate content but show great range in their bulk mineralogy (15 – 90% carbonate). Although dispersed framboidal pyrite is less common and smaller throughout this section, aggregate framboids, euhedral crystals, and rosettes are commonly found on and within the larger litho- and bio-clasts. These phases contribute to an average 2% total pyrite ranging from 1 to 4% bulk mineralogy. Although textural grading is not common, soft sediment deformation is often observed. Fusulinids, foraminifera, crinoids, thin-shelled mollusks, brachiopods, sponge spicules, and rugose corals have all been identified in thin section (Baumgardner and Hamlin, 2012).

Skeletal pack/grainstones make up a lithofacies opposite the siliceous mudstones described earlier in this system. These rocks are interpreted as turbidity deposits and typically overlie debris-flow deposits in a seemingly conformable and co-genetic relationship. These rocks contain far less clay (avg. 8%) and TOC (avg. 0.37%). Typically, this facies is observable

as medium to light gray in color and is composed of silt- and very fine sand-sized carbonate grains with medium sand- to pebble-sized bioclasts. Sections commonly contain significant amounts of diagenetic quartz when the total weight percent of quartz exceeds 50%. Skeletal grains ≤6 mm include fusulinids, crinoids, echinoids, thin-shelled mollusks, and rare trilobites. Bed thickness ranges from <1 to 80 cm and average 18 cm with distinct beds containing finely-laminated (<1 mm) layers. These layers allow observation of low-angle cross-sets and sharp erosional contacts depicting partial Bouma sequences. Soft sediment deformation is seen to a greater degree than in the mudrocks but lesser degree than in the conglomerates. Pyrite is present as clusters of euhedral crystals up to 250 µm along bedding planes or in quartz cement. The total range of pyrite composition ranges from 1 to 12% with an average of 2% bulk weight. At maximum concentrations, pyrite fills intragranular pores within fossils as amorphous masses or rhombic crystals in clusters up to 700 µm in diameter (Baumgardner and Hamlin, 2012).

1.4 Research Objectives and Hypothesis

1.4.1 *Research Objectives*

The purpose of the research project is to provide a detailed assessment of the chemostratigraphy and paleoceanography of the Wolfcamp Formation in the Midland Basin of West Texas. Major research objectives within this overarching goal include the following: 1) determination of the mechanism(s) driving change in environmental redox conditions, 2) determination of cyclic relationships between geochemical conditions that reflect changes in paleo-conditions (paleo-climate and –oceanography) during deposition, 3) Provide insight into geochemical variations caused by unique sediment influx conditions occurring during Pennsylvanian – Permian time in the Midland Basin, 4) indicate zones of enhanced organic preservation and accumulation for future oil and gas exploration, and 5) create a sequence stratigraphic model for the entire section.

1.4.2 *Hypothesis*

Initial observations based on large scale sequence stratigraphy and chemo-stratigraphy suggests the following hypotheses regarding the depositional environments and paleoceanography of the Pennsylvanian – Permian section of the Midland formation in West Texas. Chiefly, two differing mechanisms contributed to large scale anoxia-euxinia throughout the vertical section. 1) Discrete pulses of low-stand carbonate influxes created extensive anoxic zones dominated by detrital influence. These zones limited the exposure of organic carbon to oxygen by rapid burial and compaction, thus enhancing organic preservation. Additionally, these episodes provided a coincidental increase in porosity through diagenesis, recrystallization, and dissolution associated with an increase in the carbonate fraction received from the debris/turbidite flows. 2) Episodes characterized by a high degree of water column stratification caused by the cessation of bottom-water currents and limited marginal marine erosional capabilities, thus, drastically reducing sedimentation rates across the basin. Predominant sediment influx at this point slowed while the continual influx of micro-nutrients promoted primary production throughout the basin. The increase in primary production coupled with a highly stratified water column controlled an increase in organic accumulation and preservation. Also, differential deposition of Late Pennsylvanian – Early Permian clastics occurred into a restricted basin setting with tectonically and glacially driven changes in basin hydrography and sediment source. Massive carbonate factories surrounding the basin contributed high degrees of sediment influx and spurred an increase in biologic activity. Vast abundance of rocks representing transitional periods between basin conditions combined with the rare appearance of lithologic end members suggests a dynamic system. Ultimately, the Leonardian and Wolfcampian mudrocks appear to be a hydrocarbon-enriched source and reservoir system with significant opportunity for economic hydrocarbon production.

CHAPTER 2

METHODS

2.1 Core Information

2.1.1. Cores Analyzed

Mechanical properties in relation to fluid flow, wettability, and geochemistry are factors of immense importance in the characterization of an oil or gas play. Intimate knowledge of these properties is best gained through detailed core sampling and analysis. This process allows geologists and engineers the ability to empirically test subsurface material in order to provide evidence indicative of detailed nuances of complex hydrocarbon systems. Past failures in the Midland Basin Spraberry trend have been linked to the deficiency of detailed core-based research on the play. A general lack of historically preserved core is the main culprit responsible for this problem (Montgomery et al., 2000), but is closely followed by poor core maintenance and destructive analytical techniques. Recent initiatives to broaden the database

Table 1. Information for cores used in study housed at the BEG.

Core Name	Operator	County	Location (Lat/Long)	API Number	XRF Unit(s)	
					Majors	Traces
GW Glass B 3	Gulf Oil Corp	Martin	32.1652975 / -102.0929409	42317001300000	UTA-1 UTA-2	X
OL Greer 1	Pan American	Reagan	31.5005152 / -101.5669656	42383101890000	UTA-1 BEG	UTA-2
OL Greer 2	Pan American	Reagan	31.5110470 / -101.5700495	423831057500	UTA-2	BEG
Ricker Rupert	Pan American	Reagan	31.5294462 / -101.5056299	423831051900	UTA-2	BEG

Table 2. Intervals analyzed and sample density by formation and core.

Formation Name	GW Glass B 3		OL Greer 1		OL Greer 2		Ricker Rupert	
	Foot Intervals	Number of Samples	Foot Intervals	Number of Samples	Foot Intervals	Number of Samples	Foot Intervals	Number of Samples
Sprayberry	8373-8744	325						
Dean	9094-9340	214						
Lower Leonard			7700-8087	387	7748-8130	127	7635-7959	50
Wolfcamp			8088-8558	469	8640-9515	143	8310-8995	194
Pensylvanian	10350-10402	35						
Strawn	10434-10549	71						
Atoka	10713-10787	152						

of Midland Basin cores in vertical and horizontal orientations have given rise to a renewed momentum for analytical core-based research. The non-destructive nature of HH-ED- XRF analysis, to be discussed below, fits well into this scheme.

All cores used for geochemical analysis are housed at the Core Research Center Repository of the Texas Bureau of Economic Geology (BEG) in Austin, TX. Tables 1 and 2 describe one core in Martin County and four cores located in Reagan County of West Texas and their related sample analysis. **Figures 3** and **5** show the location and stratigraphic settings of all cores. The present study is heavily biased by results received from the detailed analysis of the OL Greer 1 core due to its impeccable condition and continuity through the section of study. Detailed core descriptions by Robert Baumgardner aided in the interpretation of geochemical results. The OL Greer 2 and Ricker Rupert core results are used to support bulk geochemical trends seen in the OL Greer 1 core. Major elemental concentrations obtained from the GW Glass B 3 core are used as a comparison between the Wolfcamp formation and the surrounding Spraberry, Dean, Pennsylvanian, Strawn, and Atokan mudrocks.

2.2 Hand-Held Energy Dispersive X-Ray Fluorescence (HH-ED-XRF) Analysis

2.2.1. HH-ED-XRF Analysis

Past geochemical and chemostratigraphic studies have relied on Wavelength-Dispersive X-Ray Fluorescence (WD-XRF), Inductively-Coupled Plasma (ICP) Mass

Spectrometry (ICP-MS), Instrumental Neutron Activation Analysis (INAA), or Stationary (bench-top) Energy Dispersive X-Ray Fluorescence (ED-XRF) for quantitative data retrieval (Rowe et. al., 2011). Although reliable, these methods are often destructive, time consuming, and limited to the lab. Primary bulk core-based geochemistry attained in this project was efficiently collected through the use of Hand-Held Energy Dispersive X-Ray Fluorescence (HH-ED-XRF) on cores housed in the Bureau of Economic Geology core repository located in Austin, Texas, using the method outlined by Rowe et al. (2012). Initial results were passed through a matrix-specific calibration which will be further discussed in the mudrock calibration section. This process allows for instant results while protecting the integrity of valuable drill cores. The current calibration has the ability to analyze major elements heavier than sodium and trace elements: Ba, V, Cr, Ni, Cu, Zn, Rb, Sr, Y, Zr, Nb, Mo, Th, and U. This calibration has been used successfully in a number of recent theses (Hoelke, 2011; Hughes, 2011; Mainali, 2011).

Geochemical measurements were taken from the four cores at previously marked locations spaced at approximately one-foot (0.3 m) intervals. A Bruker Tracer III-V HH-ED-XRF spectrometer was used to obtain metal concentrations in each sample. The instrument was supported by a Bruker supplied plastic stabilizing platform accessory and powered by a dedicated power-strip to limit electrical fluctuations. Samples were placed on a stabilizing platform attachment fitted to the nose of the instrument immediately above a 3 by 4 mm elliptical beam window. Sensitivity of the instrument decreases by the inverse square of the distance from this window and its subsequent silicon detector (SiPIN) beneath the window. In order to optimize this distance, a clean flat surface was needed. Much time and effort was spent adhering to this detail in order to increase the consistency and accuracy of the measurements. Whenever possible, the cores were analyzed on the slabbed side after thorough cleaning and drying was performed. In the cases where slabbed core was not available, a Dremel grinding hand tool was used to create a flat surface.

Two phases of data acquisition were undertaken on each marked stratum. Major and trace metals were each sampled for 180 seconds. The site was chosen using a number of criteria. Because we were attempting to assess a 1 ft. interval of core by a 3 by 4 mm scan, a site was chosen that best represents the entire interval. Major lithoclasts were avoided while sharp changes in lithology were often straddled. Obviously, this procedure is limited by our visual capability but has proven to be quite reliable.

Elements that emit characteristic K-shell x-rays between 1.25 – 7.06 kV are considered low-energy spectrum or major elements. A vacuum pump filter provided by Bruker was used in major elemental acquisition due to the filtering properties of air between the silicon detector (SiPIN) and the sample window. A maximum tolerance of 2 µTorr was allowed but 0 µTorr was usually observed. This study used a total of 3 different instruments (named: BEG, UTA-1, and UTA-2) with slight variations in actual output due to variability associated with the manufacture of the x-ray tube and electronics.

High-energy, trace elemental, settings were optimized to study elements that emit unique x-ray signatures between 6.92 and 19.80 kV. The instruments were set to emit rhodium x-rays at 40 kV and 28 µA for this analysis with the same individual instrumental variability mentioned before. This procedure required a Cu-Ti-Al filter, placed between the detector and the sample window to attenuate low-energy x-rays from interfering with the targeted high-energy x-ray spectra.

Table 3. Lowest Detectable Measurements for XRF Instruments

Element	Accepted Value[a]	Instrument 1 (UTA-1) Measured Value[b]	σ (n=7)[b]	LDM[c]	Instrument 2 (1st UTA-2) Measured Value[b]	σ (n=7)[b]	LDM[c]
Mg (%)	0.67	0.80	0.09	0.17	0.85	0.14	0.28
Al (%)	4.96	5.39	0.14	0.28	5.32	0.11	0.22
Si (%)	32.6	33.7	0.2	0.5	33.1	0.4	0.8
P (%)	0.07	0.05	0.03	0.07	0.09	0.03	0.06
S (%)	3.34	2.18	0.10	0.20	2.27	0.09	0.18
K (%)	2.07	2.31	0.09	0.18	2.22	0.07	0.14
Ca (%)	0.13	0.23	0.03	0.06	0.24	0.02	0.04
Ti (%)	0.23	0.27	0.02	0.04	0.27	0.02	0.03
Mn (%)	0.015	0.012	0.001	0.002	0.013	0.001	0.003
Fe (%)	2.93	2.55	0.06	0.12	2.52	0.06	0.13
Ba (ppm)	2090	1884	376	753	1706	300	600
V (ppm)	928	1114	68	137	1110	80	159
Cr (ppm)	110	98	13	26	106	14	27
Ni (ppm)	130	153	26	52	150	20	40
Cu (ppm)	83	147	20	40	87	12	23
Zn (ppm)	823	844	96	191	880	74	147
Th (ppm)	8.4	9	1	2	9	1	2
Rb (ppm)	122	123	12	25	131	12	25
U (ppm)	18.1	17	6	11	22	4	8
Sr (ppm)	75.5	87	5	10	93	9	18
Y (ppm)	35.4	34	3	5	36	2	4
Zr (ppm)	80.3	95	7	13	96	6	13
Nb (ppm)	9	9	1	2	9	1	2
Mo (ppm)	79	83	4	9	82	3	6

A - Values for major elements from lithium borate-fused disc analysis by WD-XRF at SGS; values for trace elements (ppm) from sodium borate fusion dissolution and analysis by ICP-MS.

B - Average HH-ED-XRF measured values (n = 7) and standard deviations (s) for reference material RTC-W-260, a black shale from the Devonian Woodford Formation of West Texas.

C - Limit of Determination of a Method (LDM) calculated according to Rousseau

2.2.2. Mudrock Calibration

Raw datum collected at both high and low energy settings were passed through a matrix-specific calibration that resulted in quantitative percentages and estimated parts per million (ppm) elemental concentrations at each measured stratum. The calibration was developed over several years by the use of five commercially available standards and eighty-five in-house materials (Rowe et. al., 2012). These materials are: five international shale standards, seven from the Devonian-Mississippian Ohio Shale, twenty from the Pennsylvanian Smithwick Formation of Central Texas, twenty-seven from Devonian Mississippian Woodford formation from West Texas, fifteen from the Late Cretaceous Eagle Ford formation of South Texas, and sixteen from the Mississippian Barnett Formation of North Central Texas. The eighty-five in-house materials were taken from clean flat drill cores. Each of these ninety reference material was pressed in a Carver press to forty tons with a forty millimeter die using a boric acid backing. A TM Engineering pulverizer with trace metal grade stainless steel pulverizing cups and pucks was used to pulverize each in-house reference into a 200 mesh powder. Eight grams of powdered reference was attained from each reference material and analyzed for major and trace elements using wavelength-dispersive x-ray fluorescence (WD-XRF and inductively-coupled plasma mass spectrometry (ICP-MS), respectively.

The completed calibration process yields quantified relative percentages in low-energy metals heavier than sodium and total quantity (ppm) of high-energy trace metals from raw HH-ED-XRF spectra of unknown samples. The low energy calibration quantifies the following elements: Mg, Al, Si, P, S, K, Ca, Ba, Ti, V, Cr, Mn, and Fe. The high energy calibration quantifies the following elements: Ni, Cu, Zn, Th, Rb, U, Sr, Y, Zr, Nb, and Mo. The limits of determination of a method (LDM) for each element in relation to two instruments are provided in Table YY (Rousseau, 2001). More details about the calibration process as well as the

processing of raw spectra from unknowns through a calibration spreadsheet are described further in Rowe et al., 2011.

2.3 Additional Geochemical Analysis

2.3.1. Sample Preparation

Powder samples for Total Inorganic Carbon (TIC) and stable isotopes of Carbon ($\delta^{13}C$, TOC) and Nitrogen ($\delta^{15}N$, TN) were drilled using a standard hand-held drill with a hardened carbide tipped masonry drill bit. The sample site was chosen to best mimic the HH-ED-XRF scan site. Slabbed core was cleaned and sampled on the exact opposite side of the core immediately corresponding to the scan site. In the occurrence of extremely fissile or damaged sample sites care was taken to select an analogous powder sample to the previously scanned site.

2.3.2. Total Inorganic Carbon (TIC)

Samples from the GW Glass B 3, and OL Greer 1 cores were analyzed for their total inorganic carbon (TIC) content using a UIC, Inc. coulometer equipped with a CM5230 acidification module with average unknown standard deviations of less than 0.5 percent (Engleman et al 1985). Samples were weighed out between 3.000 to 5.000 mg. For TIC analysis, weighed samples are acidified at 70°C with ten percent (10%) phosphoric acid (H_3PO_4).

2.3.3. Total Organic Carbon (TOC) and Organic Carbon Isotopes ($\delta^{13}C_{org}$)

Analysis of total organic carbon (TOC), total nitrogen (TN), and stable isotopic compositions of TOC ($\delta^{13}C_{org}$) and TN ($\delta^{15}N$) was performed on powdered samples that were weighed into silver capsules (Costech Analytical, Inc. #41067) and acidified with six percent (6%) sulfurous acid (H_2SO_3) until complete elimination of carbonate phases (Verardo et al., 1990). These samples were analyzed at the University of Texas at Arlington using a Costech 4010 elemental analyzer interfaced with a Thermo Finnigan Conflo IV device to a Thermo

Finnigan Delta-V isotopic ratio mass spectrometer (IRMS). Isotopic results are reported in per mil (‰) relative to V-PDB for $\delta^{13}C_{org}$ and air for $\delta^{15}N$. The average standard deviations were 0.11‰ and 0.07‰ for $\delta^{13}C_{org}$ and $\delta^{15}N$ of USGS-40 glutamic acid (IAEA-8573), respectively, and 1.07% and 0.08% for the TOC and TN of USGS-40, respectively, and 0.13 for C/N. The average standard deviations for unknown samples analyzed in triplicate were 0.10‰ for $\delta^{13}C$, 0.12‰ $\delta^{15}N$, 0.02% for TOC, 0.01% for TN, and 0.18 for C/N.

CHAPTER 3

RESULTS

3.1 General Data

The detailed core description, mentioned earlier, by B.E.G. staff provided general constraints and parameters in which much of the study was based. Also, prior observations and trends perceived in analogous mudrock systems were taken into consideration. Modern analogs like the Black Sea, Papua New Guinea, and the Cariaco Basin served as quality referents for and bottom-water euxinia, pore-water dynamics, and basin hydrographics, respectively.

Results for the geochemical analysis were observed at several scales. Cross-plots consisting of all cores and formations are presented to show broad, basin scale changes in bulk geochemistry. Additionally, individual wells and formations are compared for observance of small scale environmental changes through time.

3.1.1. XRF Data

Graphs of X-ray fluorescence data described in the previous sections will be presented in weight percent (e.g. % Si), parts per million (e.g. ppm Mo), whole number ratios (e.g. Fe/Ti), or as an enrichment factor expressed by the following equation:

$$EF = (\text{element in ppm/Al in ppm})_{\text{sample}} / (\text{element in ppm/Al in ppm})_{\text{standard}}$$

All cross plots present the data in their respective units of measurement. Bulk geochemistry was observed for each zone of interest as well as for the overall system to discern trends at

multiple scales. Samples with negative values were retained in order to note overall trends and relative interactions between elements.

3.1.2. XRD Data

X-Ray diffraction results will be shown in weight percent (e.g. % Illite) versus depth. Plots showing bulk lithology will be presented versus depth with corresponding percentages represented by graphic comparison.

3.1.3. TIC Data

Total inorganic carbon (TIC) percentages will be shown in weight present (e.g. % TIC) in cross-plots and verses depth. After observing geochemical, XRD, and well-log relationships, these data suggest that the vast majority of TIC measured is found in the carbonate fraction.

3.1.4. $\delta^{13}C_{org}$ and *TOC Data*

Measurements of $\delta^{13}C_{org}$ are presented as per mil (‰) excursions while total organic carbon (TOC) depicts enrichment normalized by total weight percent (e.g. % TOC).

3.1.5 Chemostratigraphic Data

Chemostratigraphic data for the OL Greer 1 core is plotted verses depth in four figures. One figure depicts major elemental data used in the observance of bulk mineralogy and sediment provenance of the mudrock. The second figure shows trace elemental enrichment factors (EF) used to determine redox conditions of the depositional environment over time. The third figure presents non-XRF data including isotopic enrichments, TIC, and TOC plotted versus depth. The last figure depicts XRD results along-side an integrated bulk lithology interpretation plotted versus depth.

3.2 Integrated Data

3.2.1. Calcite-Clay-Quartz Ternary Diagram

Ternary plots represent the use of normalized data to utilize a simplified three phase lithologic system. The major constituents in average grey shale, defined by Wedepohl (1971,

1991), are compared to the Wolfcamp formation through the application of calcium oxide (CaO), alumina (Al_2O_3), and silica (SiO_2).

3.2.2. Cross-Plot Diagrams

Cross plots of major and trace elements versus aluminum or titanium are used to represent the presence of each element in clay or non-clay mineral phases. Instrumental limitations in the resolution of aluminum created distinct zones of negative weight percent Al. To avoid complications and illogical results, titanium or chromium was commonly used as the clay proxy normalization factor. Established covariance between the elements iron, potassium, calcium, and silica to titanium provide sufficient linkage to the detrital fraction in the Midland Basin. Several other relationships will be discussed as they are presented.

3.3 Results by Core

3.3.1 All Cores

Cross-plots portraying all samples from all wells show strong linear correlations between potassium and titanium (K/Ti), potassium and aluminum (K/Al), and titanium and aluminum (Ti/Al) (**Figures 17 and 18**). Comparisons between iron versus aluminum and titanium (Fe/Al, Fe/Ti) (**Figure 17**) depict two distinct relationships. The Glass B3 core shows a line of regression representing iron composition to be 0.4 – 0.8 percentage units lower than in the Greer 1, Greer 2, and Ricker Rupert cores. A plot of iron versus silicon (Fe/Si) (**Figure 17**) depicts a trend in the Glass B3 core opposite the trend seen in the Greer 1, Greer 2, and Ricker Rupert cores. Similarly, a Calcite-Clay-Quartz ternary diagram (**Figure 15**) reveals that Glass B3 samples concentrate along the silica dilution line from the defined average grey shale while Greer 1, Greer 2, and Ricker Rupert samples trend ninety degrees away, along the carbonate dilution line.

3.3.2 Glass B3 Core

Although **Figure 19** shows the titanium versus aluminum (Ti/Al) trend to be linear in the Glass B3 core, negative aluminum values are concentrated in samples taken from the

Penn/Strawn and Atokan Formations. Data-points off of the linear trend created by silicon-aluminum and silicon-titanium cross-plots (**Figure 21**) concentrate in the Spraberry Formation. Similarly, the conflicting trend observed in the iron-silicon cross-plot (**Figure 22**) is strongly influenced by samples located in the Spraberry and Dean intervals. Iron-titanium and iron-aluminum cross-plots (**Figures 22 and 23** respectively) show a moderately linear trend with frequent occurrences of samples with increased iron concentration in the Spraberry and Dean Formations. Cross-plots comparing calcium (Ca), manganese (Mn), iron (Fe) and magnesium (Mg) to Total Inorganic Carbon (TIC) (**Figure 24**) show very little correlation with much higher TIC values (6 – 11 percent) concentrated in the Penn/Strawn and Atokan samples.

The Spraberry interval contains the highest average total organic carbon (TOC) (1.40%), ranging from 0.07 to 5.6% (**Figure 25**). The Dean interval averages 1.02% TOC and ranges from 0.34 to 1.4 (**Figure 25**). The Pennsylvanian, Strawn, and Atokan intervals average 0.89% TOC and range from 0.09 to 5.62% (**Figure 26**). The average TOC content of the entire core is 1.15%. Spikes in TOC and TIC composition seem to be in distinct pulses rarely thicker than 40 ft. in the Spraberry and Dean intervals, while the Penn/Strawn and Atokan sections show extensive intervals containing 10 – 12 percent TIC. $\delta^{13}C_{org}$ values remain between -27 – -29‰ through the Spraberry and Dean Formations while the Penn/Strawn and Atokan intervals show episodes of drastic negative excursions reaching -30‰ in some strata. $\delta^{13}C_{org}$ positive excursions generally covary with TIC content in the Spraberry and Dean intervals. Covariance between the negative excursions and TIC values are predominant in the Penn/Strawn, and Atokan intervals.

3.3.3 Greer 1, Greer 2, and Ricker Rupert Cores

The Greer 1, Greer 2, and Ricker Rupert cores show many similarities due to their close proximity and stratigraphic correlation. Titanium-aluminum plots (**Figures 29 and 35**) show strong linear trends. Silicon-titanium (**Figure 30, 36, and 39**) and silicon-aluminum (**Figure 29 and 35**) cross-plots exhibit linear trends with significant silicon “pull-off.” Potassium-aluminum

trends (**Figure 29, 35, and 38**) also show similarities, while further inspection into the Greer 1 core revealed that samples containing exceptionally high K/Al values were concentrated into two distinct intervals (7700-7850 and 8250-8350 ft.) (**Figure 29**), while potassium-titanium trends showed very little linear deviation (**Figures 30, 35, and 38**). Iron-aluminum and iron-titanium cross-plots show a strong linear trend with significant iron "pull-off" (**Figures 30, 36, and 38**). Iron-silicon cross-plots (**Figures 30 and 36**) reveal an increasing degree of scatter with increasing values. Calcite-Clay-Quartz ternary diagrams (**Figures 8, 34, and 38**) indicate a trend along the carbonate dilution line with significant influence, although to a lesser degree, from silica dilution. Further assessment of the Greer 1 core revealed the concentration of lithologic end-members into the defined zones shown in **Figure 11** and described in the discussion.

TOC measurements taken from samples in the Greer 1 core reveal an average organic content of 2.89% ranging from 0.06 to 6.42% (**Figure 11**). The Leonardian interval contains an average of 3.15% TOC, ranging from 0.27 to 6.13%. The Wolfcamp interval contains an average of 2.7% TOC, ranging from 0.6 to 6.42%. $\delta^{13}C_{org}$ values range from -25 – -29‰ with four significant thick (200 – 300 ft.) shifts noted on **Figure 10**, as well as several smaller (<20 ft.) shifts.

XRD analysis (**Figure 13**) supported many bulk lithological implications inferred by XRF relationships. The Greer 1 core showed predominantly illite as the clay type with discrete traces of mixed illite/smectite. Small dolomite spikes (20 – 40%) are measured in the Leonardian section, while large spikes (40 – 80%) are recorded in two intervals within the Wolfcampian interval. The presence of pyrite seems to be ubiquitous. Quartz, plagioclase and potassium feldspar dominate non-clay or –carbonate phase bulk lithology with an average weight percent of 32, 7, and 3 respectively.

Enrichments of silicon, potassium, and iron (**Figure 12**) are observed in the Wolfcamp Formation between 8200 – 8380 ft. while significant zones of calcium enrichment are located

from 7710 – 8085 ft. and 8380 – 8560 ft. Total aluminum composition remains fairly constant. EF plots reveal several distinct zones of elemental enrichment. Strata between 8100 and 8200 ft. show an increase in vanadium (V), chromium (Cr), manganese (Mn), iron (Fe), copper (Cu), zinc (Zn), and uranium (U). Relative depletion of these same elements with the addition of molybdenum (Mo) is seen at 7945 ft. Uranium, zinc, and vanadium appear to be highly variable throughout the Leonardian section but fairly constant through the Wolfcampian interval (**Figure 12**).

A great deal of cyclicity is seen between 7800 – 8460 ft. in the XRD, TOC and TIC data (**Figures 11 and 13**). The cycles are typically 10 – 20 ft. thick and involve converse relationships between the carbonate and clay fractions. Although this system is dominated by clay and carbonate, quartz, potassium feldspar, plagioclase, dolomite, and pyrite also make up a substantial portion of the bulk lithology.

CHAPTER 4

DISCUSSION

4.1 Bulk Geochemistry

The bulk geochemistry of cores through the Wolfcamp Formation is useful in the identification of changes in the general mineralogy throughout the system. Cross-plots of major elements versus aluminum or titanium help to determine mineral phases in which the element is present. Similarly, a cross-plot of total inorganic carbon (TIC) versus percent calcium (%Ca) suggests the mineral phase in which calcium is predominantly present. Cross-plots of total organic carbon (TOC) versus copper, nickel, and zinc can determine whether these minerals are found primarily in mineral or non-mineral phase (i.e. organic matter). Co-variation (or lack thereof) in major elements, like silica and aluminum, also provides insight into the basic lithological character of rocks. Similarly, the presence or absence of redox-sensitive trace metals is highly indicative of changes in bottom-water redox conditions throughout the evolution of the basin.

4.1.1. Major Elements

Major elements, such as aluminum, potassium, and titanium, are reliable clay-type indicators. Distinct ratios of these elements typically show strong linearity when bound primarily in clay mineral phases such as illite or mixed illite/smectite. As such, strong linear trends in K/Al, Ti/Al, and K/Ti cross-plots, as well as XRD results, convey a dominant illite clay-type throughout the Pennsylvanian-Permian section of the Midland Basin (**Figures 13, 29, and 30**). XRD results relate strata showing potassium enrichment to intervals containing 4 – 6%

potassium feldspar. This indicates a shift in detrital sediment source at two distinct intervals (8400 and 7800 ft.).

Although silicon exhibits a strong linear trend with aluminum and titanium (**Figures 29 and 30**), considerable enrichment occurs in relation to the clay proxies. This "pull-off" is indicative of silicon present in a mineral phase other than clay. It is not clear whether the source is this excess silica is biogenic or detrital. The most realistic conclusion would be that it is a combination of both. The large expanse of time involved in the deposition of these rocks presents opportunity for considerable microfossil (sponge spicules and radiolarian) and sand (aeolian or shelf) accumulation leading to eventual lithification into chert or quartz.

Due to a diverse reactive nature, iron is found in many phases. Like silicon, a strong linear relationship is observed in cross-plots of iron versus aluminum and titanium (**Figure 30**), with significant "pull-off." This relationship indicates that iron is predominantly found in the clay fraction while substantial enrichments suggest presence in alternate mineral phases. XRD (**Figure 13**) and visual core analysis find considerable amounts of iron to be bound in pyrite (framboidal, euhedral, and rosettes).

Strong linear trend between total inorganic carbon (TIC) and calcium (**Figure 31**) provides a reliable geochemical proxy for carbonates. Little deviation from this line suggests that the vast majority of calcium is bound in carbonate phases. It is believed that data-points below the Ca/TIC trend line are a result of instrumental or sampling errors during analysis. TIC shows little to no trend in cross-plots of manganese and magnesium, suggesting little to no presence of these elements in the carbonate fraction. Similarly, iron shows depletion with TIC enrichment suggesting the lack of presence as iron carbonate (siderite).

4.1.2. Trace Elements and TOC

Moderate linear trend between trace elements like copper (Cu), nickel (Ni), and zinc (Zn), (**Figure 28**) suggests their association with TOC as environmental micronutrients.

Although the relationship is weak, it appears that nickel is more closely related to organic preservation than zinc.

4.1.3. Calcite-Clay-Quartz Ternary Diagrams

Ternary diagrams for all four cores were plotted to determine the composition of each formation in relation to average marine grey shale (**Figure 15**). Similarities between the Greer 1, Greer 2, and Ricker Rupert cores were extensive due to the proximity of the cores. The Glass core allows for a larger scale view of basin evolution.

Although the Spraberry and Dean Formations prove to be closer analogs to Wolfcamp mudrocks, several distinct differences are seen in their ternary diagrams (**Figures 8, 9, and 15**).

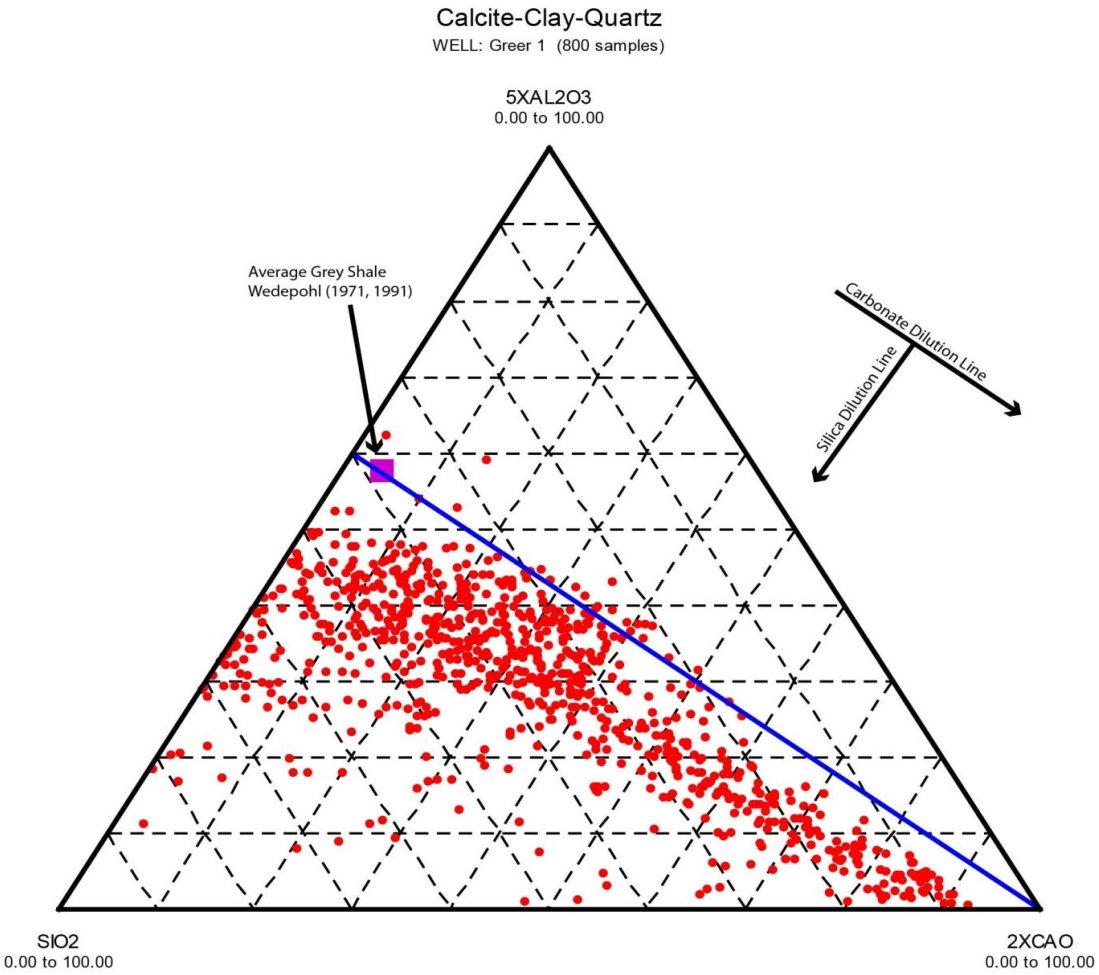

Figure 8. Calcite-Clay-Quartz ternary diagram for the Greer 1 core. Average grey shale marked by the purple square.

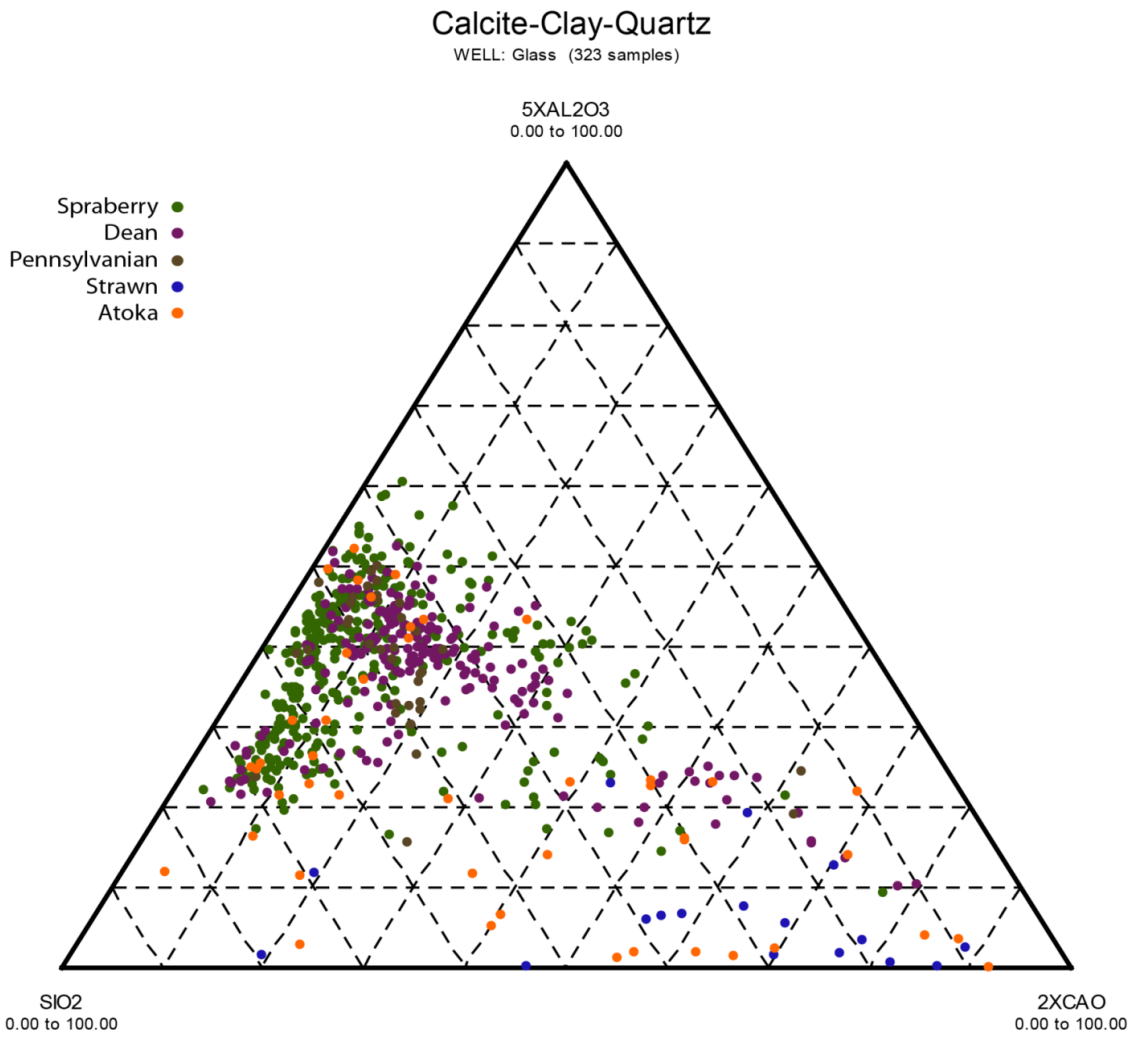

Figure 9. Calcite-Clay-Quartz ternary diagram for the Glass core. Formations are depicted by color.

The most glaring variance is based on the observation that Wolfcamp samples lie along the carbonate dilution line, while Glass samples (especially Spraberry and Dean) plot along the silica dilution line ninety degrees clockwise (**Figures 8 and 9**). Strawn and Atokan strata plot along the carbonate dilution line but are vastly more enriched in silica than Wolfcamp samples. The succession of these stratal and lithologic differences gives insight into the overall sediment source changes of the Midland Basin during the time of deposition.

As the oldest strata analyzed in this study, Atokan and Strawn clastics plot as nearly pure sandstones and argillaceous limestone. These rocks infer the shallow nature of the early Midland Basin and intense terrigenous and shelfal contribution to the system. The lithology gradually changes in the Pennsylvania Formation as clay is introduced into the system. This shift could be indicative of basin deepening and the resultant sediment source shift to clay and silica (biogenic and/or terrigenous). The Wolfcamp Formation provides evidence of a clay and carbonate dominated basin with significant terrigenous influx. This trend is suggestive of basin deepening and increased accommodation, resulting in shelfal carbonate erosion into the basin via debris flows and turbidites. Finally, the Dean and Spraberry Formations provide evidence for continued deepening by returning to another two-lithology dominated system, this time devoid of carbonate influence and a shift to a more arid climate.

4.1.4. Stable Isotopes of Organic Carbon ($\delta^{13}C_{org}$)

Although useful, it is quite difficult to interpret a direct causal relationship between environmental influences and excursions seen in $\delta^{13}C_{org}$ values. Ideally, several other isotope values (e.g. $\delta^{15}N$, $\delta^{18}O$, $\delta^{87}Sr$ . . .) should be used in concert to proclaim, with much certainty, that a particular change was the result of a few variables. Because environmental influences on stable carbon isotopes of organic matter span such a broad degree of realms, this study will make the general assumption that the principal factor driving negative $\delta^{13}C_{org}$ excursions is an increase in primary production. This assumption is supported by the covariant relationships seen in preserved TOC and micronutrient influx (Fe, Zn, and Ni) in zones of $\delta^{13}C_{org}$ negative excursion. Conversely, we will assume that positive excursions will be primarily triggered by drastic decreases biologic activity, thus causing a subsequent reduction in primary production. Secondarily, increased influx of C_3 land plants during periods of high detrital infiltration will be assumed to also have negative influence on $\delta^{13}C_{org}$ values, although to a lesser degree. Increases in water age can sometimes have a significant influence on $\delta^{13}C_{org}$ values. It is

assumed that the dynamic nature of this system minimized the influence of aging water columns on $\delta^{13}C_{org}$ values.

The large scale negative excursion, marked by a blue arrow in **Figure 10,** suggests an increase in the amount of primary production and influx of terrestrial C_3 plants as the basin evolved. Four smaller shifts in $\delta^{13}C_{org}$ values marked by red lines, ranging 150 – 300 feet of thickness, coincide with zones of varying oxygenation to be described in the following sections. Negative excursions at this scale are likely caused by cyclic pulses of increased biologic productivity and with an additional small degree of influence from an increase in water-mass aging gradients (Hohbein et al., 2012). The cyclic nature of this section is also exhibited at the Wolfcampian-Leonardian boundary by the sudden increase in glacial frequency and ice volume seen in **Figures 7 and 10**. The drastic eustatic sea-level drop created increased basin restriction and thus decreased deep water renewal time. It is difficult to resolve the negative excursion seen in the uppermost strata of the study. It may be caused by water column stagnation from extensive high-stand conditions, a drastic increase in deep-water primary production, or an influx of terrestrial (C_3) sediment. Samples from younger strata must be observed in order to place this excursion in a larger context. Lastly, small scale $\delta^{13}C_{org}$ excursions (10 – 40 ft.; marked by the green box in **Figure 10**) reveal brief episodes of intense heavy carbon excursions. These intervals are indicative of third-order cyclicity created by periodic water stagnation and depleted primary production following biologic explosions and subsequent increased primary production created by nutrient influx. This phenomenon is observed by the appearance of drastic increases in deep-water production (negative $\delta^{13}C_{org}$ excursions) directly following sudden enrichments in micronutrients like Fe, Zn, Cu, and Ni (**Figure 12**). It is believed that the zone marked by the yellow box in **Figure 12** (8100 – 8190 ft.) represents an influx of these micronutrients and ultimately resulted in the significant positive $\delta^{13}C_{org}$ shift marked by the green box in **Figure 10** after a brief lag period.

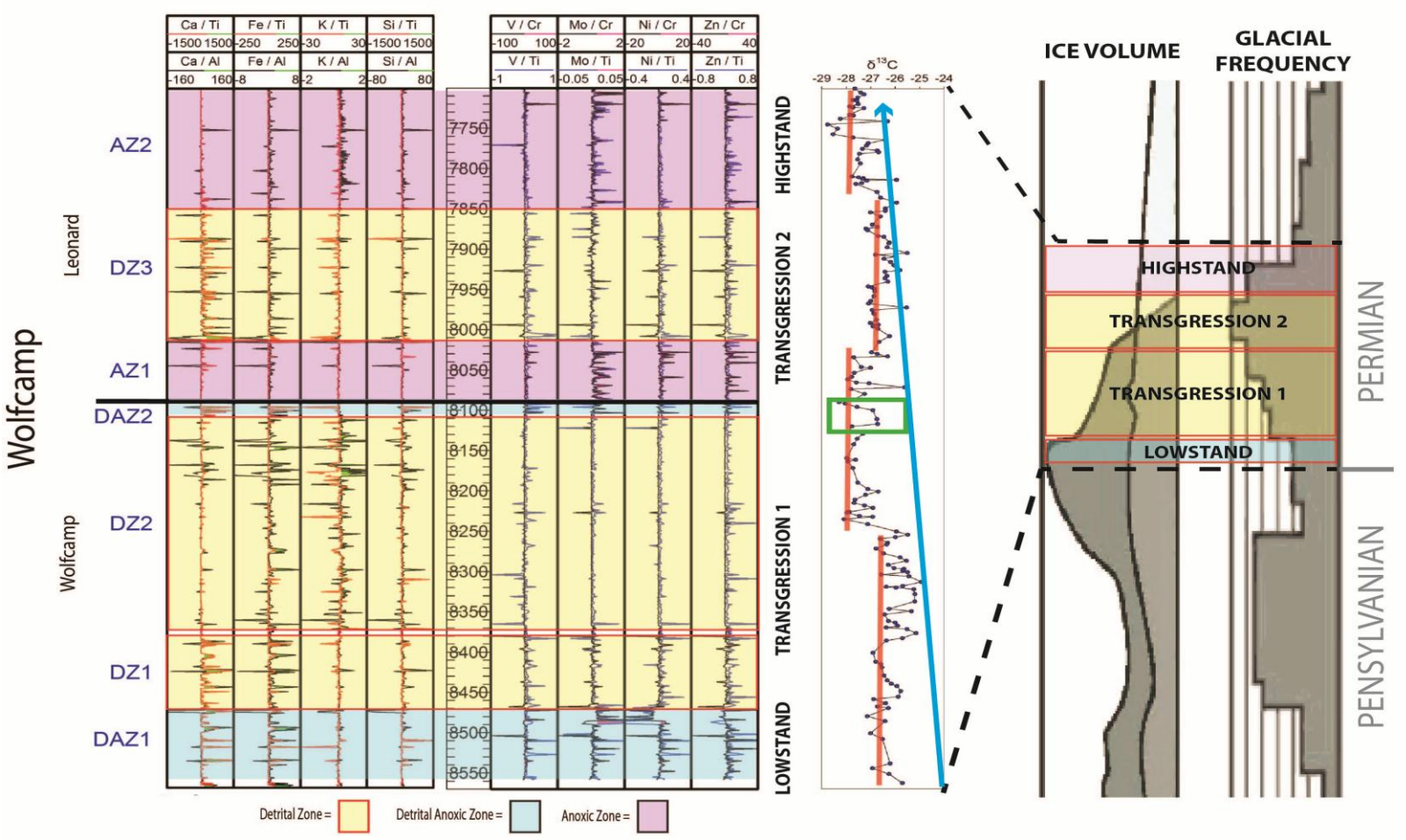

Figure 10. Chemostratigraphy of the Greer 1 core correlated to Late Paleozoic Ice Age (LPIA) ice volume and glacial frequency. Defined zones of varying depositional oxygenation represented by colored boxes and correlated to sequence stratigraphic systems. Three scales of carbon isotope excursion shown by blue arrow, red lines, and green box.

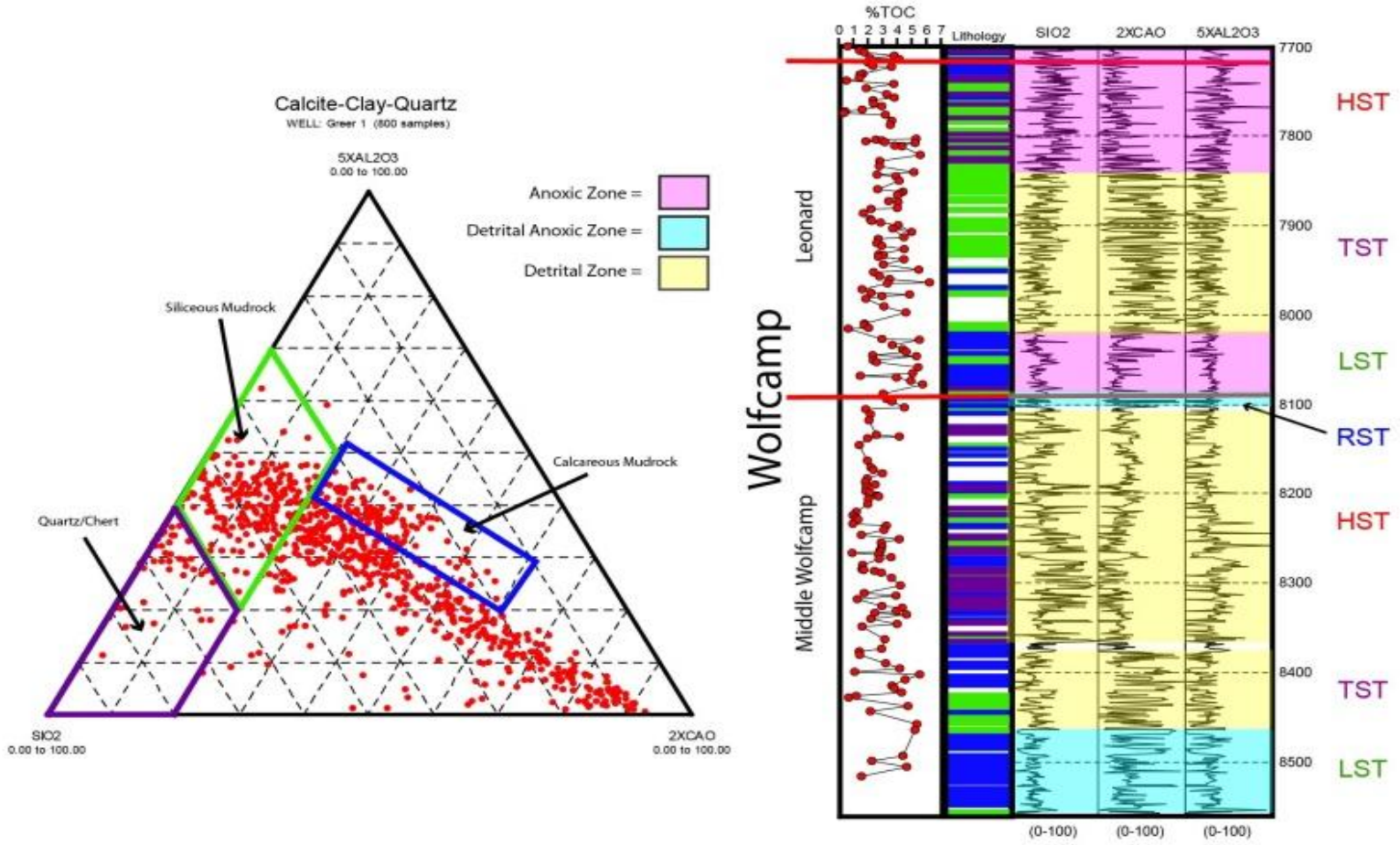

Figure 11. Calcite-Clay-Quartz ternary diagram of the Greer 1 core with polygons representing lithologic end-members of the Wolfcamp strata correlated to sequence stratigraphy, %TOC, and defined zones of varying depositional oxygenation.

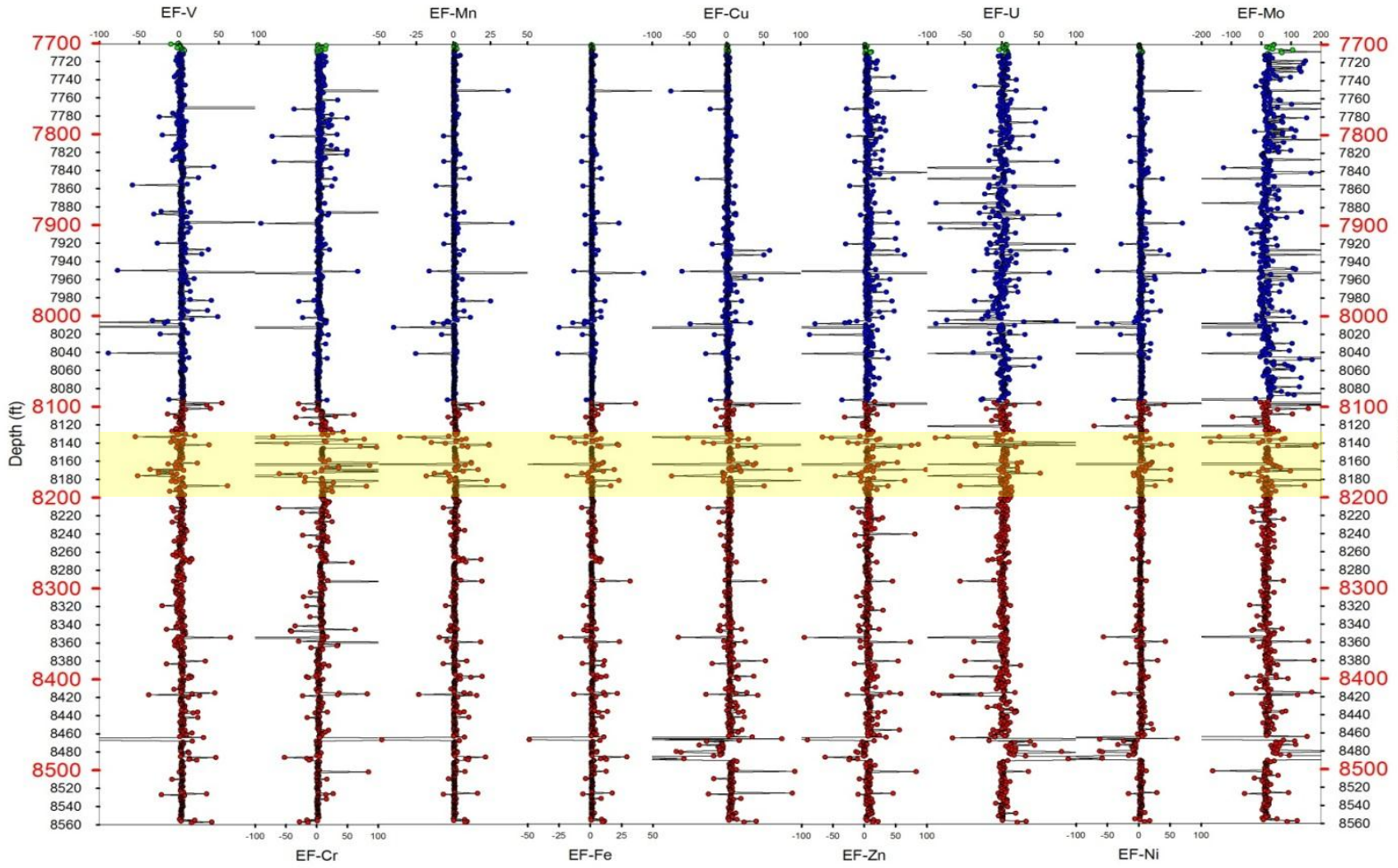

Figure 12. Enrichment Factors (EFs) for the Greer 1 core plotted versus depth. Formations indicated by color. Yellow box denotes a zone of micronutrient enrichment

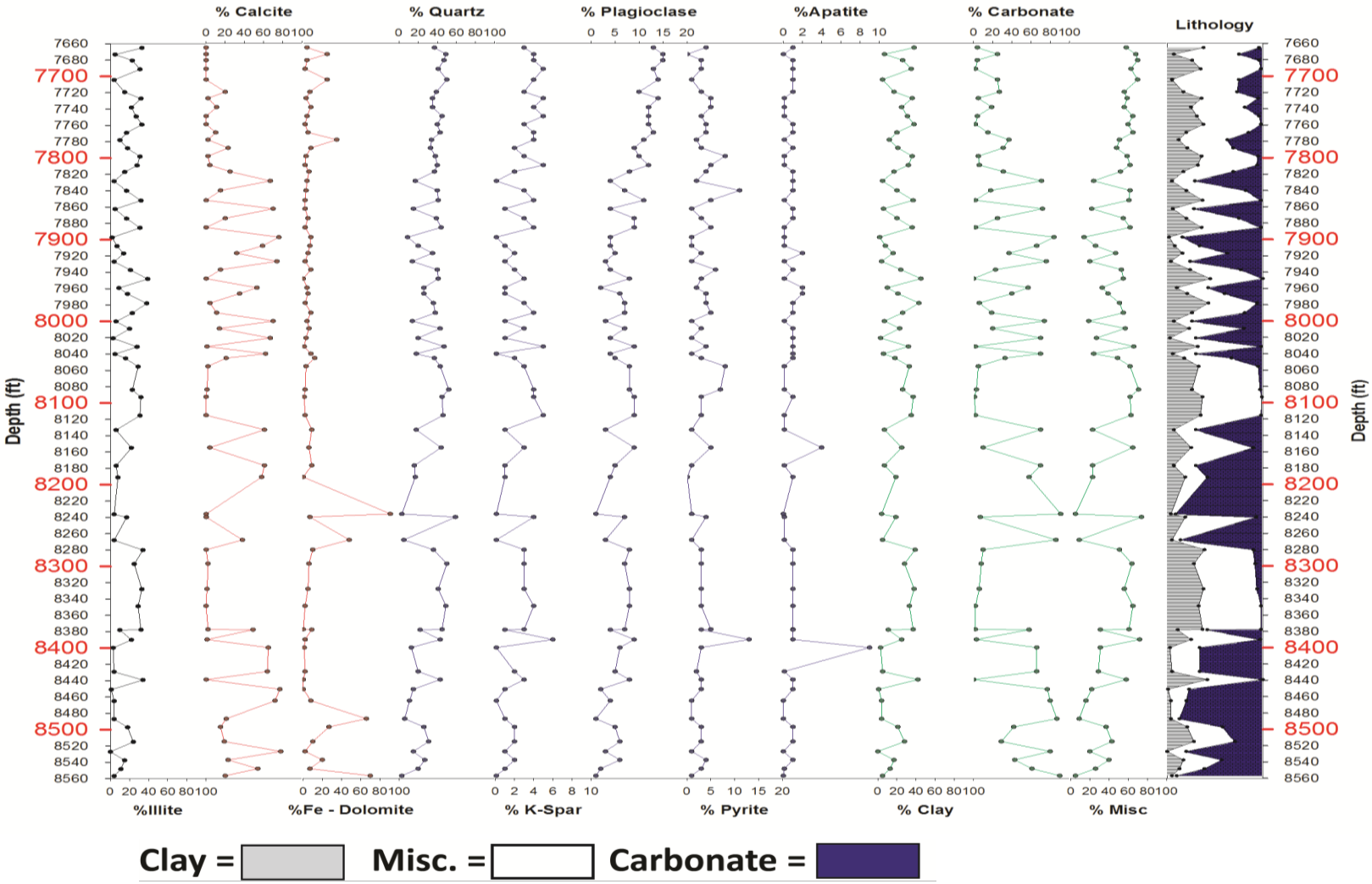

Figure 13. XRD data plotted versus depth of the Greer 1 core. Bulk lithology composition represented graphically on right.

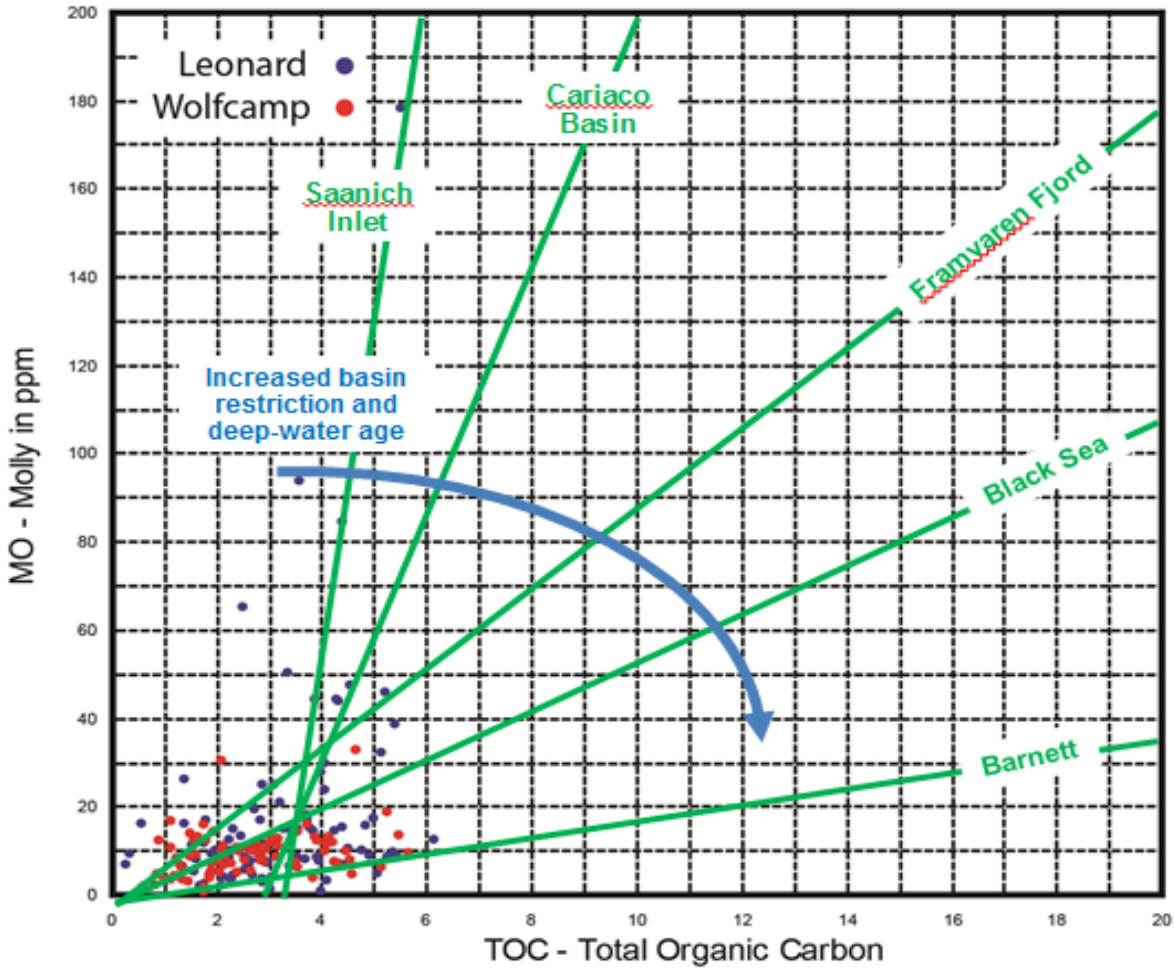

Figure 14. Molybdenum versus TOC cross-plot showing Wolfcamp and Leonard samples from the Greer 1 core in relation to several analogs. Blue arrow depicts an increase in basin restriction and deep-water age.

4.2 Paleoceanography

4.2.1 Physical Paleoceanography

4.2.1.1 Basinal Restriction

A general correlation has been made through recent study between hydrographic restriction and an increased stratification of the water column in a basin (e.g. Rimmer, 2004; Algeo and Lyons, 2006; Rowe et al., 2008). Observed relationships of molybdenum-total organic carbon can be used to reflect the degree of hydrographic restriction of the sub-pycnoclinal water mass in marine basins (Algeo and Lyons, 2006). Water circulation plays a

particularly important role in basin depositional environment and in specific biogeochemical cycles (Algeo and Rowe, 2011). **Figure 14** shows the cross-plot of molybdenum versus TOC for the Greer 1 core. The green lines represent empirical trends of analogous basins, both modern and ancient. The blue arrow represents an increase in basin restriction and deep-water age. The results indicate the Midland Basin to be a restricted during Wolfcampian deposition to a degree that is analogous to the Black Sea and Fort Worth Basin. A secondary trend is seen in Leonardian samples that could represent an increase in ocean mixing due to eustatic sea-level rise.

4.2.2. Chemical Paleoceanography

4.2.2.1 Redox Indicators

Relative enrichment of trace metals in the form of enrichment factors (EFs) were used to evaluate the redox character of the Wolfcamp Formation. An EF near one represents levels similar to that of average crustal abundance and is thusly indicative of relatively normal deposition rates (Calvert and Pedersen, 1993; Crusius et al., 1996). EF values increase after episodes of syn- or post-depositional enrichment of elements. Knowledge of the thermodynamic behavior of an element along-side relative enrichment can be telling of the syn- or post-depositional environments. Significant and prolonged enrichment of redox sensitive trace metals normalized to aluminum, titanium, or chromium (clay proxies) substantiate suboxic – anoxic deposition.

As the most reliable redox indicator, the appearance of molybdenum will have priority as an indicator of suboxic – euxinic deposition (Dean et al., 1997; McManus et al., 2006; Rimmer, 2004). **Figure 10** shows two particular zones of molybdenum enrichment normalized to clay. Indications of anoxic deposition are corroborated by similar enrichments of vanadium, nickel, and zinc. Lack of enrichment in calcium, iron, or silica in anoxic zones at depths 8015 – 8090 and 7700 – 7850 suggests minimal influence from detrital sources. These zones will be referred to as Anoxic Zone 1 (AZ1) and Anoxic Zone 2 (AZ2) respectively. Although these

Table 4. Average %TOC and carbon isotope values in the Greer 1 core organized by zone.

Depths	Zone	AVG %TOC	AVG $\delta^{13}C$
8015-8090	AZ1	3.20	-27.34
7700-7850	AZ2	2.68	-27.32
8380-8560	DAZ1	3.71	-26.52
8090-8115	DAZ2	4.16	-26.98
8380-8470	DZ1	2.85	-26.40
8115-8380	DZ2	2.65	-26.71
7850-8015	DZ3	3.31	-26.60

zones have little detrital influence, XRF and XRD results (**Figures 10 and 13**) indicate an enrichment of K bound in potassium feldspar throughout AZ2. **Table 4** shows the average %TOC and $\delta^{13}C_{org}$ values of each zone. AZ1 and AZ2 have similar $\delta^{13}C_{org}$ values but AZ2 %TOC is slightly lower. This infers similar degrees of terrestrial organic (C_3) input and primary production in both zones, while an increased influx of terrestrial potassium feldspar into AZ2 actively diluted the TOC.

Zones coupling trace elemental and detritus enrichments are observed at depths 8470 – 8560 and 8090 – 8115 (**Figures 10 and 11**). These zones will be referred to as Detrital-Anoxic Zone 1 (DAZ1) and Detrital-Anoxic Zone 2 (DAZ2) respectively. These zones show particular enrichments in Fe, Ca, and TOC. **Table 4** reveals that DAZ1 and DAZ2 contain the highest %TOC values throughout the section and a positive excursion in the $\delta^{13}C_{org}$ values on the order of +1.2‰. This suggests an episode of particularly high sedimentation rate coupled with high rates of burial and compaction and an overall decrease in primary production.

Lastly, three zones of significant detrital influence without substantial evidence of anoxic depositional conditions were observed at 8380 – 8470, 8115 – 8380, and 7850 – 8015 ft. These zones will be referred to as Detrital Zone 1 (DZ1), Detrital Zone 2 (DZ2), and Detrital Zone 3 (DZ3) respectively. DZ1 and DZ3 show similar influence of Ca and Fe in relation to clay proxies as well as slight enrichments of redox sensitive trace metals like Mo and V. DZ2 shows a shift to Fe and K as the dominant terrigenous material and virtually no trace metal

accumulations. Like AZ2, XRD results indicate that the K is primarily bound in potassium feldspar. **Table 4** shows similar $\delta^{13}C_{org}$ values in all detrital zones and slight increases in %TOC in DZ1 and DZ3. It is believed that these slight increases are resultant of enhanced preservation from intermittent episodes of oxygen depletion, indicated by faint appearances of Mo, V, Ni, and Zn.

4.3 Sequence Stratigraphy

Although it is difficult to resolve sequence stratigraphic systems through traditional core-based study, chemostratigraphy provides well defined shifts in depositional environment and sediment character that can lead to reliable implications of sequence stratigraphic boundaries. Integration of XRF, XRD, $\delta^{13}C_{org}$, basin dynamics, and paleoclimate will be analyzed in order to outline a potential sequence stratigraphic framework for the interval of study. It is important to note that the linkages of sequence stratigraphic tracts were established before paleoclimate data integration. These suppositions were based on several vital assumptions and known limitations of this method. First, due to the near depo-center setting of the study area, it is conceded that the ideal appearance of all system tracts is not probable. Additionally, due to the limitations of core-based study, tracts will not be based on stratal lapping relationships or sedimentary structures. Thirdly, past interpretations of differential rates of subsidence will be integrated as two distinct events. Mazzullo and Reid (1989) concluded that Middle Wolfcampian clastics were deposited in a regime of low to moderate rates of subsidence with punctuated episodes of increased subsidence, relative to the Upper Wolfcamp Formation. Thus, we will assume that this interval subsided at a fairly consistent rate with sudden events of drastic subsidence. Conversely, the assumption will be made that the Upper Wolfcamp was influenced to a greater degree by subsidence. Additionally, it is believed that the scale of this study combined with an indication of a high degree of basin restriction, as well as implications given by previous studies, provide strong evidence of a eustatically-driven system (Crowell, 1978; Veevers and Powell, 1987; Mazzullo and Reid, 1989). Furthermore, this study will

assume that the LPIA was the primary factor affecting sea level in the basin. Primary results are based on major shifts in the character of sediment influx and implications of varying degrees of oxygenation in the sediment. Therefore, the results presented were initially attained exclusively through geochemical analysis and later refined by paleoclimate estimates.

There is great possibility for confusion when classifying sequence stratigraphic systems tracts using chemostratigraphy in a basin setting. Geochemical signatures represent changes in sediment character and oxygenation of bottom waters. These changes, when occurring far from the sediment source, can have rather sizeable lag times in response to changes in basin dynamics. Adding to the difficulty, different responses can possibly have substantially dissimilar lag times. For example, increased accommodation and erosional capacity that leads to regular sediment input (via debris flows and turbidites) into the basin can occur nearly simultaneously with sea-level fall. Conversely, trace metal accumulation from a stratified water-column (via increases in basin restriction) related to the same sea-level fall could occur much later. Thus, general time-event-strata connections should be relatively equivocal. Due to this limitation, traditional sequence stratigraphic systems tracts will not be defined. Instead, simple interpretations of the most likely basin conditions will be presented for each major change in geochemical character.

The Late Paleozoic Ice Age (LPIA) greatly influenced global sea levels from the Mississippian through the Permian (**Figure 7**) (Blakey, 2008; Fielding et al., 2008). **Figure 10** relates total ice volume, glacial frequency and the chemostratigraphic definitions previously reached. In the late Pennsylvanian, global temperatures began to drop, creating significant glacial volume from the poles into the lower latitudes (~30°) (Fielding et al., 2008). Rapid eustatic sea-level drop created sediment representative of lowstand conditions in the rocks earlier defined as DAZ1. Located near the equator, the Midland Basin was subject to relatively high rates of erosion, typical of a tropical environment (Mazzullo and Reid, 1989; Blakey, 2008;

Fielding et al., 2008; Flamm, 2008). Therefore, low sea levels contributed two prominent situations: 1) an increase in an incising erosional front, thus intense sedimentation of the shelf carbonate shelves into the basin, and 2) an increased basinal restriction, ultimately hindering circulation. Evidence of each effect is seen by the significant enrichment in detrital indicators and redox-sensitive trace metals in **Figure 10**.

Transgressive sediment deposits are typically thin to absent in shelf and slope clastics because much of the eroded sediment is deposited at the bottom of the shelf slope or farther into the basin through mass-waste flows. An increase in the presence of debris flows and turbidites through this section suggests a combination of sea-level rise and subsidence. LPIA estimates (**Figure 7**) concur, showing a drastic decrease, followed by a steady decline in ice volume. The increased erosion on carbonate factories, along the continental shelf, deposited strata dominated by a well-mixed oxygenated influx of Ca and Fe. This event, labeled Transgression 1 in **Figure 10**, also records a shift around 8370 ft. in sediment character as the erosional front approached a terrigenous sediment source of differing character. Here, we observe a change in the chemical character of introduced detritus from Ca to the K. This shift, depicted by DZ1 and DZ2, is indicative of the shoreline surpassing the shelfal carbonate factories, reaching and possibly exceeding the previous beachfront. XRD results (**Figure 13**) through this section support this claim by revealing the K to be primarily bound in potassium feldspar.

The transition into Leonardian time is marked by a sudden shift into anoxic – euxinic bottom waters. This interval, labeled Transgression 2, coincides with a considerable increase in the rate of ice volume depletion and the highest glacial frequency of the LPIA. DAZ2 serves as the transitional stratal package from oxic to anoxic-euxinic bottom-waters. Although the system was still transgressing, an obvious shift in basin dynamics occurred here. The drastic and sudden cessation of detrital input suggests an event effecting either accommodation or

erosional capabilities around the basin. It is hypothesized that the increase in tectonic activity during the Upper Wolfcamp led to a diversion of sediment. The subsequent detritus starvation led to oxygen depletion by increased primary production seen in $\delta^{13}C_{org}$ estimates. Continued nutrient input elsewhere supported increased biologic activity throughout the basin. Sediment and biological rain increased the bulk lithology percentages of clay and quartz, seen in **Figure 13**, through this section. Transgression 2 persisted with another shift in sediment character marked by DZ3. Here, the system returned to similar conditions described in DZ1 (part 1 of Transgression 1). Detrital input was reestablished and dominated by Ca and Fe. Additionally, evidence of discreet episodes of anoxia-euxinia is seen in the redox sensitive trace metal enrichment curves (**Figure 10**). High degrees of cyclicity observed in XRD results (**Figure 13**), trace metals, and $\delta^{13}C_{org}$ along-side the appearance of transitional lithologies (**Figure 11**) and glacial frequency estimates (**Figure 13**) suggest this period to be the most dynamic system in the study.

Finally, the uppermost section progresses into the most extreme highstand condition of the study. Strong and sudden appearance of redox sensitive trace metals implicate severe anoxia – euxinia resultant of a stratified water-column. Once again, potassium feldspar influx seems to replace Ca as previously noted in the DZ2 transgression, but with an overall drastic reduction in sediment volume. This shift is most likely a result of extremely high sea levels and the subsequent transgression of the erosional front beyond previously eroded terrigenous terrain. This theory, much like DZ1, is also supported by the large negative excursion in $\delta^{13}C_{org}$ values indicating an increase in production from the added nutrient flux. Much like AZ1, primary production throughout the basin was being supported by the nutrient influx at the margins. The great expanse of the entire basin at this point led to a local increase in the oxygen-minimum zone, therefore a higher degree of basin-centered anoxia – euxinia. The expanse and level of completeness of this tract is unknown due to the limitations created by the scope of this project.

CHAPTER 5

CONCLUSIONS

5.1 Conclusions

The integration of geochemical proxies and basin dynamics has provided insight into the paleoceanography of the Pennsylvanian – Permian section of the Midland Basin. Reconstruction of the paleoceanography at several scales delivered solid theories and hypotheses into the redox conditions of bottom waters and related sediments during Wolfcampian and Leonardian deposition. Chemostratigraphic variance illuminated differences in sedimentation rates and sourcing through a number of oceanographic settings. These differences provided the ability to make correlations to sequence stratigraphic boundaries and systems from the late Pennsylvanian to the Early Permian period.

1. The chemical paleoceanography of the Pennsylvanian – Permian section of the Midland Basin reveals that the strata were deposited beneath bottom waters ranging from oxic to euxinic conditions. Appearance of such a vast array of environments was primarily produced by changing basin dynamics associated with glacial-driven eustatic sea-level fluctuations and sedimentation rates.

2. The mudrocks of the Wolfcamp and Leonard Formations are considered to be rich (averaging 3.2%) in TOC. Three scales of $\delta^{13}C_{org}$ cyclicity contribute to an overall negative excursion in younger sediments representing an overall increase in primary production and degree of C_3 land plant organic sediment influx.

3. The bulk geochemistry of the Wolfcamp Formation indicates that it is composed primarily of siliceous and calcareous mudrocks with significant influence from genetically-related muddy carbonate-clast conglomerates (debris flows), and skeletal packstone/grainstones (turbidites).

4. Multiple mechanisms provided several distinct anoxic zones of varying sediment influence. Highest average %TOC values (3.93%) are present in detritus dominated anoxic zones associated with increased erosion and high rates of sedimentation, compaction, and burial.

5. Chemostratigraphy successfully integrates into sequence stratigraphy showing that Wolfcampian – Leonardian clastics were deposited under varying degrees of oxygenation through a full, LPIA-driven lowstand – highstand cycle.

5.2 Future Study

Future work in the area should focus on refining the basin wide extent and correlation of defined zones of differential bottom-water oxygenation. Also, similar studies should be extended down section into the older strata in order to compare the source and reservoir potential of additional anoxic zones. In addition, a small scale geochemical analysis should be completed on zones of transition between oxic and anoxic bottom-water conditions. XRF analysis at one inch, rather than one ft., over transitional intervals between defined zones of interest could provide much needed insight into the actual mechanism driving changes in pore-water chemistry. Also, isotopic analysis should be expanded to include oxygen ($\delta^{18}O$), nitrogen ($\delta^{15}N$), and strontium ($\delta^{87}Sr$) in order to further refine our understanding of the climate, sediment sourcing, productivity, and age of the rocks. Finally, work should be done to observe the effect that debris flows and turbidites have on the chemistry, geo-mechanics, and porosity of the Wolfcampian and Leonardian mudrocks.

APPENDIX A

ADDITIONAL FIGURES

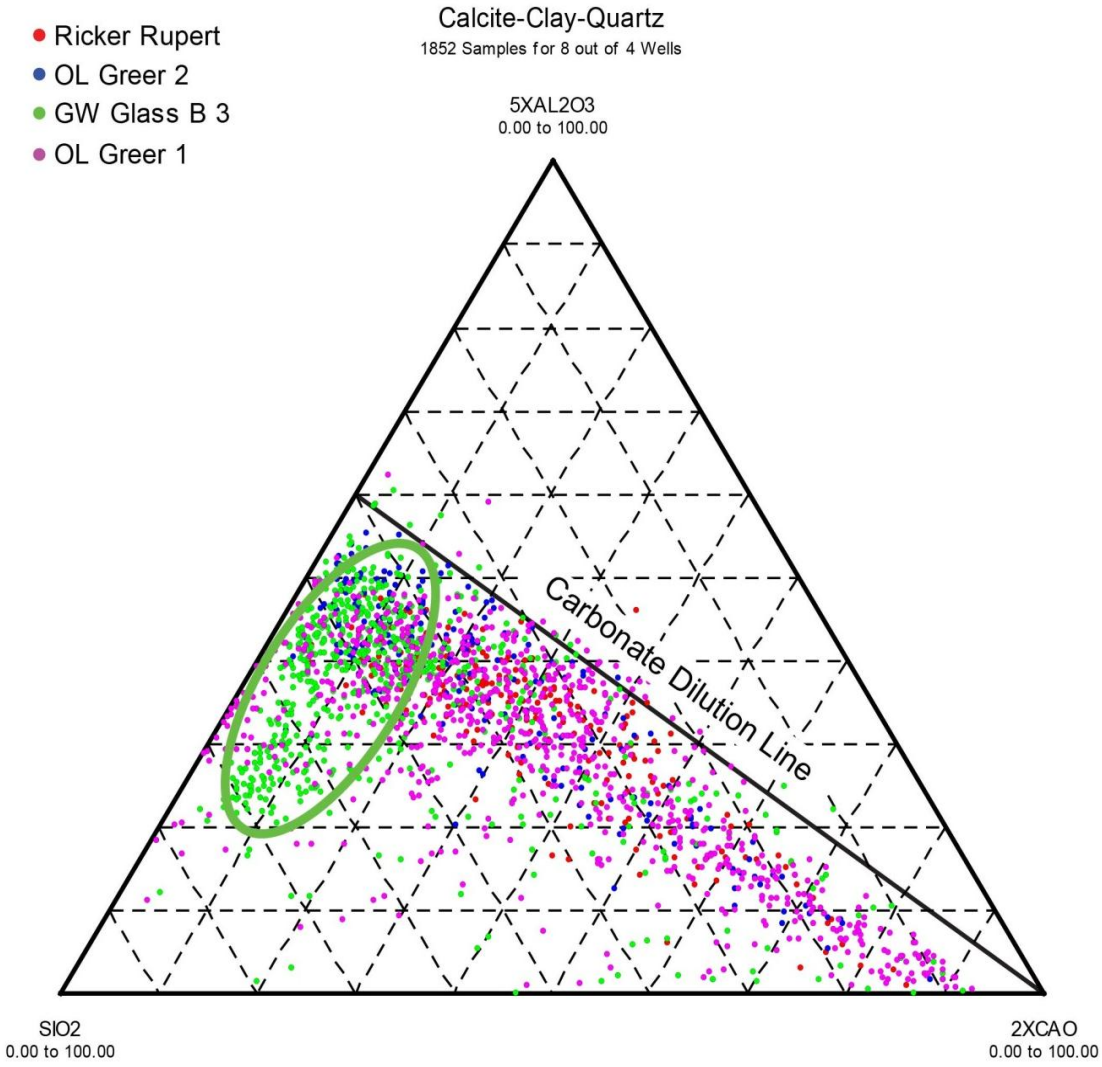

Figure 15. Calcite-Clay-Quartz ternary diagram with all samples plotted in relation to the carbonate dilution line. Green ellipsoid represents Glass samples.

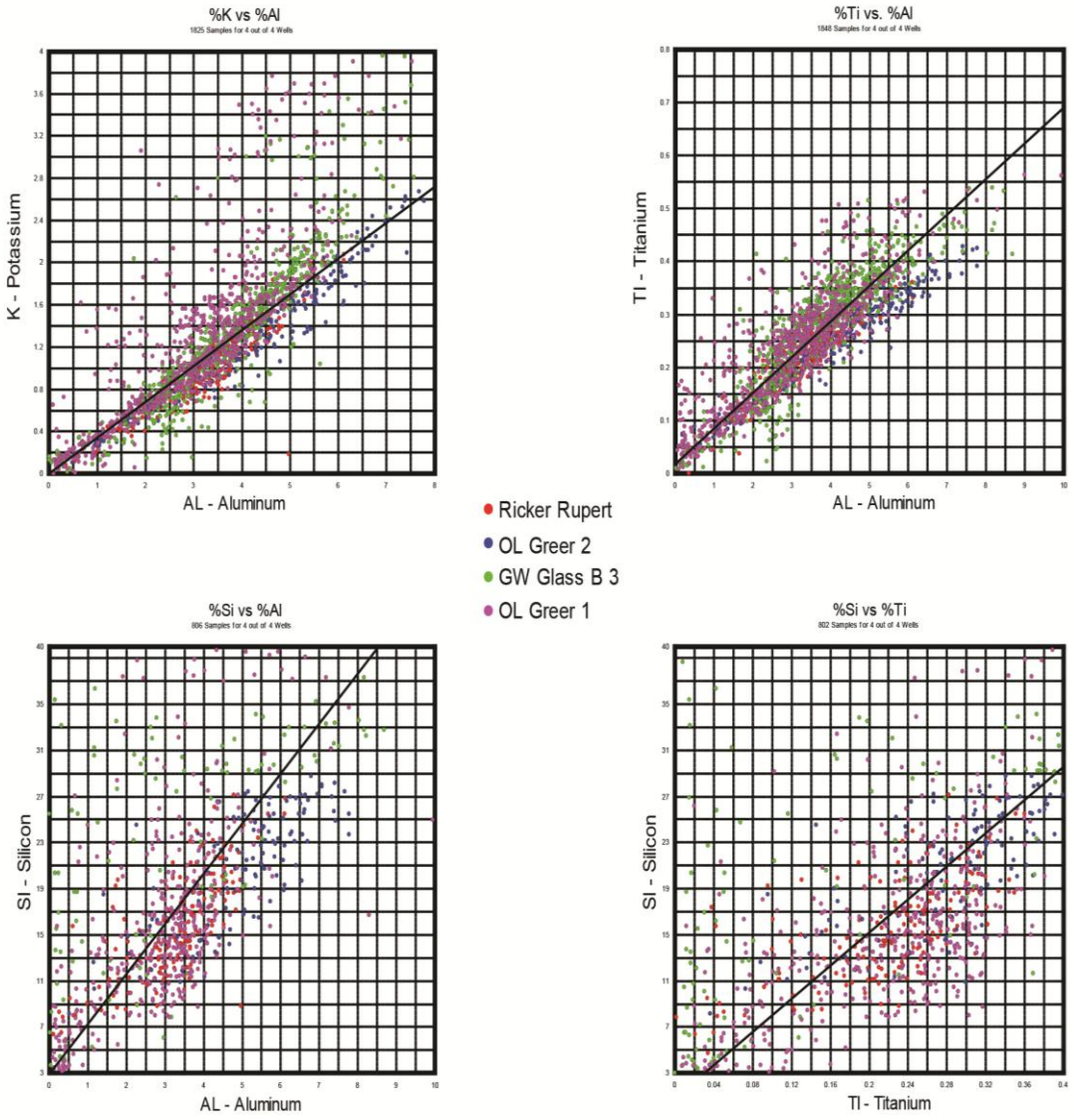

Figure 16. Cross-plots for all samples from all cores in the study showing best fit lines for K, Al, Si, and Ti ratios. Cores represented by colors indicated in the legend.

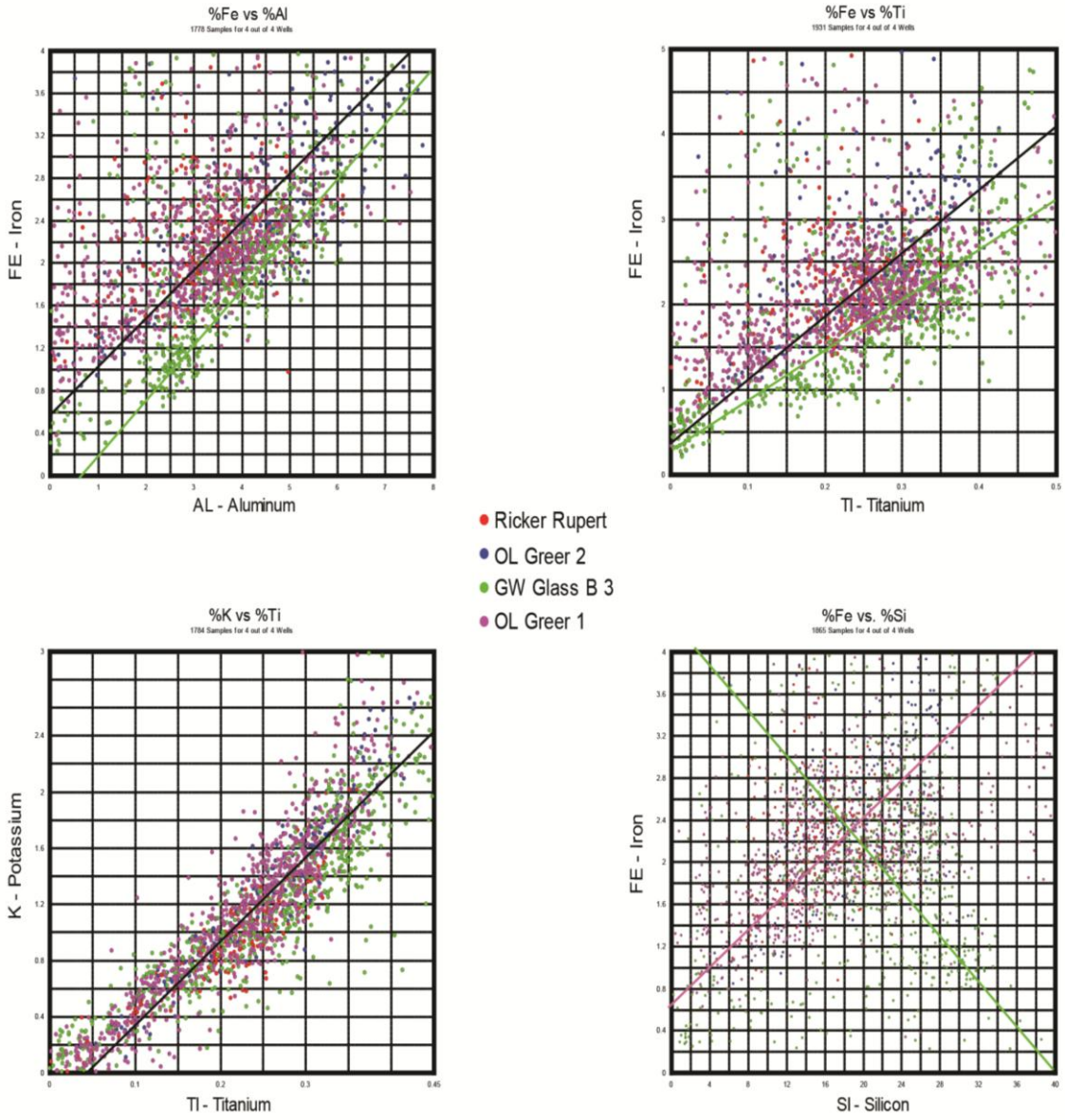

Figure 17. Cross-plots for all samples from all cores in the study showing best fit lines for K, Al, Si, Fe, and Ti ratios. Cores represented by colors indicated in the legend.

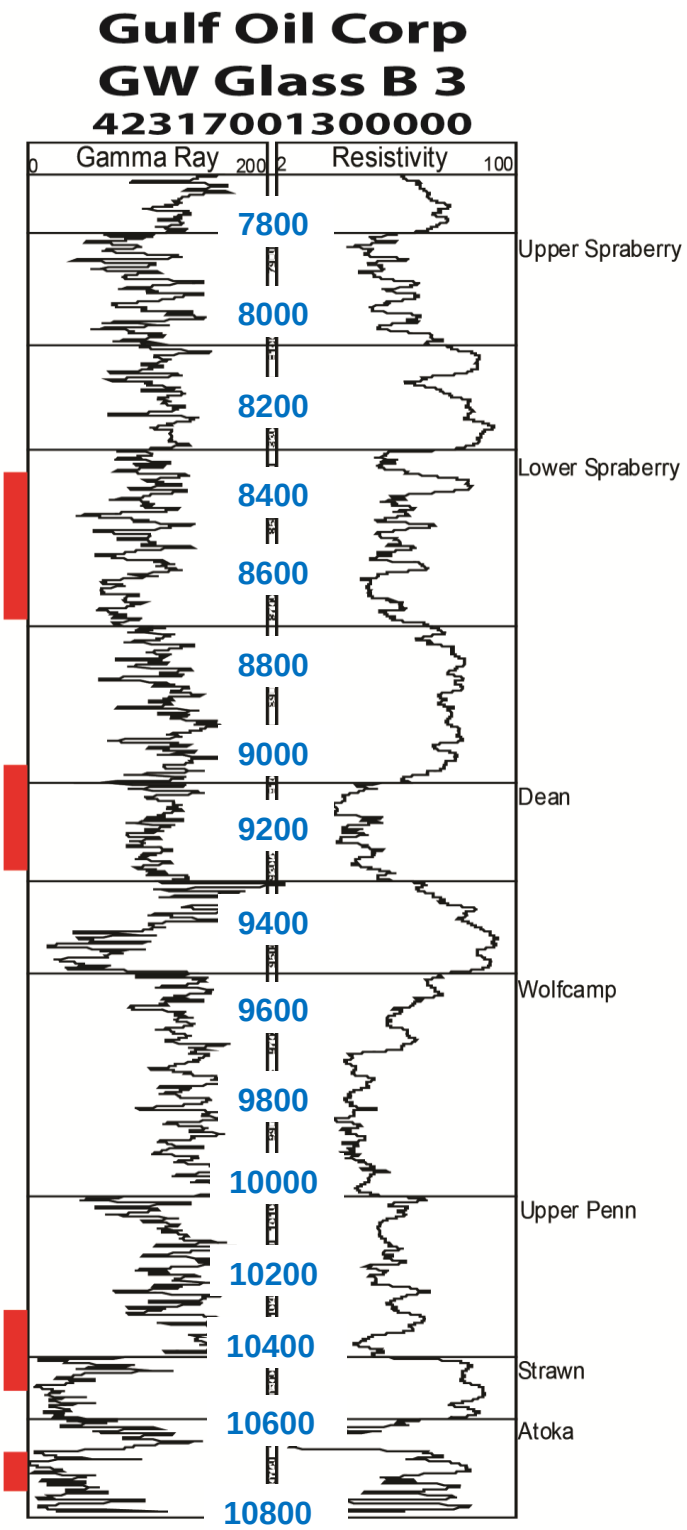

Figure 18. Glass core well log with intervals of study marked by red rectangles.

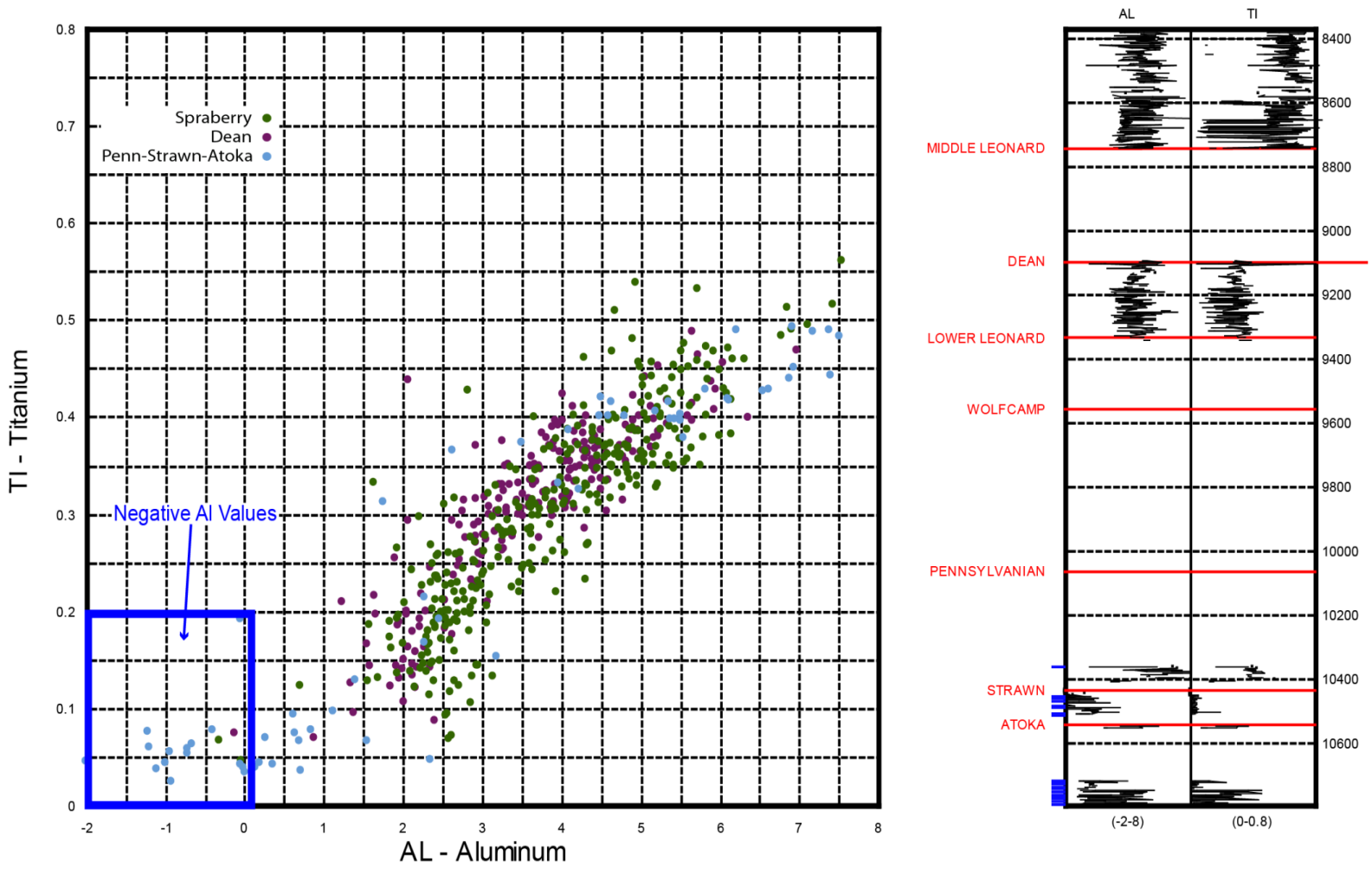

Figure 19. Aluminum versus Titanium trend highlighting the concentration of negative aluminum values in the Strawn and Atoka Formations due to a lack of instrumental calibration for the lithology.

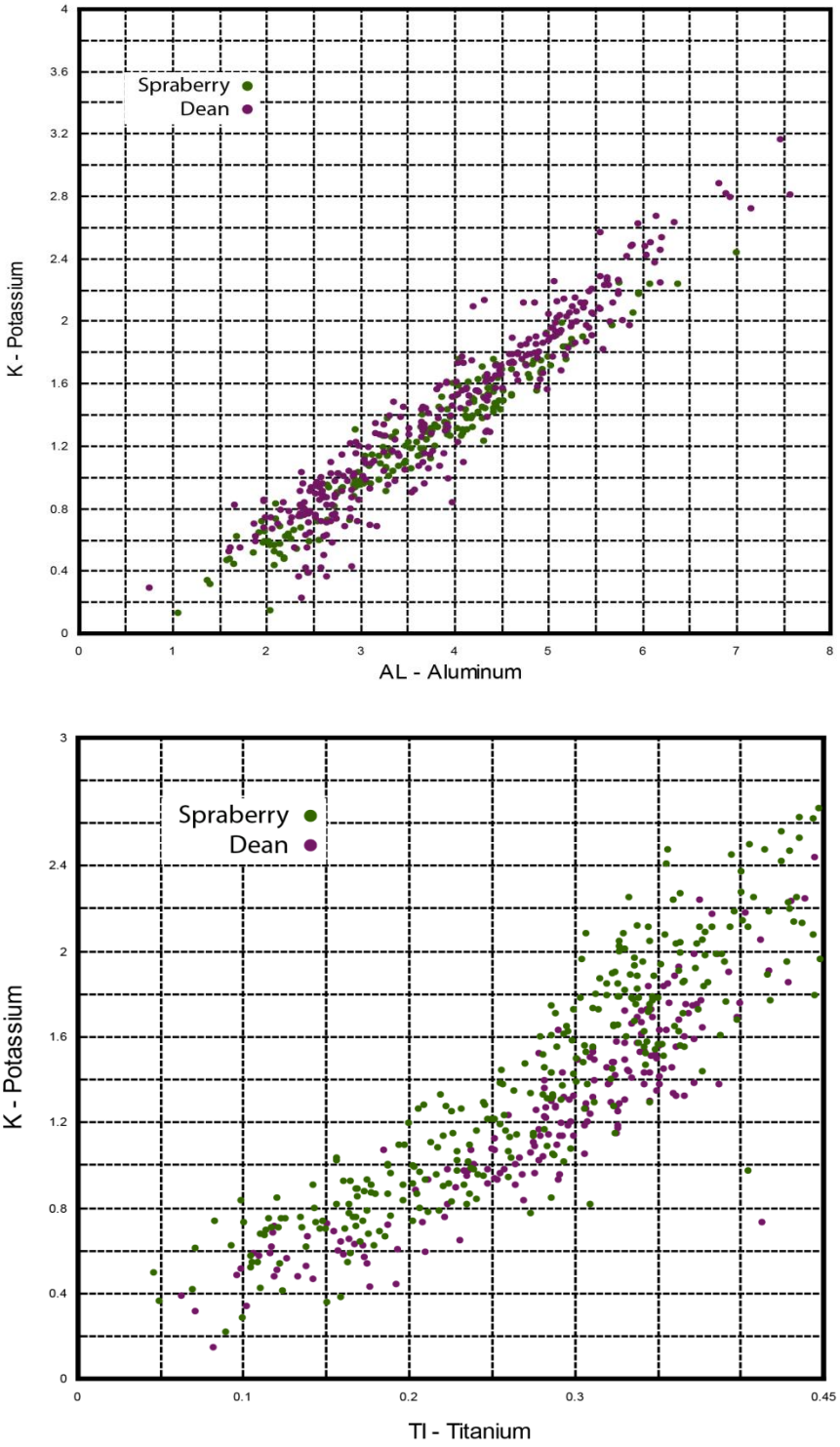

Figure 20. Cross-plots for the Glass core of K vs. Al and Ti of samples through the Spraberry and Dean Formations.

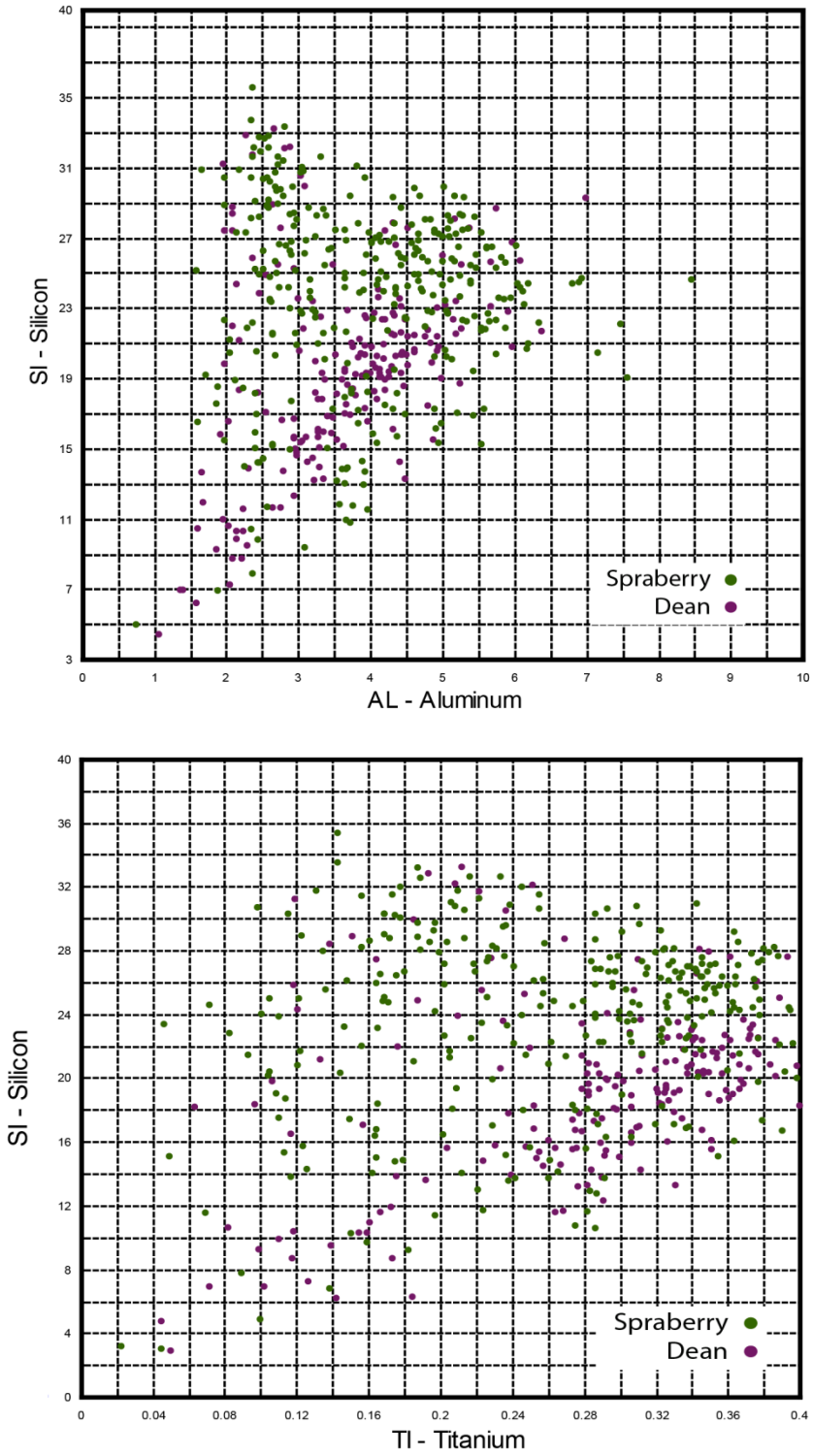

Figure 21. Cross-plots for the Glass core of Si vs. Al and Ti of samples through the Spraberry and Dean Formations.

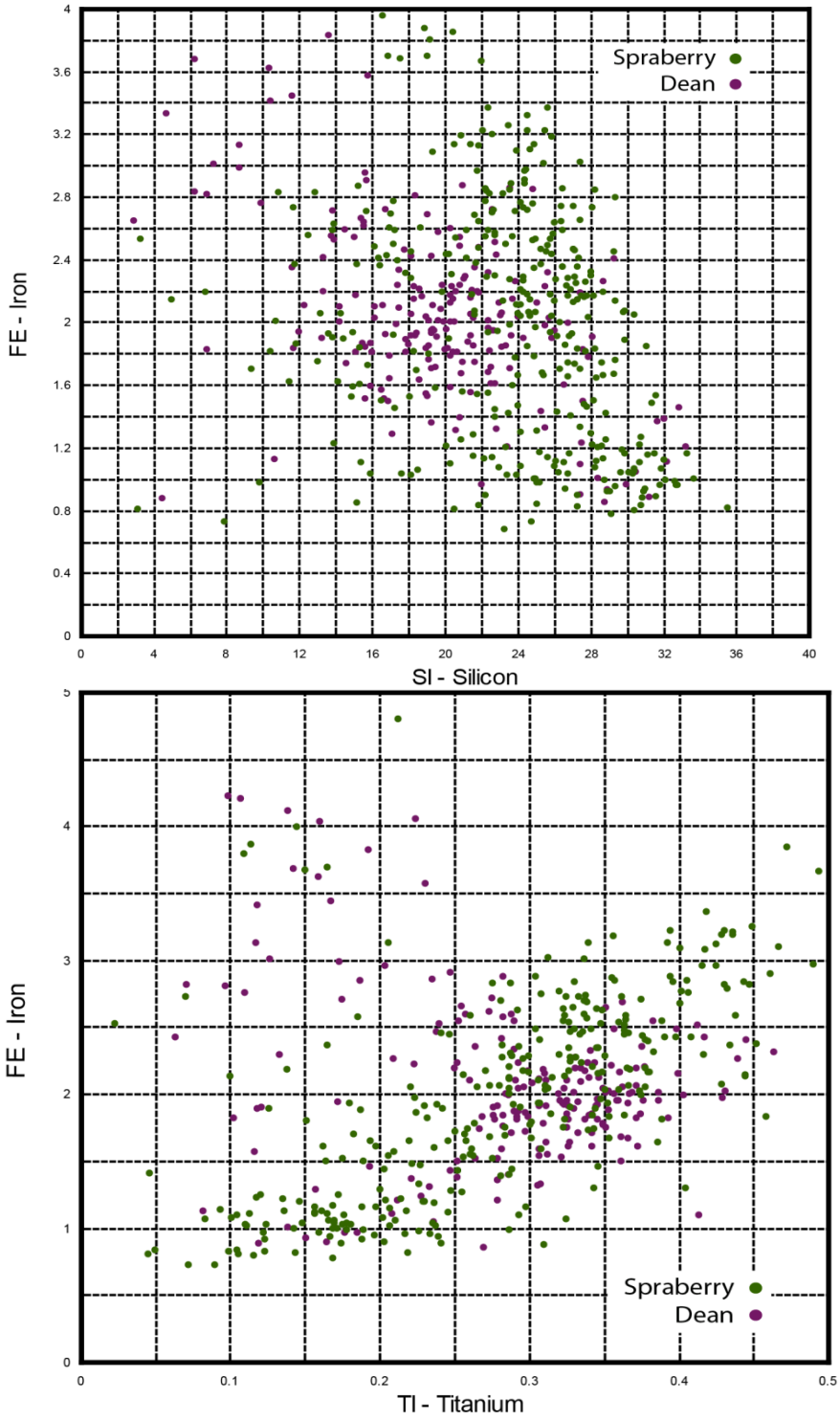

Figure 22. Cross-plots for the Glass core of Fe vs. Si and Ti of samples through the Spraberry and Dean Formations.

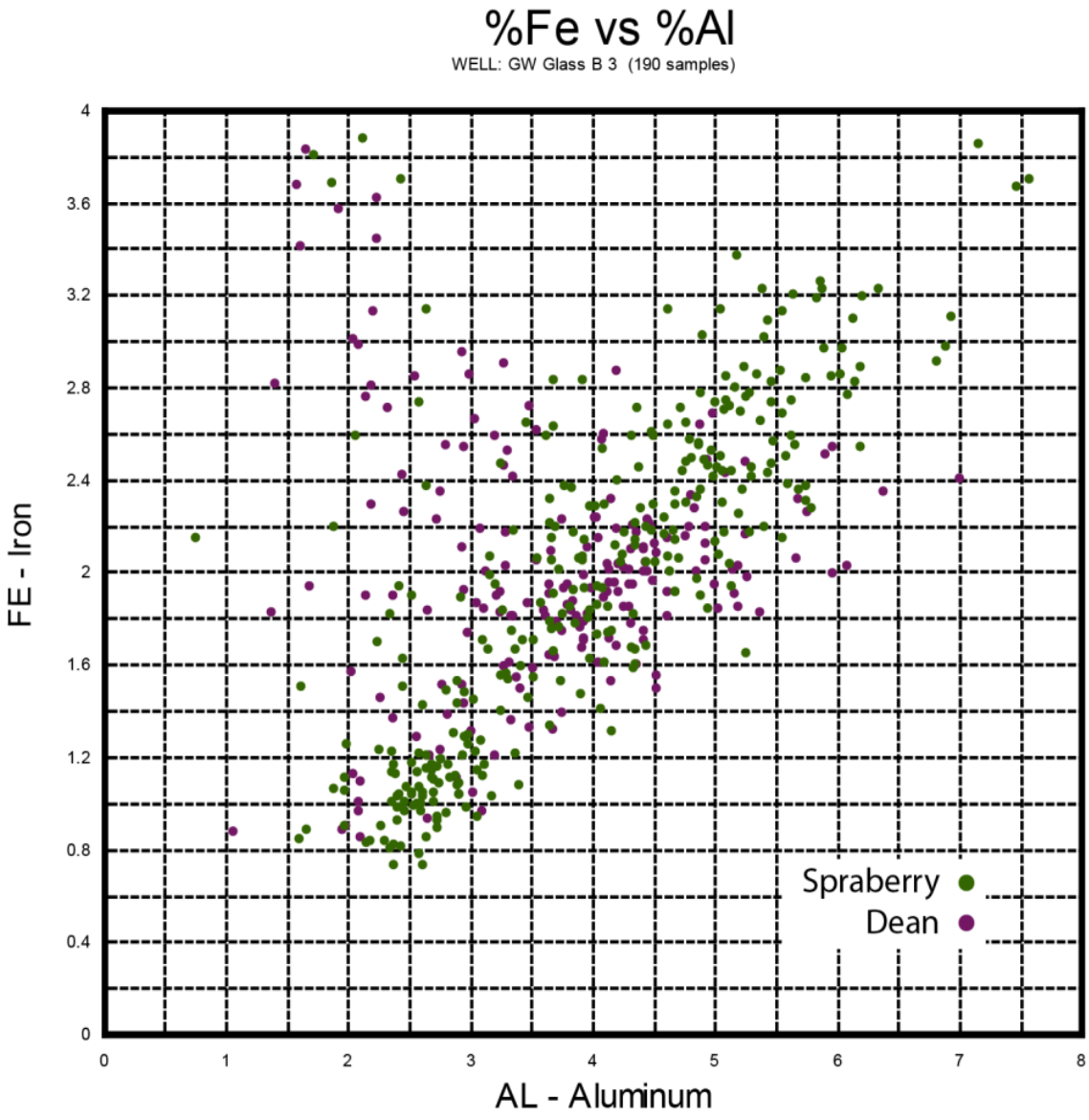

Figure 23. Cross-plot for the Glass core of Fe vs. Al of samples through the Spraberry and Dean Formations.

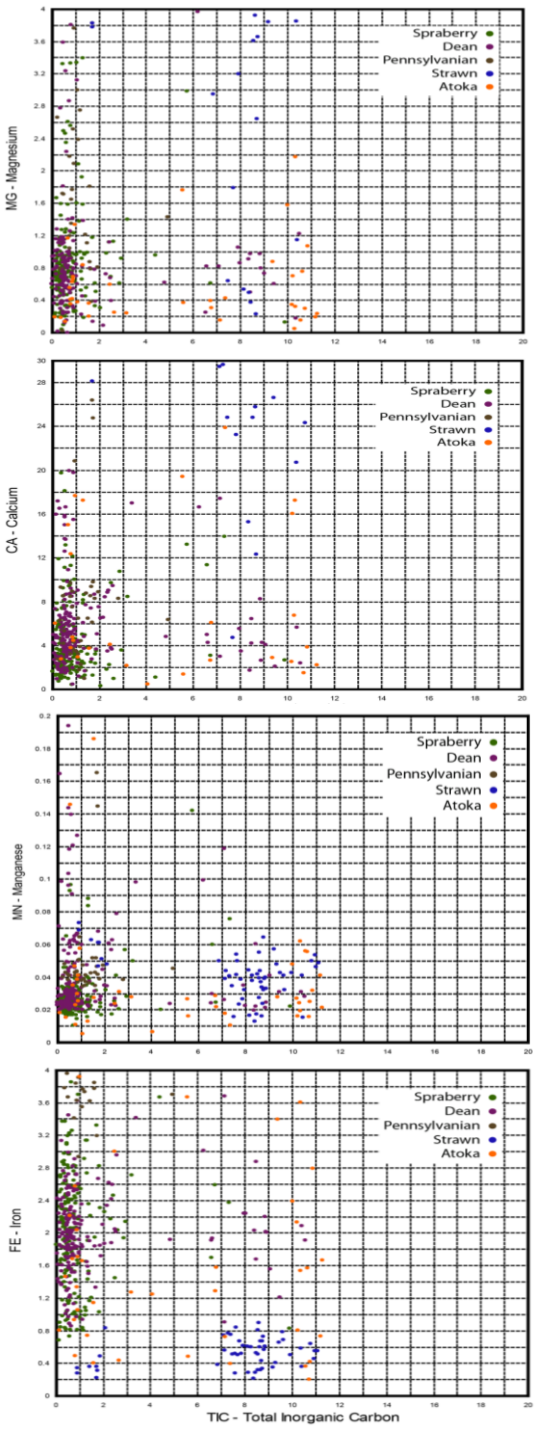

Figure 24. Mg, Ca, Mn, and Fe plotted vs. TIC for all Glass core samples. Formations are represented by colors

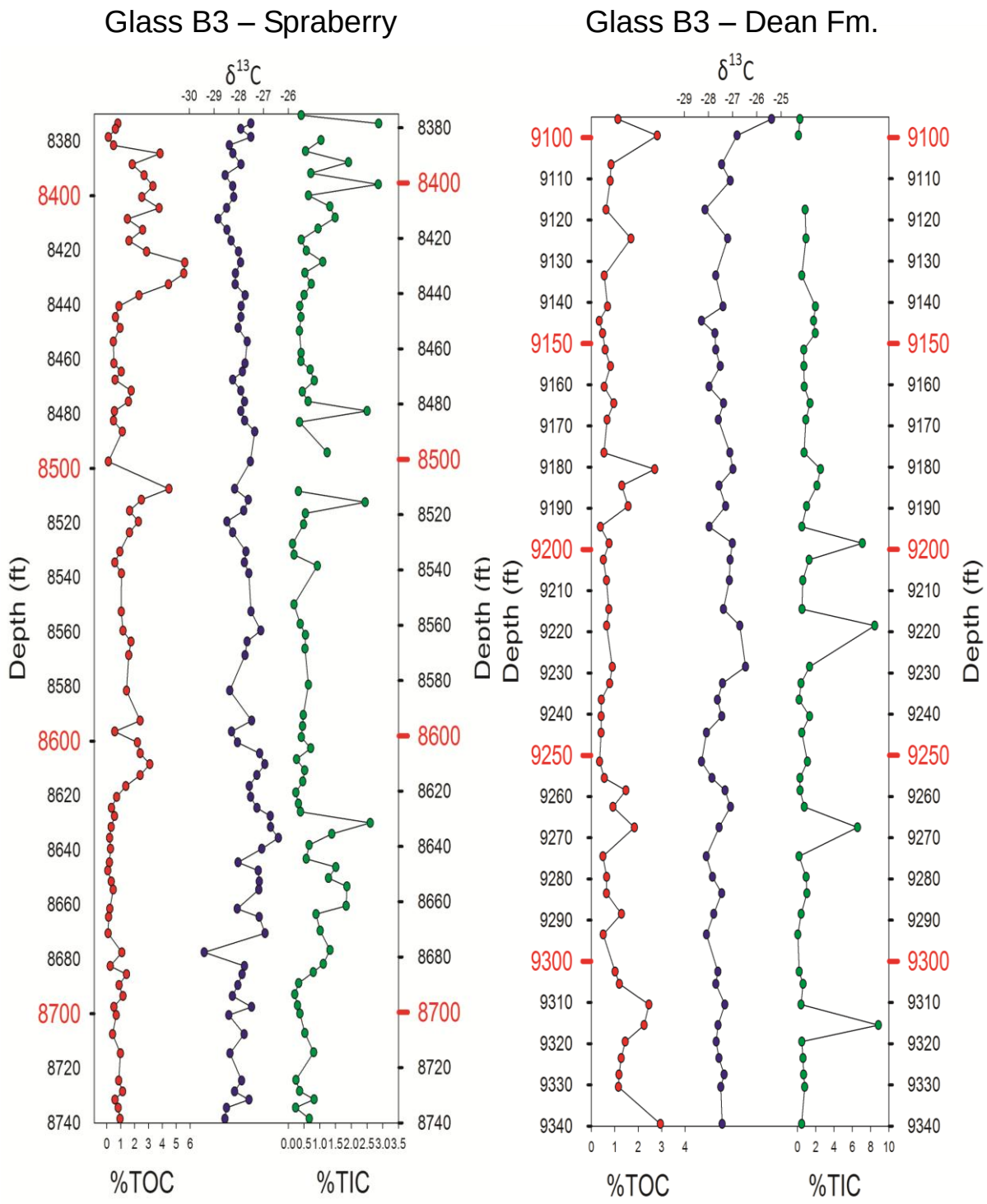

Figure 25. %TOC, %TIC, and carbon isotopes for samples through the Spraberry and Dean Formations in the Glass core.

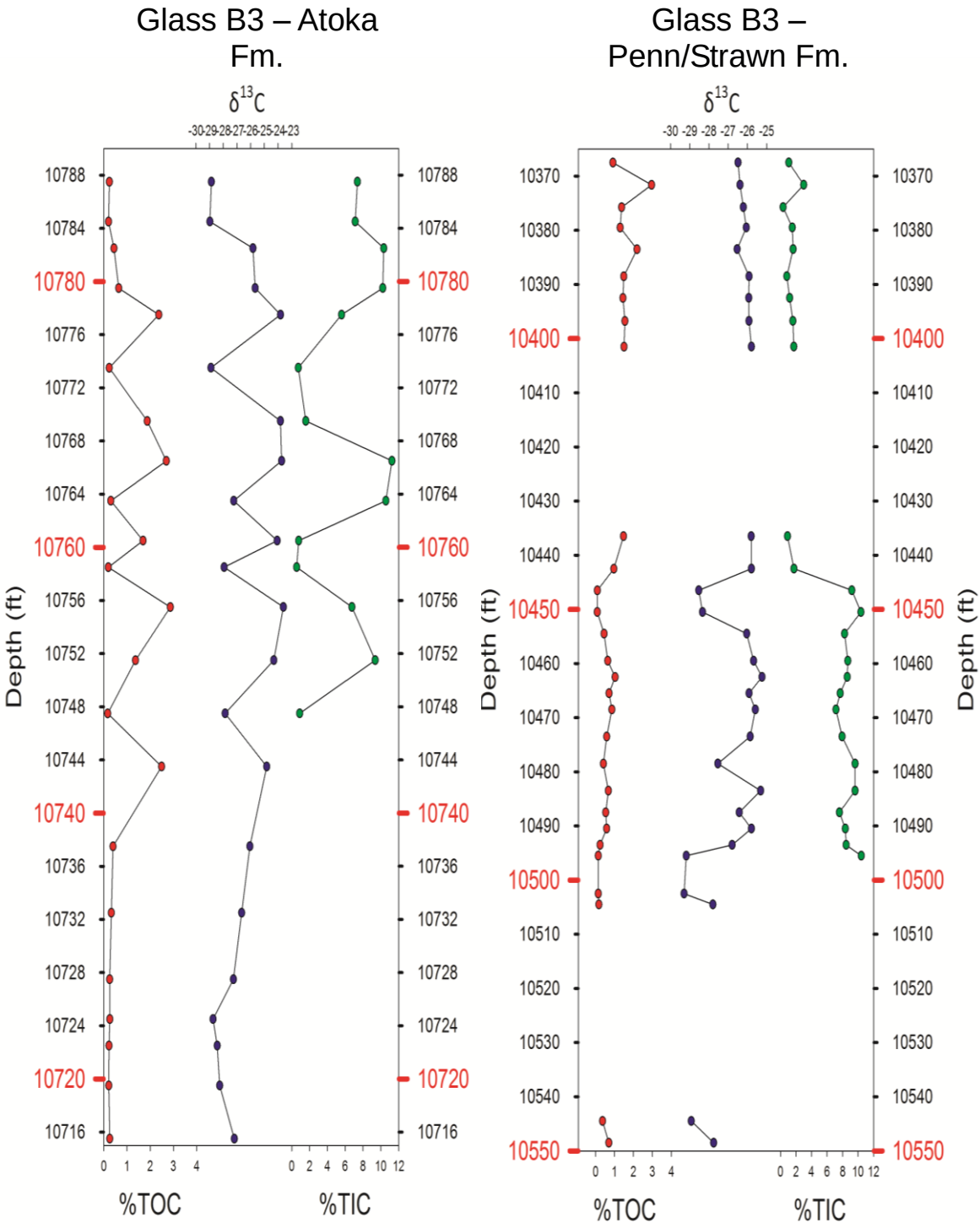

Figure 26. %TOC, %TIC, and carbon isotopes for samples through the Penn/Strawn and Atoka Formations in theGlass core.

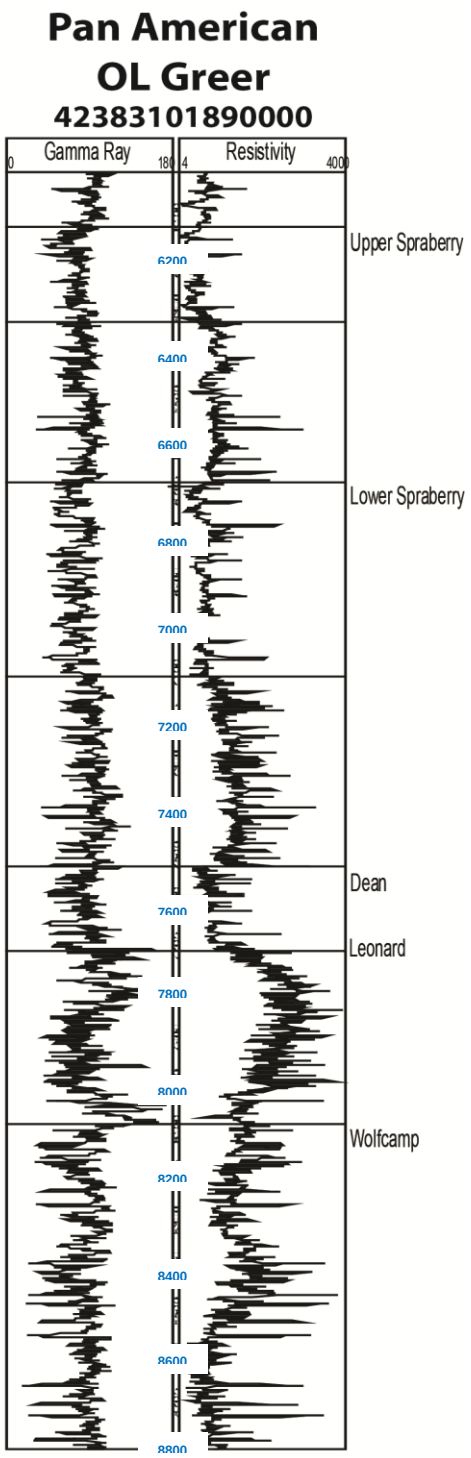

Figure 27. Greer 1 well log with annotated formation tops.

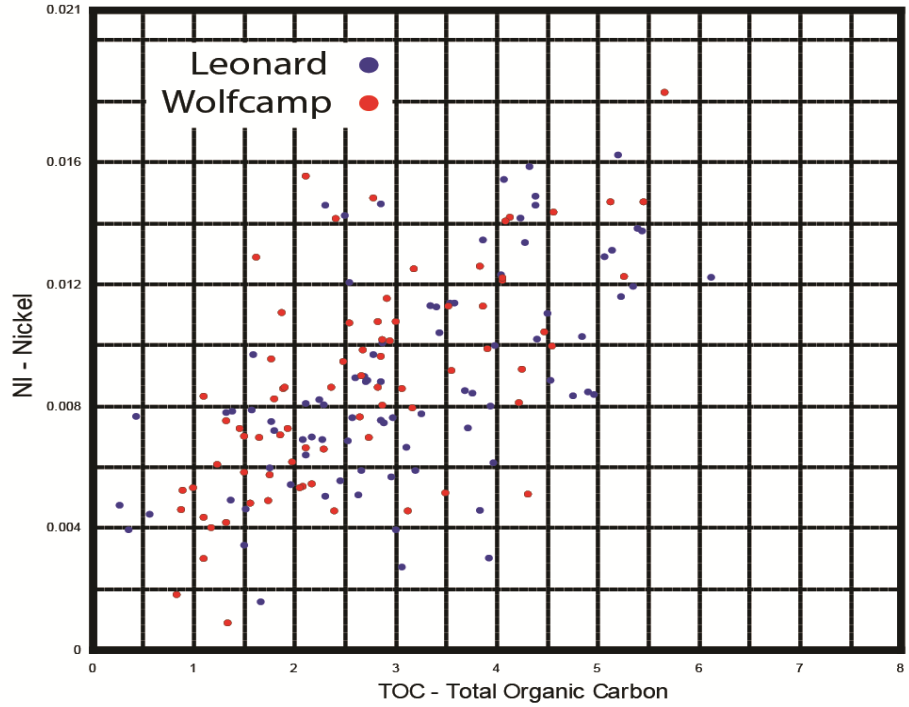

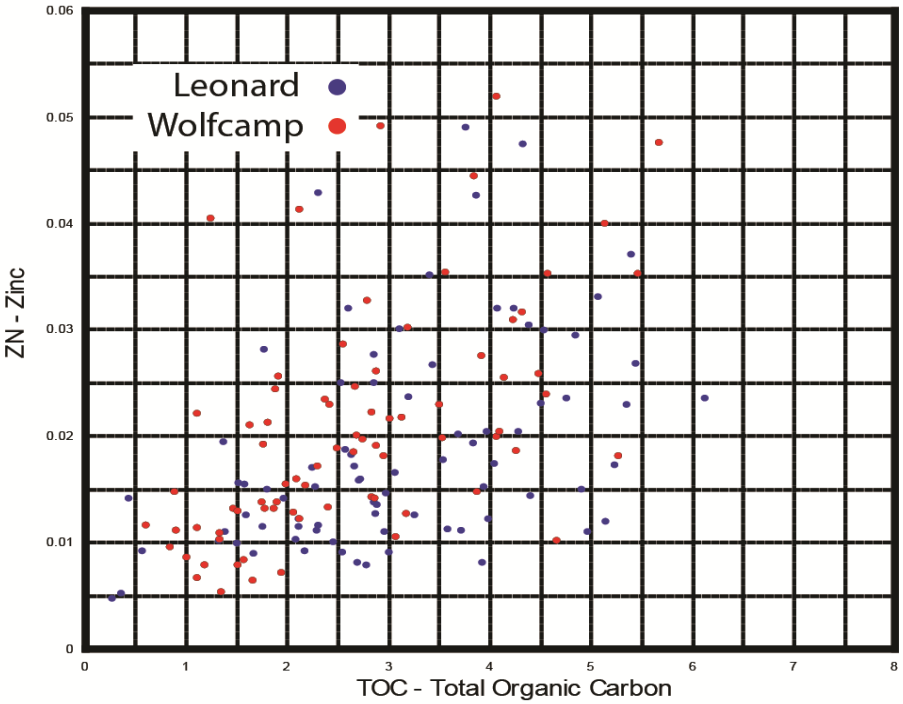

Figure 28. Greer 1 cross-plots of TOC vs. Zn and Ni.

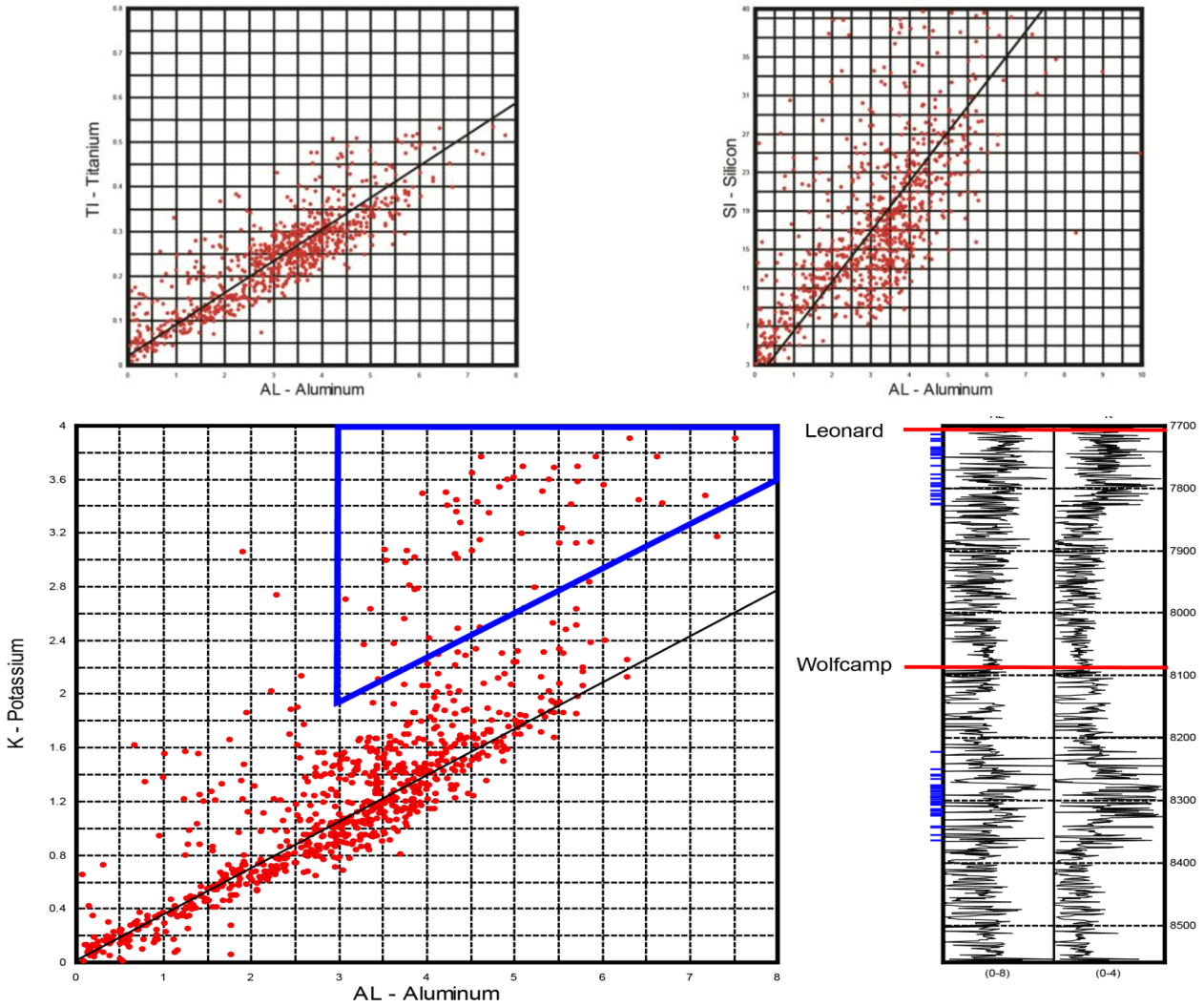

Figure 29. Greer 1 cross-plots of Al vs. Ti, Si and K. Substantial K enrichment shown to be concentrated into to stratigraphic intervals.

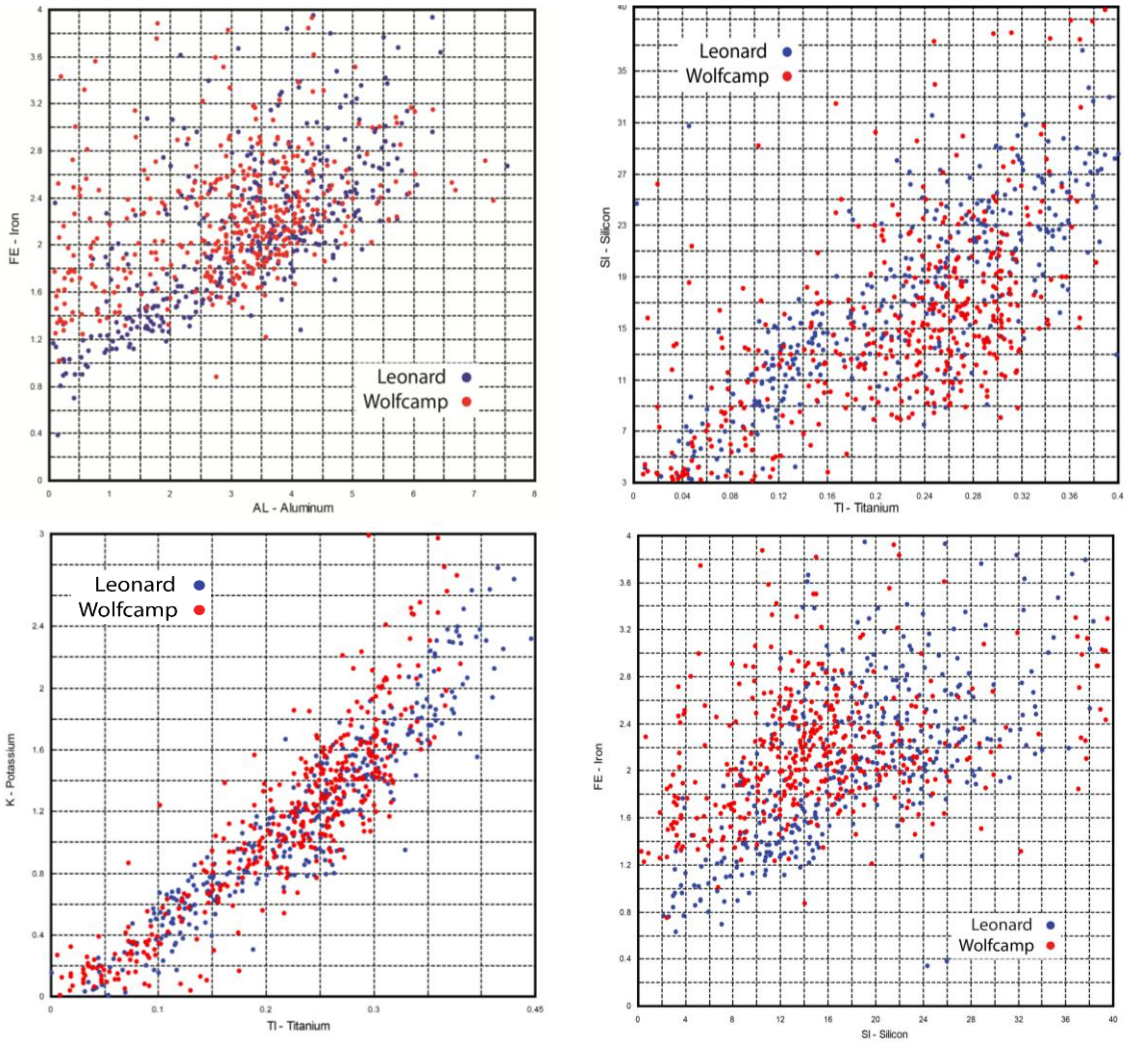

Figure 30. Greer 1 cross-plots for Fe, Al, Ti, K, and Si.

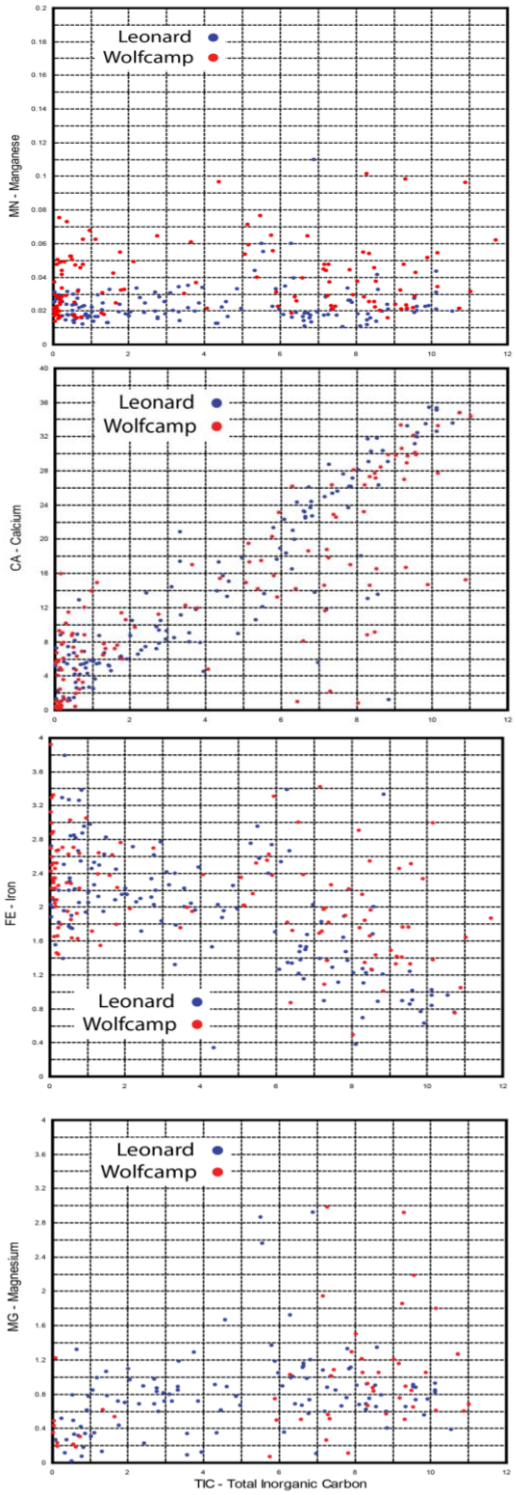

Figure 31. Greer 1 cross-plots of Mn, Ca, Fe, and Mg vs. TIC.

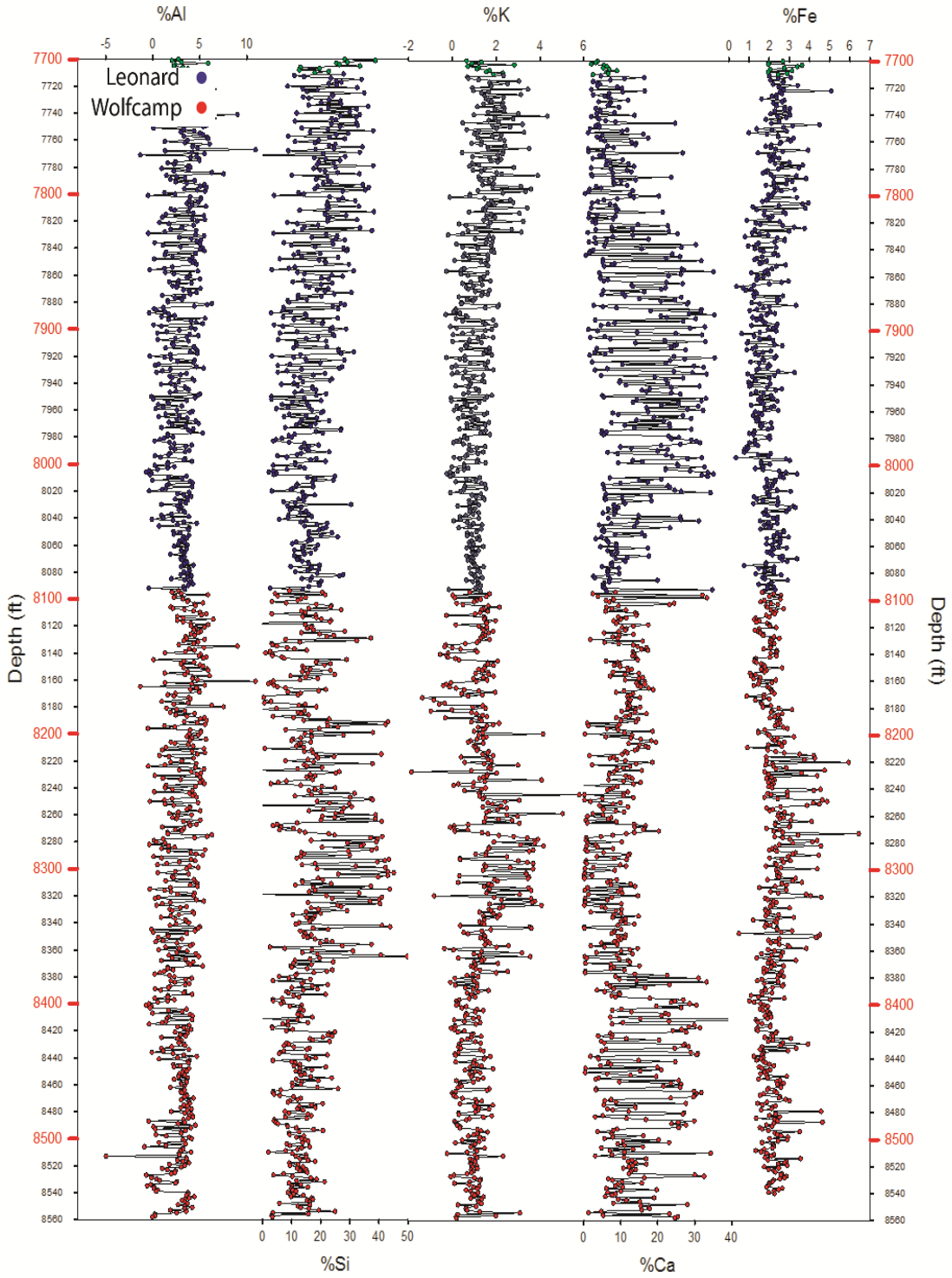

Figure 32. Major elemental chemostratigraphy of the Greer 1 core.

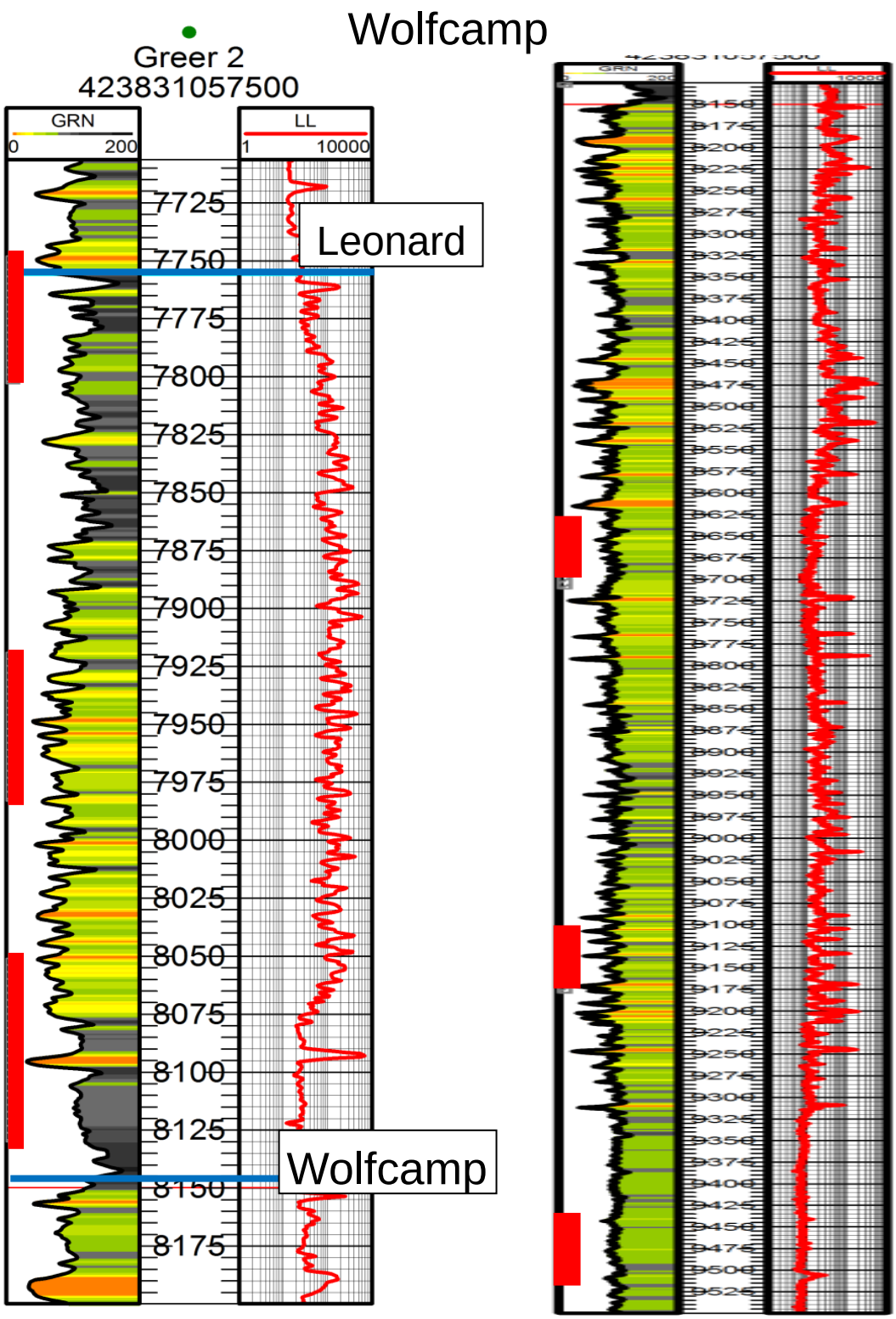

Figure 33. Greer 2 well log through the Leonard and Wolfcamp Formations with scanned intervals marked by red rectangles.

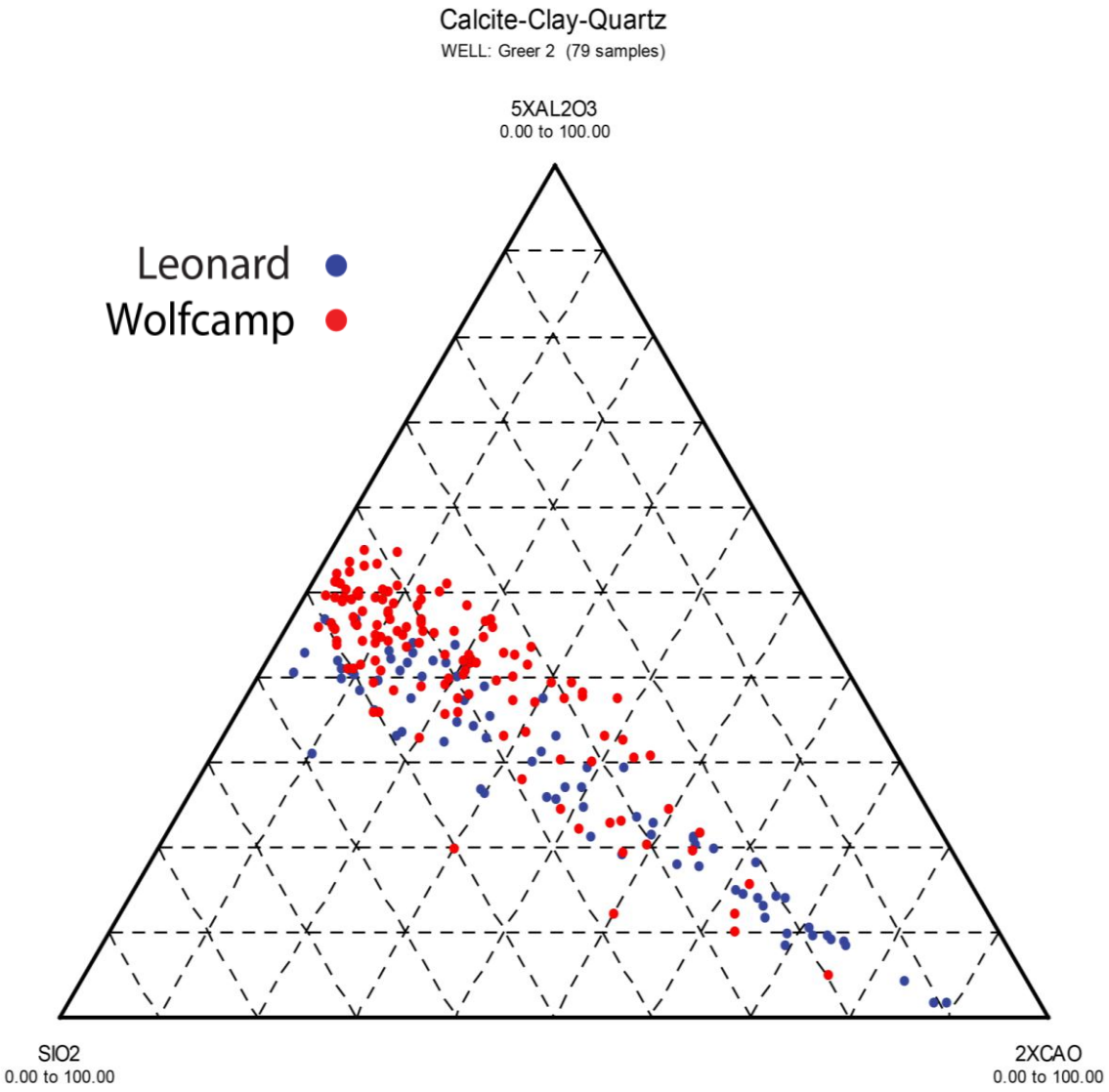

Figure 34. Greer 2 Calcite-Clay-Quartz ternary diagram.

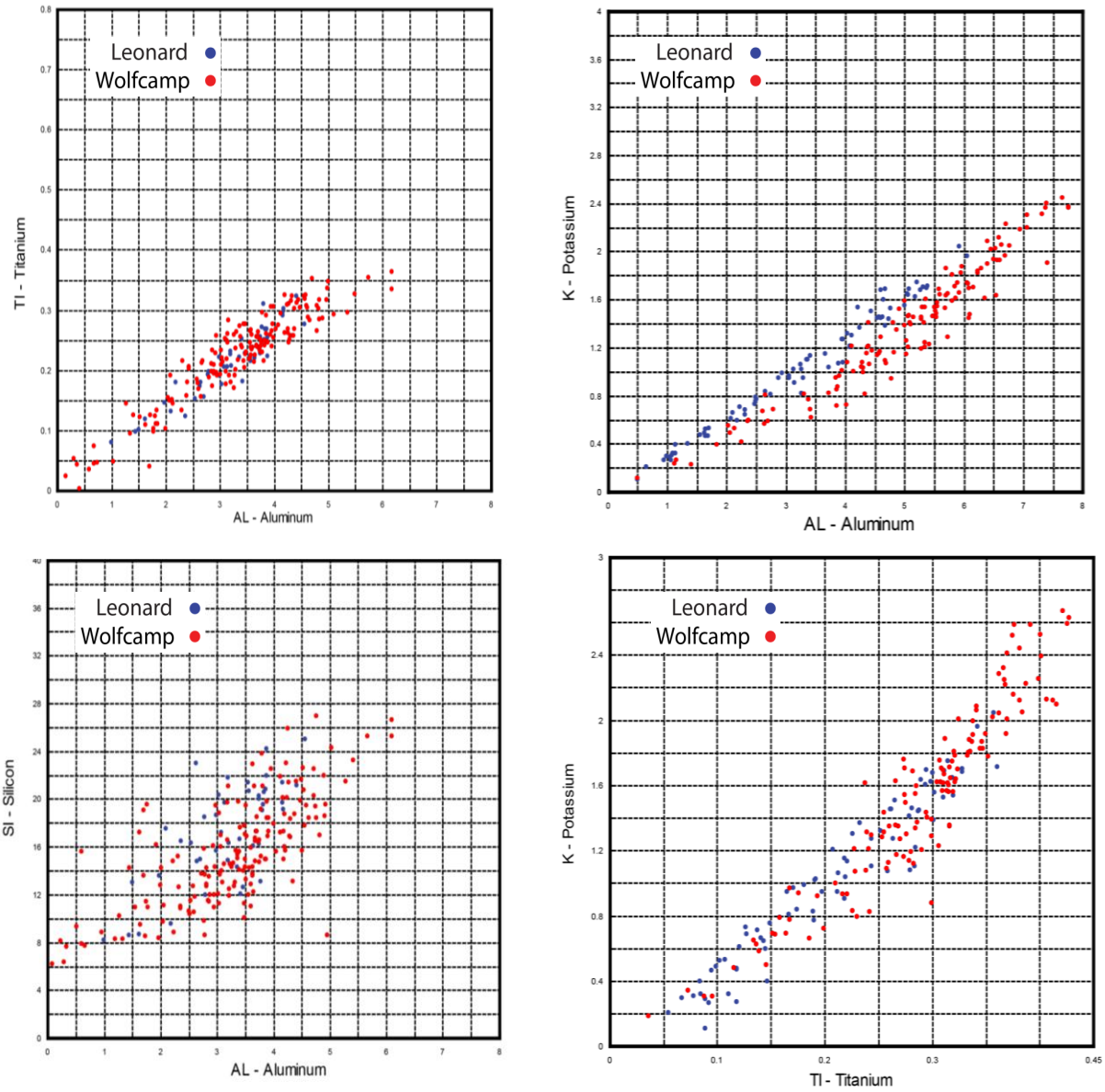

Figure 35. Greer 2 cross-plots of Ti, Al, K, and Si.

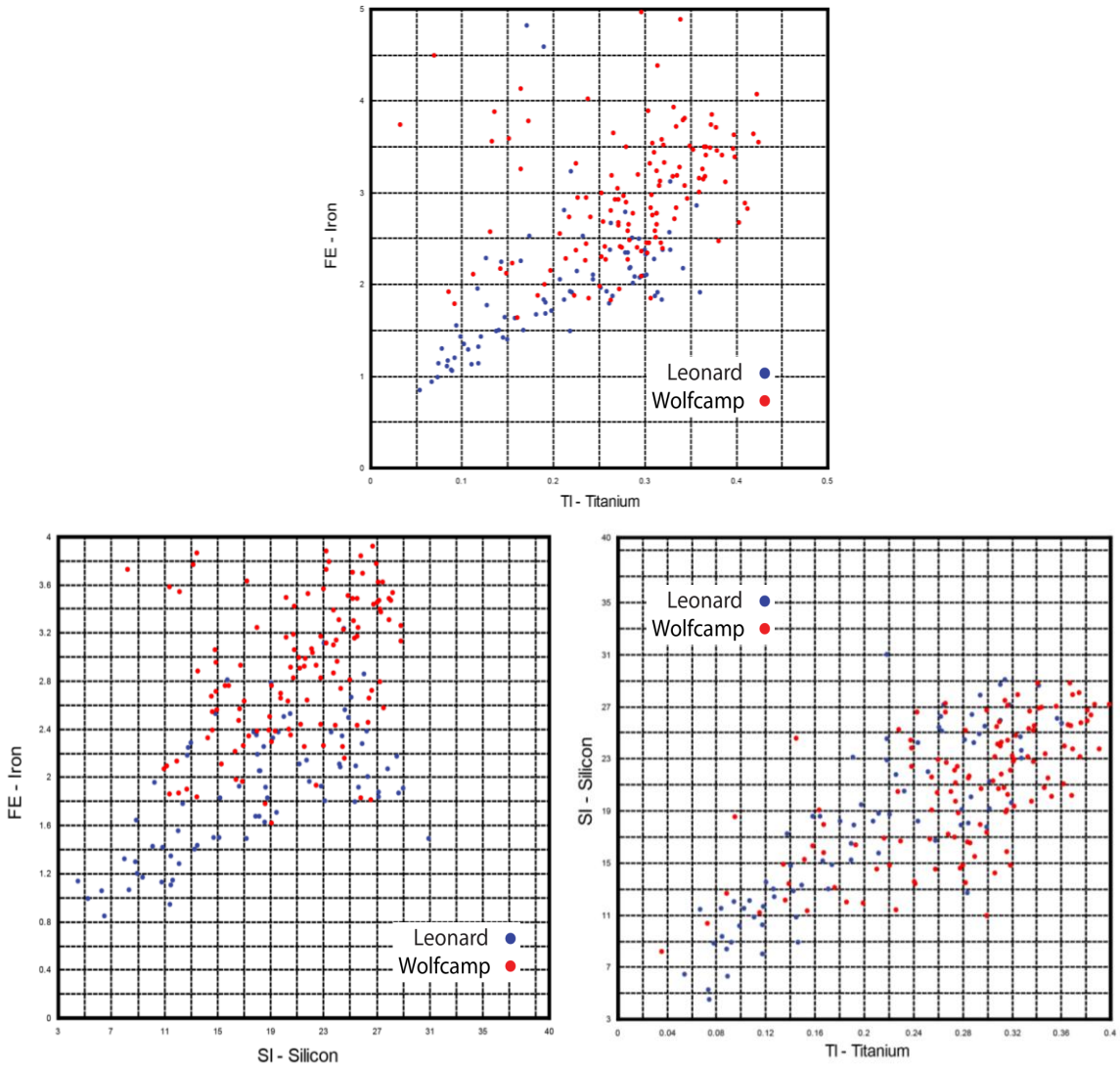

Figure 36. Greer 2 cross-plots of Si, Ti, and Fe.

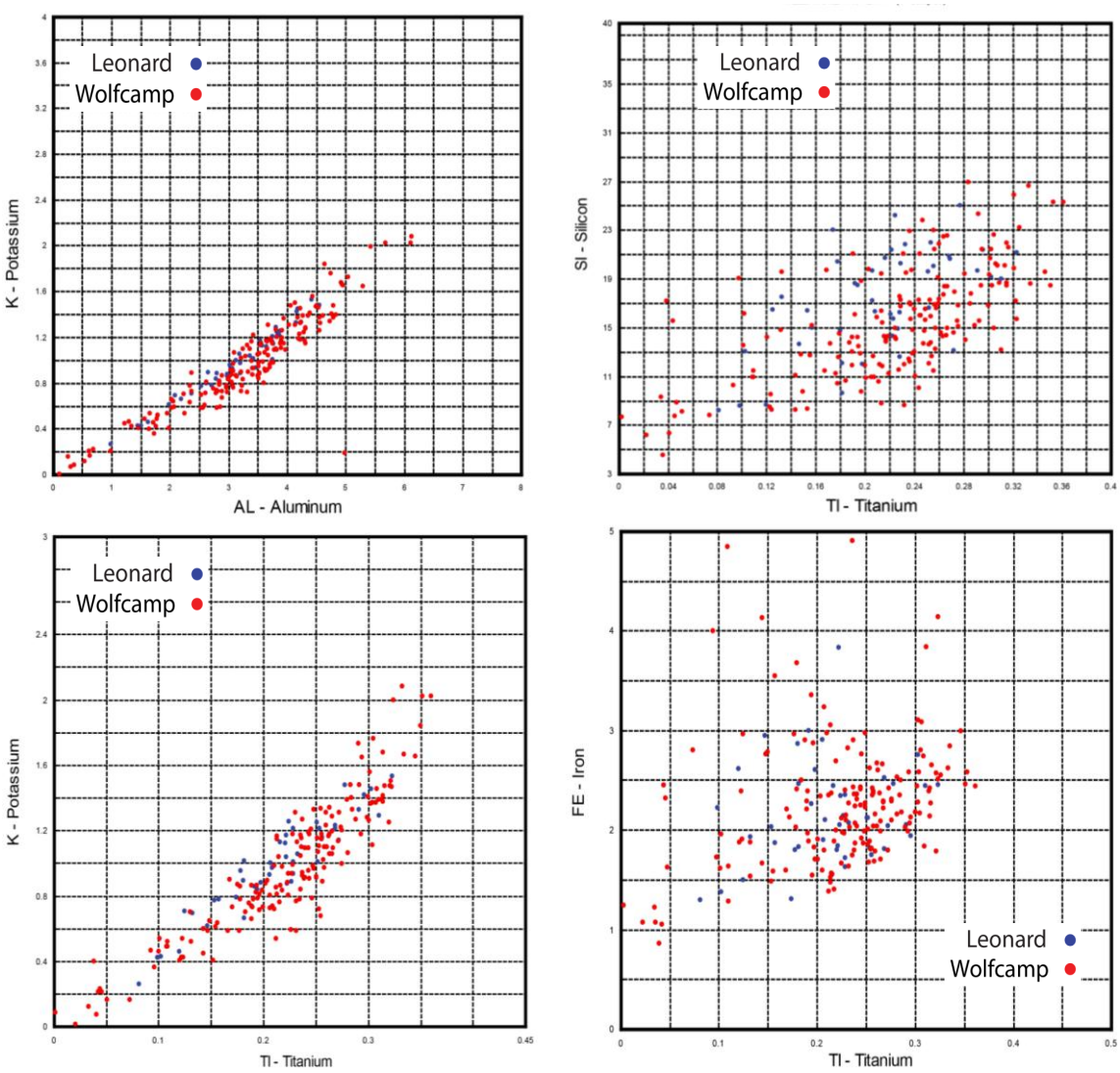

Figure 37. Ricker Rupert cross-plots of K, Al, Si, and Ti.

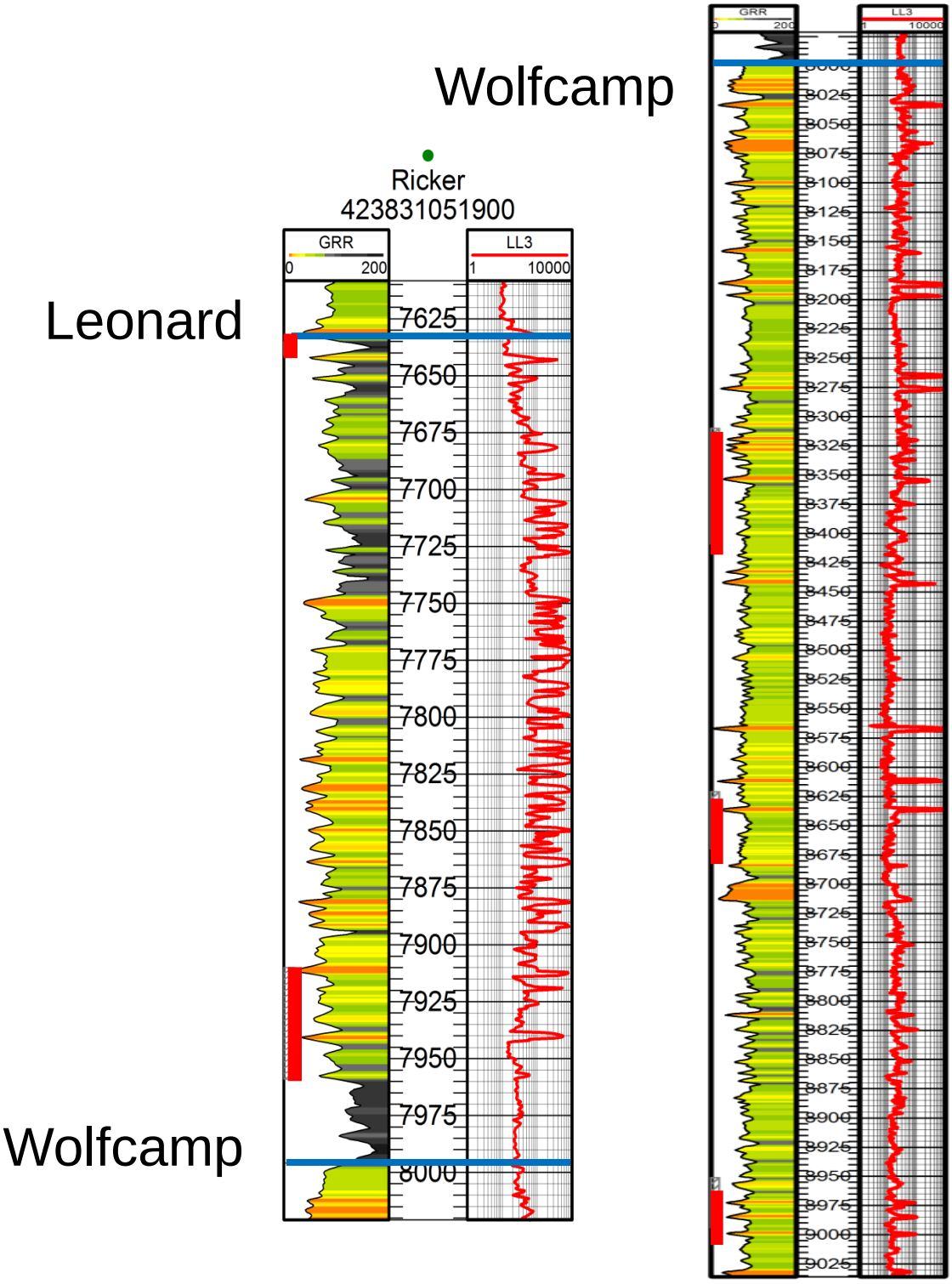

Figure 38. Ricker Rupert well log with scanned intervals marked with red rectangles.

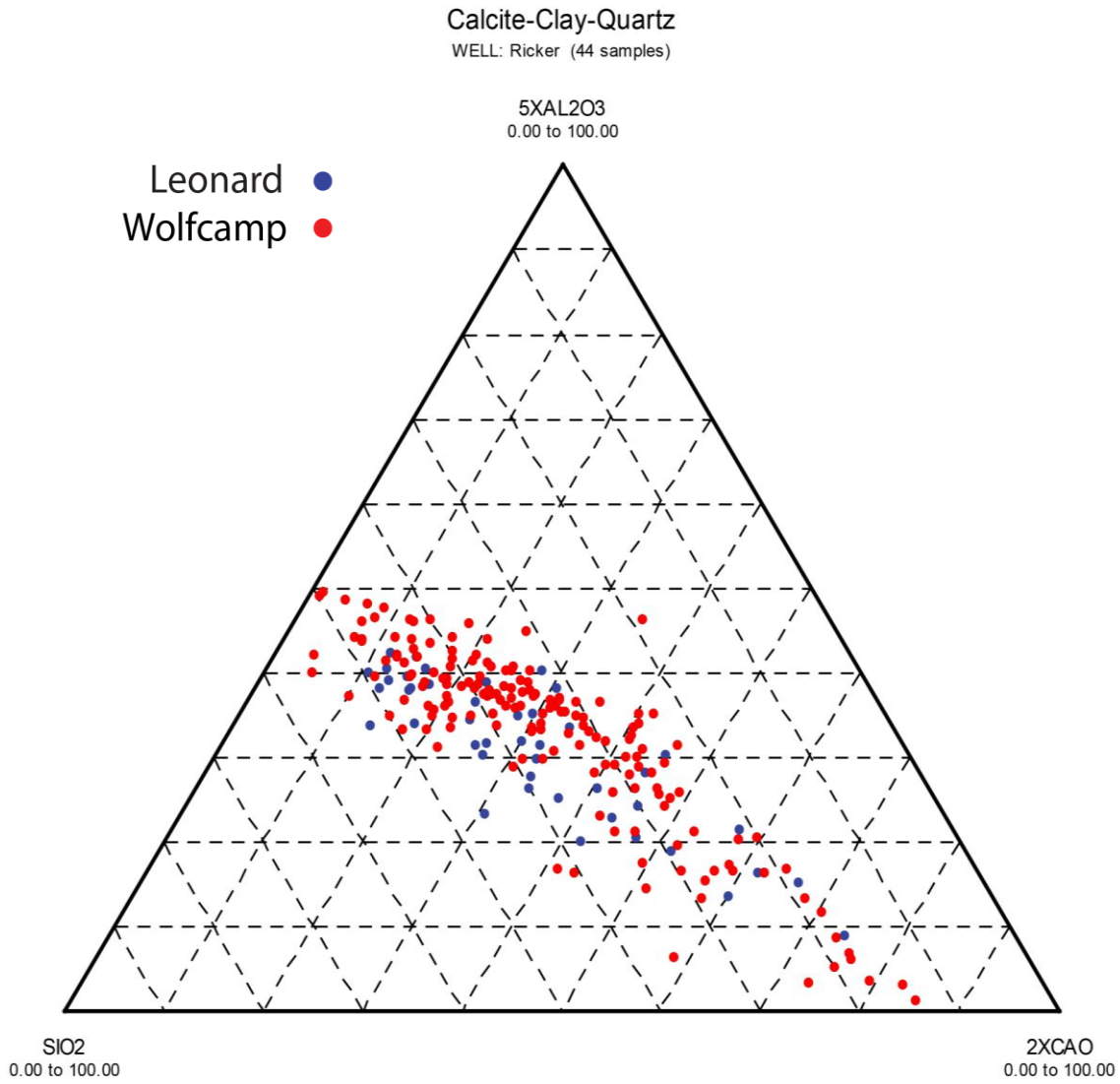

Figure 39. Ricker Rupert Calcite-Clay-Quartz Ternary diagram

REFERENCES

Adams, J.A.S., and Weaver, C.E., 1958. Thorium-to-uranium ratios as indicators of sedimentary processes: example of concept of geochemical facies: AAPG Bulletin, v. 42, p. 387-430.

Adams, J.E., Cheney, M.G., DeFord, R.K., Dickey, R.I., Dunbar, C.O., Hills, J.M., King, R.E., Lloyd, E.R., Miller, A.K., and Needham, C.E., 1939. Standard Permian section of North America: Assoc.Petroleum Geologists Bull, v. 23, p. 1673-1681.

Aller, R.C., Hannides, A., Heilbrun, C., and Panzeca, C., 2004. Coupling of early diagenetic processes and sedimentary dynamics in tropical shelf environments: The Gulf of Papua deltaic complex: Continental Shelf Research, v. 24, p. 2455-2486.

Alnaji, N., 2012. Permian Basin Geology Master's Thesis. Online. http://sepmstrata.org/nassir-thesis-site/CHAPT07.html (accessed March 2, 2012).

Algeo, T.J. and Maynard, J.B., 2004. Trace-metal behavior and redox facies in core shales of Upper Pennsylvanian Kansas-type cyclothems. Chemical Geology. 206: 289-318.

Algeo, T.J. and Lyons, T.W., 2006. Mo-total organic carbon covariation in modern anoxic marine environments: implications for analysis of paleoredox and paleohydrographic conditions. Paleoceanography, v. 21, p. 1016.

Algeo, T.J., Lyons, T.W., Blakey, R.C., and Over, D.J. 2007. Hydrographic conditions of the Devono–Carboniferous North American Seaway inferred from sedimentary Mo–TOC relationships. Palaeogeography, Palaeoclimatology, Palaeoecology. 256: 204–230.

Algeo, T.J., Maynard, J.B., 2008. Trace-metal covariation as a guide to water-mass conditions in ancient anoxic marine environments. Geosphere. Oct 2008, v. 4, no. 5; 872-887.

Algeo, T.J. and Rowe, H.D. 2011, In press. Paleoceanographic applications of trace-metal concentration data. Chemical Geology.

Algeo, T.J. and Tribovillard, N. 2009. Environmental analysis of paleoceanographic systems based on molybdenum–uranium covariation. Chemical Geology. 268: 211–225.

Archer, D., Morford, J., and Emerson, S., 2002. A model of suboxic sedimentary diagenesis suitable for automatic tuning and gridded global domains: Global Biogeochem.Cycles, v. 16, p. 1017.

Arthur, M.A., Sageman, B.B., 1994. Marine black shales: depositional mechanisms and environments of ancient deposits. Annual Reviews in Earth and Planetary Science. 22: 499–551.

Arthur, M.A., and Sageman, B.B., 2005. Sea-level control on source-rock development: perspectives from the Holocene Black Sea, the mid-Cretaceous Western Interior Basin of North America, and the Late Devonian Appalachian Basin: SPECIAL PUBLICATION-SEPM, v. 82, p. 35.

Assareh, E., Behrang, R., Assareh, R., Hedayat, N., 2011. Global Electricity Consumption Estimation Using Particle Swarm Optimization (PSO). World Academy of Science, Engineering and Technology. 79.

Ball, Mahlon, 1995. Permian Basin Province (044), in Gautier, D.L., Dolton, G.I., Takahashi, K.T., and Varnes, K.L., eds., 1995 National assessment of United States oil and gas resources—Results, methodology, and supporting data: U.S. Geological Survey Digital Data Series DDS-30.

Baumgardner, R., Hamlin, S., 2012. Permian Wolfcamp and Lower Leonard formations: Core-Based study of Basinal Lithofacies in the Wolfberry Play, Reagan County, Midland Basin, Texas: Extended Abstracts MSRL March Meeting. p. 170-181.

.Berner, R.A., 1984. Sedimentary pyrite formation: an update: Geochimica Et Cosmochimica Acta, v. 48, p. 605-615.

Berner, R.A., 1982. Burial of organic carbon and pyrite sulfur in the modern ocean: its geochemical and environmental significance: Am.J.Sci, v. 282, p. 451-473.

Berner, R.A. and Raiswell, R., 1983. Burial of organic carbon and pyrite sulfur in sediments over Phanerozoic time: a new theory. Geochimica et Cosmochimica Acta. 47: 855–862.

Berrang, P., and Grill, E., 1974. The effect of manganese oxide scavenging on molybdenum in Saanich Inlet, British Columbia: Marine Chemistry, v. 2, p. 125-148.

Blakey, R.C., 2008. Gondwana paleogeography from assembly to breakup—A 500 my odyssey: Resolving the Late Paleozoic Ice Age in Time and Space: Geological Society of America Special Paper, v. 441, p. 1-28.

Bohacs, Kevin M. 1998, Contrasting Expressions of Depositional Sequences in Mudrocks from Marine to non-Marine Environs, in Schieber, J., Zimmerle, W., and Sethi, P., eds., Shales and mudstones I.: E. Schweizerbart'sche Verlagsbuchhandlung (Nagele u. Overmiller), 33-78.

Bohacs, Kevin M., Grabowski Jr, G., Carroll, A., Mankeivicz, P., Miskell-Gerhardt, K., Schwalbach, J., Wegner, M., Simo, J.A., 2005. Production, Destruction, and Dilution – the Many Paths to Source-Rock Development. SEPM Special Publication, no. 82, pp. 62-101.

Böse, E., 1917. The permo-carboniferous ammonoides of the Glass mountains, west Texas, and their stratigraphical significance: The University.

Bowker, K.A., 2007. Barnett Shale gas production, Fort Worth Basin: issues and discussion: AAPG Bulletin, v. 91, p. 523.

Broadhead, R.F., Jianhua, Z., and Raatz, W.D., 2004. Play Analysis of Major Oil Reservoirs in the New Mexico Part of the Permian Basin: Enhanced Production Through Advanced Technologies: New Mexico Bureau of Geology & Mineral Resources.

Brumsack, H.J., 1989. Geochemistry of recent TOC-rich sediments from the Gulf of California and the Black Sea: Geologische Rundschau, v. 78, p. 851-882.

Brumsack, H.J. 2006. The trace metal content of recent organic carbon-rich sediments: Implications for Cretaceous black shale formation. Palaeogeography, Palaeoclimatology, Palaeoecology. 232: 344-361.

Calvert, S.E. 1987, Oceanographic controls on the accumulation of organic matter in marine sediments. Geological society Special Publication. 26: 137-151.

Calvert, S., and Karlin, R., 1991. Relationships between sulphur, organic carbon, and iron in the modern sediments of the Black Sea: Geochimica Et Cosmochimica Acta, v. 55, p. 2483-2490.

Calvert, S., Karlin, R., Toolin, L., Donahue, D., Southon, J., and Vogel, J., 1991. Low organic carbon accumulation rates in Black Sea sediments: .

Calvert, S.E. and Pedersen, T.F. 1993. Geochemistry of recent oxic and anoxic marine sediments: implications for the geological record. Marine Geology. 113: 67–88.

Campbell, C.V., 1967. Lamina, laminaset, bed and bedset: Sedimentology, v. 8, p. 7-26.

Carll, J.F., 1880. The geology of the oil regions of Warren, Venango, Clarion and Butler Counties. *Pa. Geol. Surv.* 3, 482.

Catuneanu, O., Abreu, V., Bhattacharya, J., Blum, M., Dalrymple, R., Eriksson, P., Fielding, C.R., Fisher, W., Galloway, W., and Gibling, M., 2009. Towards the standardization of sequence stratigraphy: Earth-Science Reviews, v. 92, p. 1-33.

Chernykh, V.V., and Ritter, S.M., 1997. Streptognathodus (Conodonta) succession at the proposed Carboniferous-Permian boundary stratotype section, Aidaralash Creek, northern Kazakhstan: Journal of Paleontology, p. 459-474.

Comer, J.B., 1991. Stratigraphic Analysis of the Upper Devonian Woodford Formation, Permian Basin, West Texas and Southeastern New Mexico: Bureau of Economic Geology, University of Texas at Austin, .

Cooper, G.A., Grant, R.E., 1969. New Permian Brachiopods from West Texas. Smithsonian Contributions to Paleobiology. No. 1, 1-31.

Crowell, J., 1978. Gondwana glaciation, cyclothems, continental positioning, and climatic change: American Journal of Science, v. 278, no. 10, p 1345-1372.

Cruse, A., Lyons, T., and Hannigan, R., 2007. Sedimentary Trace Metal-Organic Interactions as Proxies for Oceanic Redox Conditions, *in* AGU Fall Meeting Abstracts. p. 242.

Crusius, J., Calvert, S., Pedersen, T., Sage, D., 1996. Rhenium and molybdenum enrichments in sediments as indicators of oxic, suboxic and sulfidic conditions of deposition. Earth and Planetary Science Letters. 145: 65–78.

Curtis, J.B., 2002. Fractured shale-gas systems: AAPG Bulletin, v. 86, p. 1921.

Cys, J., and Gibson, W., 1988, Pennsylvanian and Permian geology of the Permian Basin region: Frenzel Et Al, p. 277-289.

David Z., P., 1994. Seawater as the source of minor elements in black shales, phosphorites and other sedimentary rocks: Chemical Geology, v. 114, p. 95-114, doi: 10.1016/0009-2541(94)90044-2.

Davydov, VI, Glenister, BF, Spinosa, C., Ritter, SM, Chernykh, BR, Wardlaw, BR, and Snyder, WS, 1995, Proposal of Aidaralash as GSSP for the base of the Permian System: Permophiles, no. 26, p. 1-9.

Dean,W.E. and Arthur, M.A. 1989. Iron–sulfur–carbon relationships in organic-carbon-rich sequences I: Cretaceous western interior seaway. American Journal of Science. 289: 708–743.

Dean, W., Gardner, J., Piper, D., 1997. Inorganic geochemical indicators of glacial – interglacial changes in productivity and anoxia on the California continental margin. Geochim. Cosmochim. Acta. 61, pp. 4507 – 4518.

Demaison, G.J. and Moore, G.T. 1980. Anoxic environments and oil source bed genesis. American Association of Petroleum Geologists Bulletin. 64: 1179–1209.

Dutkiewicz, A., Volk, H., Ridley, J., and George, S., 2004. Geochemistry of oil in fluid inclusions in a middle Proterozoic igneous intrusion: implications for the source of hydrocarbons in crystalline rocks: Organic Geochemistry, v. 35, p. 937-957.

Dutton, S.P., Eugene, M.K., Broadhead, R.F., Breton, C.L., Raatz, W.D., Ruppel, S.C., and Kerans, C., 2004. Play Analysis and Digital Portfolio of Major Oil Reserves in the Permian Basin: Application and Transfer of Advanced Geological and Engineering Technologies for Incremental Production Opportunities. Bureau of Economic Geology. 408.

Eby, G.N., 2004. Principles of environmental geochemistry: Brooks/Cole Pub Co, .

Energy Information Administration, 2012. Countries - U.S. Energy Information Administration (EIA). Online. http://www.eia.gov/countries/ (accessed February 18, 2012).

Ernst, W., 1970. Geochemical facies analysis. Meth. Geochem Geophys. 11, p. 1-152

Ettensohn, F.R., 1985a. The Catskill Delta complex and the Acadian orogeny: a model. In: Woodrow, D.L., Sevon, W.D. (Eds.), The Catskill Delta Spec. Pap. Geol. Soc. Am., vol. 201, pp. 39 – 49.

Fielding, C.R., Frank, T.D., and Isbell, J.L., 2008. The late Paleozoic ice age—A review of current understanding and synthesis of global climate patterns: Resolving the Late Paleozoic Ice Age in Time and Space.Geological Society of America, Special Papers, v. 441, p. 343-354.

Flamm, Douglas S. 2008, Wolfcampian Development of the Nose of the Eastern Shelf of the Midland Basin, Glasscock, Sterling, and Reagan Counties, Texas. Department of Geological Sciences Master's Thesis. Brigham Young University. 1-54.

Gastaldo, R.A., DiMichele, W.A., and Pfefferkorn, H.W., 1996. Out of the icehouse into the greenhouse: A late Paleozoic analogue for modern global vegetational change: Gsa Today, v. 6, p. 1-7.

Given, R.K., and Lohmann, K.C., 1986. Isotopic evidence for the early meteoric diagenesis of the reef facies, Permian Reef Complex of West Texas and New Mexico: Journal of Sedimentary Research, v. 56, p. 183-193.

Grainger, P., 1984. The classification of mudrocks for engineering purposes: Quarterly Journal of Engineering Geology and Hydrogeology, v. 17, p. 381-387.

Hallberg, R.O., 1981. Recycling of heavy metals at the redoxcline: GFF, v. 103, p. 125-126.

Hallberg, R.O., and Халлберг, P.O., 1976. A Geochemical Method for Investigation of Paleoredox Conditions in Sediments/Геохимический метод исследований условий палеоредокса в осадках: Ambio Special Report, p. 139-147.

Harris, L.D., 1978. The eastern interior aulacogen and its relation to Devonian shale gas production, *in* Preprints for Second Eastern Gas Shales Symposium: US Department of Energy, Morgantown Energy Technology Center, METC/SP-78/6, p. 55-72.

Harris, L.D., de Witt Jr, W., and Colton, G., 1970. What are possible stratigraphic controls for gas fields in eastern black shale: Oil Gas J.;(United States), v. 76, .

Heckel, P.H., 1986, Sea-level curve for Pennsylvanian eustatic marine transgressive-regressive depositional cycles along midcontinent outcrop belt, North America:Geology, v. 14, 330-334.

Hedges, J.I., and Keil, R.G., 1995. Sedimentary organic matter preservation: an assessment and speculative synthesis: Marine Chemistry, v. 49, p. 81-115.

Hills, J.M., 1972. Late Paleozoic sedimentation in west Texas Permian basin: AAPG Bulletin, v. 56, p. 2303-2322.

Hills, J.M., 1984, Sedimentation, tectonism, and hydrocarbon generation in Delaware basin, West Texas and southeastern New Mexico: American Association of Petroleum Geologists Bulletin, v. 68, 250-267.

Hoak, T., Sundberg, K., and Ortoleva, P., (1998), Overview of the Structural Geology and Tectonics of the Central Basin Platform, Delaware Basin, and Midland Basin, West Texas and New Mexico, DOE/PC/91008, No. 23, Pt. 8, p. 1-49.

Hoelke, J., 2011, Chemostratigraphy and paleoceanography of the Mississippian Barnett Formation, Southern Fort Worth Basin, Texas, USA. Department of Geological Sciences Master's Thesis. University of Texas at Arlington. 1- 96.

Hohbein, M. W., Sexton, P.F., Cartwright, J.A., 2012. Onset of North Atlantic Deep Water production coincident with inception of the Cenozoic global cooling trend. Geology, v. 40, no. 3, p. 255-258.

Holbrook, J.M., and Dunbar, R.W., 1992. Depositional history of Lower Cretaceous strata in northeastern New Mexico: Implications for regional tectonics and depositional sequences. Bulletin of the Geological Society of America, v. 104, p. 802.

Holdich, Stephen A., 2003. The Increasing Role of Unconventional Reservoirs in the Future of the Oil and Gas Business. Journal of Petroleum Technology, November. 34-79.

Holdich, Stephen A., 2006. Tight Gas Sands. Journal of Petroleum Technology, June. 84-90.

Holser, W., and Kaplan, I., 1966. Isotope geochemistry of sedimentary sulfates: Chemical Geology, v. 1, p. 93-135.

Horak, R. L., 1985, Tectonic and hydrocarbon maturation history in the Permian basin: Oil & Gas Journal, May 27, v. 83, no. 21, p. 124– 129.

Hovorka, S.D., 1998. Characterization of bedded salt for storage caverns: case study from the Midland Basin: Open File Report, Bureau of Economic Geology. p. 1-101.

Hughes, E., 2011. Chemostratigraphyand paleoenvironment of the Smithwick Formation, Fort Worth Basin, San Saba County, Texas. Department of Geological Sciences Master's Thesis. University of Texas at Arlington. 1-93.

Hunt, T.S., (1861). Bitumens and mineral oils. *Montreal Gazette*, March 1.

Jenkyns, H.C., 2010. Geochemistry of oceanic anoxic events: Geochem.Geophys.Geosyst, v. 11, p. Q03004.

Jones, B. and Manning, A.C. 1994. Comparison of geochemical indices used for the interpretation of palaeoredox conditions in ancient mudstones: Chemical Geology, v. 111, p. 111-129.

Kim, E.M. and Ruppel, S.C., 2005. Oil and Gas Production in Texas. Bureau of Economic Geology Pub. 2.

Klinkhammer, G., and Palmer, M., 1991. Uranium in the oceans: where it goes and why: Geochimica Et Cosmochimica Acta, v. 55, p. 1799-1806.

Krumbein, W.C., 1951. Occurrence and lithologic associations of evaporites in the United States: Journal of Sedimentary Research, v. 21, p. 63-81.

Kvenvolden, K.A., and Squires, R.M., 1967. Carbon isotopic composition of crude oils from Ellenburger group (Lower Ordovician), Permian Basin west Texas and eastern New Mexico: American Association of Petroleum Geologists Bulletin, v. 5, p. 1293-1303.

Leventhal, J., and Finkelman, R., 1987. Uranium in the Vermillion Creek core samples: US Geological Survey Professional Paper, v. 1314, p. 171.

Leventhal, J., and Goldhaber, M., 1977. New data for uranium, thorium, carbon, and sulfur in Devonian black shale from West Virginia, Kentucky, and New York, *in* Proceedings, first eastern gas shales symposium, Morgantown, , p. 259-296.

Lyons, T.W., and Berner, R.A., 1992. Carbon-sulfur-iron systematics of the uppermost deep-water sediments of the Black Sea: Chemical Geology, v. 99, p. 1-27.

Lyons, T.W., and Severmann, S., 2006. A critical look at iron paleoredox proxies: New insights from modern euxinic marine basins: Geochimica Et Cosmochimica Acta, v. 70, p. 5698-5722.

Lyons, T.W., Werne, J.P., Hollander, D.J., and Murray, R., 2003. Contrasting sulfur geochemistry and Fe/Al and Mo/Al ratios across the last oxic-to-anoxic transition in the Cariaco Basin, Venezuela: Chemical Geology, v. 195, p. 131-157.

Mackenzie, F.T., 2005. Sediments, diagenesis, and sedimentary rocks: Elsevier Science, .

Magyar, B., Moor, H., and Sigg, L., 1993. Vertical distribution and transport of molybdenum in a lake with a seasonally anoxic hypolimnion: Limnology and Oceanography, p. 521-531.

Mainali, Pukar, 2011. Chemostratigraphy and the paleoceanography of the Bossier-Haynesville Formation, East Texas Basin, TX and LA, USA. Department of Geological Sciences Master's Thesis. University of Texas at Arlington. 1- 80.

Mazzullo, S.J., and A. M. Reid, 1988, Stratigraphic architecture of Pennsylvanian and Lower Permian Facies, Northern Midland Basin, Texas, *in* B. K. Cunningham, ed., Permian and Pennsylvanian Stratigraphy, Midland Basin, West Texas: Studies to aid hydrocarbon exploration, Midland, Texas, West Texas Geological Society, Permian Basin Section, SEPM Publication 88-28. 1-6.

Mazzullo, S., and Reid, A., 1989. Lower Permian platform and basin depositional systems, northern Midland Basin, Texas: SEPM Special Publication, v. 44, p. 305-320.

McManus, J., Berelson, W.M., Severmann, S., Poulson, R.L., Hammond, D.E., Klinkhammer, G.P., and Holm, C. 2006. Molybdenum and uranium geochemistry in continental margin sediments: Paleoproxy potential. Geochimica et Cosmochimica Acta. 70: 4643–4662.

Milliman, J.D., 1995. Sediment discharge to the ocean from small mountainous rivers: The New Guinea example: Geo-Marine Letters, v. 15, p. 127-133.

Montgomery, S.L., Schechter, D.S., and Lorenz, J., 2000. Advanced reservoir characterization to evaluate carbon dioxide flooding, Spraberry Trend, Midland Basin, Texas: AAPG Bulletin, v. 84, p. 1247.

Montgomery, C.T., Smith, M. B., 2010. Hydraulic Fracturing History of an enduring technology. Journal of Petrophysical Technology, December. 26 -41.

Morford, J.L. and Emerson, S. 1999. The geochemistry of redox sensitive trace metals in sediments. Geochimica et Cosmochimica Acta. Vol. 63, No. 11/12, pp. 1735–1750.

Morford, J.L., Russell, A.D., Emerson, S. 2001. Trace metal evidence for changes in the redox environment associated with the transition from terrigenous clay to diatomaceous sediment, Saanich Inlet, BC. Marine Geology. 174: 355–369.

Morse, J., and Luther III, G., 1999. Chemical influences on trace metal-sulfide interactions in anoxic sediments: Geochimica Et Cosmochimica Acta, v. 63, p. 3373-3378.

OPEC, 2012. OPEC Share of World Crude Oil Reserves. Online. http://www.opec.org/opec_web/en/data_graphs/330.htm (accessed February 2, 2012).

Meyers, P.A. 1994. Preservation of elemental and isotopic source identification of sedimentary organic matter. Chemical Geology. 114: 289-302.

Meyers, P.A. 1997. Organic geochemical proxies of paleoceanographic, paleolimnologic, and paleoclimatic processes. Organic Geochemistry. Vol. 27, No. 5/6, pp 231-250.

Meyers, P.A., Bernasconi, S.M., and Forster, A. 2006. Origins and accumulation of organic matter in expanded Albian to Santonian black shale sequences on the Demerara Rise, South American margin. Organic Geochemistry. 37: 1816–1830.

Meyers, P.A., Bernasconi, S.M., and Yum, J-G. 2009A. 20 My of nitrogen fixation during deposition of mid-Cretaceous black shales on the Demerara Rise, equatorial Atlantic Ocean. Organic Geochemistry. 40: 158-166.

Meyers, P.A., Yum, J-G., and Wise, S.W. 2009B. Origins and maturity of organic matter in mid-Cretaceous black shales from ODP Site 1138 on the Kerguelen Plateau. Marine and Petroleum Geology. 26: 909-915.

Peterson, J.A., and Ohlen, H.R., 1963. Pennsylvanian shelf carbonates, Paradox basin, *in* Shelf Carbonates of the Paradox Basin, a Symposium±Four Corners Geol. Soc., 4th Field Conference, , p. 65-79.

Piper, D.Z., and Calvert, S.E., 2009. A marine biogeochemical perspective on black shale deposition. Earth-Science Review 95. 63-96.

Posamentier, H.W. and Allen, G.P. 1999. Siliciclastic sequence stratigraphy: concepts and applications. Concepts in Sedimentology and Paleontology, vol. 7. Society of Economic Paleontologists and Mineralogists (SEPM). 210 pp.

Raiswell, R. and Berner, R.A. 1986. Pyrite and organic matter in Phanerozoic normal marine shales. Geochimica et Cosmochimica Acta. 50: 1967–1976.

Raiswell, R., Buckley, F., Berner, R.A., and Anderson, T., 1988. Degree of pyritization of iron as a paleoenvironmental indicator of bottom-water oxygenation: Journal of Sedimentary Research, v. 58, p. 812-819.

Rimmer, S.M., 2004. Geochemical paleoredox indicators in Devonian–Mississippian black shales, central Appalachian Basin (USA): Chemical Geology, v. 206, p. 373-391.

Rimmer, S., Rowe, H., Taulbee, D., Hower, J., 2006. Influence of maceral content on $\delta^{13}C$ and $\delta^{15}N$ in a Middle Pennsylvanian coal. Chemical Geology. 225, p. 77-90.

Rimmer, S.M., Thompson, J.A., Goodnight, S.A., and Robl, T.L. 2004. Multiple controls on the preservation of organic matter in Devonian–Mississippian marine black shales: geochemical and petrographic evidence. Palaeogeography, Palaeclimatology, Palaeoecology. 215, p. 125–154.

Ritter, S.M., 1995. Upper Missourian-lower Wolfcampian (upper Kasimovian-lower Asselian) conodont biostratigraphy of the midcontinent, USA: Journal of Paleontology, p. 1139-1154.

Rogers, J., and Adams, J., 1969. Uranium: Handbook of Geochemistry, V, v. 4, .

Ross, C.A., 1959. The Wolfcamp Series (Permian) and new species of fusulinids, Glass Mountains, Texas: Jour, *in* Washington Acad. Sci, , p. 299-316.

Rousseau, R.M., 2001. Detection limit and estimate of uncertainty of analytical XRF results: The Rigaku Journal, v. 18, p. 33-47.

Rowe, H., Hughes, N., Robinson, K., 2012, The quantification and application of handheld energy-dispersive x-ray fluorescence (ED-XRF) in mudrock chemostratigraphy and geochemistry. Chemical Geology.

Rowe, H.D., Loucks, R.G., Ruppel, S.C., Rimmer, S.M., 2008. Mississippian Barnett Formation, Fort Worth Basin, Texas: Bulk geochemical inferences and Mo-TOC constraints on the severity of hydrographic restriction. Chemical Geology. 257: 16-25.

Rowe, H., S. Ruppel, S. Rimmer, and R. Loucks, 2009, Core-based chemostratigraphy of the Barnett Shale, Permian Basin, Texas: Gulf Coast Association of Geological Societies Transactions, v. 59, p. 675-686.

Schieber, J., Lazar, O. R., and Bohacs, K., 2010. Sedimentology and Stratigraphy of Shales: Expressions and Correlation of Depositional Sequences in the Devonian of Tennessee, Kentucky, and Indiana. AAPG 2010 Annual Convention, Field Guide for SEPM Field Trip 10. 1-15.

Schroder, S., and Grotzinger, J., 2007. Evidence for anoxia at the Ediacaran-Cambrian boundary: the record of redox-sensitive trace elements and rare earth elements in Oman: Journal of the Geological Society, v. 164, p. 175.

Schulz, H.D., 2000. Marine geochemistry: with 23 tables: Springer, .

Scotese, C., Bambach, R., Barton, C., Van Der Voo, R., Ziegler, A., 1979. Paleozoic Base Maps. The Journal of Geology, v. 87, p. 217-277.

Selley, R. C., 1998. Elements of Petroleum Geology. 2nd ed. California: Academic Press.

Silver, B.A., and Todd, R.G., 1969. Permian cyclic strata, northern Midland and Delaware basins, west Texas and southeastern New Mexico: Assoc.Petroleum Geologists Bull, v. 53, p. 2223-2251.

Slatt, R.M., 2002. Significance of Shales and Mudrocks in Oil and Gas Exploration and Reservoir Development: TRANSACTIONS-GULF COAST ASSOCIATION OF GEOLOGICAL SOCIETIES, p. 1119-1130.

Sorby, H.C., 1908. On the application of quantitative methods to the study of the structure and history of rocks. Quarterly of the Geological Society of London, 64. 171-223.

Strauss, H., and Beukes, N.J., 1996. Carbon and sulfur isotopic compositions of organic carbon and pyrite in sediments from the Transvaal Supergroup, South Africa: Precambrian Research, v. 79, p. 57-71.

Swanson, V.E., 1961. Geology and geochemistry of uranium in marine black shales: US Gov. Print. Office, .

Tourtelot, H.A., 1979. Black shale: its deposition and diagenesis: Clays and Clay Minerals, v. 27, p. 313-321.

Tribovillard, N., Algeo, T.J., Baudin, F., Riboulleau, A., 2011. Analysis of marine environmental conditions based on molybdenum-uranium covariation – Applications to Mesozoic paleoceanography. Chemical Geology.

Tribovillard, N., Algeo, T.J., Lyons, T., and Riboulleau, A., 2006. Trace metals as paleoredox and paleoproductivity proxies: An update: Chemical Geology, v. 232, p. 12-32.

Twichell, S.C., Meyers, P.A., and Diester-Haass, L. 2002. Significance of high C/N ratios in organic-carbon-rich Neogene sediments under the Benguela Current upwelling system. Organic Geochemistry. 33: 715-722.

Tyson, R., 2005. The" productivity versus preservation" controversy: cause, flaws, and resolution: SPECIAL PUBLICATION-SEPM, v. 82, p. 17.

Tyson, R.V., and Pearson, T.H., 1991. Modern and ancient continental shelf anoxia: an overview. Geologic Society London Special Publication. No. 58. 1-24.

Tyson, R.V., Wilson, R., Downie, C. 1979. A stratified water column environmental model for the type Kimmeridge Clay. Nature 277. p. 377-380.

Udden, J.A., Baker, C.L., and Bose, Emil, 1916, Review of the geology of Texas: University of Texas Bulletin, no. 44, p. 164.

Ulmer-Scholle, D.S., Scholle, P.A., and Brady, P.V., 1993. Silicification of evaporites in Permian (Guadalupian) back-reef carbonates of the Delaware Basin, West Texas and New Mexico: Journal of Sedimentary Research, v. 63, p. 955.

University of Texas Permian Basin, 1998. Comparison of Permian Basin Oil Reserves to other Producing Areas in the U.S. Online. http://ceed.utpb.edu/energy-resources/petroleum-library (accessed March 12, 2012.

Vail, P.R., Mitchum Jr., R.M., Thompson III, S. 1977. Seismic stratigraphy and global changes of sea level, part 3: relative changes of sea level from coastal onlap. In: Payton, C.E. (Ed.), Seismic Stratigraphy — Applications to Hydrocarbon Exploration. Memoir, vol. 26. American Association of Petroleum Geologists. pp. 63–81.

Verardo,D.J., Froelich, P.N., and McIntyre, A. 1990. Determination of organic carbon and nitrogen in marine sediments using the Carlo Erba NA-1500. Deep-Sea Research. 37: 157-165.

Veevers, J., Powell, C., 1987. Late Paleozoic glacial episodes in Gondwanaland reflected in transgressive-regressive depositional sequences in Euramerica: Geological Society of America Bulletin, v. 98, p. 475-487.

Vidas, H., Hughman, B., 2008. Availability, Economics, and Production Potential of North American Unconventional Natural Gas Supplies. INGAA Foundation, Inc. 1-167.

Vine, J.D., and Tourtelot, E.B., 1970. Geochemistry of black shale deposits; a summary report: Economic Geology, v. 65, p. 253-272.

Walker, J.D., and Geissman, J.W., compilers, 2009. Geologic Time Scale: Geological Society of America, doi: 10.1130/2009.CTS004R2C. ©2009 The Geological Society of America.

Walker, D.A., Golonka, J., Reid, A.M., Reid, S.A.T., 1991,The effects of late Paleozoic paleolatitude and paleogeography in the Midland basin, Texas, in M.P. Candelaria, ed., Permian basin plays – tomorrow's technology today: West Texas Geological Society Publication 91-89,141-162.

Wedepohl, K.H., 1971. Environmental influences on the chemical composition of shales and clays. In: Ahrens, L.H., Press, F., Runcorn, S.K., Urey, H.C. (Eds.), Physics and Chemistry of the Earth vol. 8, Pergamon, Oxford (1971), pp. 305–333.

Wedepohl, K.H., 1991. The composition of the upper earth's crust and the natural cycles of selected metals. Metals in natural raw materials. Natural Resources. In: Merian, E. (Ed.), Metals and Their Compounds in the Environment. VCH, Weinheim, pp. 3–17.

Wiggins, W., Harris, P., and Burruss, R., 1993. Geochemistry of post-uplift calcite in the Permian Basin of Texas and New Mexico: Bulletin of the Geological Society of America, v. 105, p. 779.

Wignall, P.B., and Myers, K.J., 1988. Interpreting benthic oxygen levels in mudrocks: a new approach: Geology, v. 16, p. 452.

BIOGRAPHICAL INFORMATION

Milton (Trey) Cortez III was born on January 28, 1981 in Clifton, Texas. Trey grew up in Clifton and graduated from high school there in 1999. He attended Baylor University for two years then entered into private industry for 8 years. After returning to full-time university studies in 2007, Trey enrolled at University of Texas at Arlington to pursue a degree in Environmental Geology. He graduated with a Bachelor of Science degree in August 2009 and continued into graduate school at the University of Texas at Arlington shortly thereafter. Trey entered the Petroleum Geology program under supervision of Dr. Harry Rowe and is scheduled to complete his Master's degree in Petroleum Geology in May, 2012. Trey begins work with Encana Natural Gas upon graduation.